pennsylvania
DEPARTMENT OF TRANSPORTATION

Determining More Effective Approaches for Grouting Shear Keys of Adjacent Box Beams

FINAL REPORT

May 31, 2010

By Maria Lopez de Murphy,
Jubum Kim, Zi Sang and Chao

The Thomas D. Larson
Pennsylvania Transportation Institute

PENNSTATE
1855

COMMONWEALTH OF PENNSYLVANIA
DEPARTMENT OF TRANSPORTATION

CONTRACT No. 510602
PROJECT No. PSU 014

DEPARTMENT OF TRANSPORTATION
UNITED STATES OF AMERICA

Technical Report Documentation Page

1. Report No. FHWA-PA-2010-014-PSU 014	**2. Government Accession No.**	**3. Recipient's Catalog No.**
4. Title and Subtitle Determining More Effective Approaches for Grouting Shear Keys of Adjacent Box Beams		**5. Report Date** May 31, 2010 **6. Performing Organization Code**
7. Author(s) Maria Lopez de Murphy, Ph.D., Jubum Kim, Ph.D., Zi Sang and Chao Xiao		**8. Performing Organization Report No.** LTI 2010-16
9. Performing Organization Name and Address The Thomas D. Larson Pennsylvania Transportation Institute The Pennsylvania State University Transportation Research Building University Park, PA 16802-4710		**10. Work Unit No. (TRAIS)** **11. Contract or Grant No.** 510602, PSU 014
12. Sponsoring Agency Name and Address The Pennsylvania Department of Transportation Bureau of Planning and Research Commonwealth Keystone Building 400 North Street, 6th Floor Harrisburg, PA 17120-0064		**13. Type of Report and Period Covered** Final Report: 10/1/08 – 5/31/10 **14. Sponsoring Agency Code**

15. Supplementary Notes
Technical Advisor: William C. Koller, PE, wkoller@state.pa.us, 814-678-7106

16. Abstract

The objective of this project was to evaluate improved design and construction practices that have the potential to reduce shear key grout failure (cracking) in PennDOT precast box beam bridges. This objective was met by conducting a state-of-the-practice literature review, numerical parametric studies, and experimental verification tests. The literature review presented four possible parameters that have the potential to reduce cracking: (1) shear key configuration, (2) grouting material, (3) transverse post-tensioning, and (4) bearing pad details. Experimental tests of shear key connections were conducted. Results from these tests were used to validate finite element models of the shear key region. A grillage analysis of a selected bridge configuration was conducted to determine the maximum live-load effects experienced by the shear key. A parametric study using finite element analysis showed that a full-depth, epoxy-grouted shear key could significantly reduce the likelihood of cracking. Moreover, the amount of post-tensioning and the effect of bearing pad at supports also play an important role in reducing the maximum tensile stress and thus cracking.

17. Key Words Shear key, grout, epoxy, cracking, bearing pad, post-tensioning, box girders		**18. Distribution Statement** No restrictions. This document is available from the National Technical Information Service, Springfield, VA 22161	
19. Security Classif. (of this report)	**20. Security Classif. (of this page)**	**21. No. of Pages** 103	**22. Price**

Form DOT F 1700.7 **(8-72)** **Reproduction of completed page authorized**

This work was sponsored by the Pennsylvania Department of Transportation and the U.S. Department of Transportation, Federal Highway Administration. The contents of this report reflect the views of the authors, who are responsible for the facts and the accuracy of the data presented herein. The contents do not necessarily reflect the official views or policies of either the Federal Highway Administration, U.S. Department of Transportation, or the Commonwealth of Pennsylvania at the time of publication. This report does not constitute a standard, specification, or regulation.

TABLE OF CONTENTS

LIST OF FIGURES

LIST OF TABLES

Executive Summary

This final report incorporates the findings from a research projected developed to evaluate design and construction practices that can reduce the likelihood of cracking of the shear key in PennDOT precast box beam bridges. The research work was supported and funded by the Pennsylvania Department of Transportation (PennDOT). Chapter 1 presents the findings of the literature review. Based on the findings, material characterizations of three grouting materials (cementitious, epoxy, and fiber-reinforced cementitious grouts) were conducted. Experimental tests of shear key connections with these grouting materials were also conducted, and results were used to verify the validity of the numerical analysis. The material characterization and experimental test results are presented in Chapter 2. Chapter 3 includes the details and results of the grillage analysis of a selected bridge configuration, which were incorporated into the finite element analysis. Chapter 4 presents the finite element analysis results of a parametric study on the shear key region. Conclusions and recommendations are summarized in Chapter 5.

The literature review presents a comprehensive state-of-the-practice on the performance of connection details of adjacent precast box beams. It was found that improved shear key design and better construction practices could reduce the likelihood of cracking in shear key. Four main factors are identified to be most influential toward the performance of the shear key: (1) shear key configuration, (2) grouting material, (3) transverse post-tensioning details, and (4) bearing pad details. Based on these findings, the research team and PennDOT decided to further explore these parameters by conducting experimental tests of selected shear key connections as well as an analytical study of the shear key region.

Material characterizations of three grouting materials—cementitious grout, epoxy grout, and fiber-reinforced cementitious grout—were conducted. Obtained properties were incorporated into the finite element analysis conducted later. Experimental tests of shear key connections with these three grouting materials were also conducted. Results indicate that epoxy grout has the highest tensile strength, fracture energy, and bond strength among three materials. These results were also used to validate the finite element models developed in this study. Numerical models developed to predict the behavior of the experimental shear tests of concrete-grout specimens were able to reflect the differences in failure modes observed in epoxy and cementitious grout specimens as well as the experimentally observed crack sequence and patterns, and strength levels.

A grillage analysis was conducted based on a selected adjacent box beam bridge configuration. Maximum moment and shear force in each shear key was determined based on several live-load combinations. Following the grillage analysis, finite element analysis of shear keys incorporating different shear key modifications such as shear key width, location, grouting depth, grouting material, transverse post-tensioning, and bearing pad details were established. It was found that a full-depth shear key tends to develop less tensile stresses compared to a partial-depth shear key under the same loading. Mid-tier shear keys and top-tier shear keys produced similar stress distributions under the same loading. When using epoxy grout, the width of the shear key did not significantly affect the stress distribution in the shear key. The

current transverse post-tensioning details, based on the analysis performed, produced inadequate compressive stress to compensate for the tensile stresses developed by the vehicle loads. Placing bearing pad directly under the shear key resulted in smaller tensile stress developed in the shear key.

In summary, using the current PennDOT shear key practices, a partial-depth shear key with cementitious grout leads to cracking under the full live load considered in this study. A recommended combination of full-depth shear key with epoxy grout is able to reduce the likelihood of cracking in the shear key. In addition, the amount of transverse post-tensioning and the effect of bearing pad at the supports were found to also play an important role in reducing the maximum tensile stresses in the shear key.

Chapter 1. Literature Review and Assessment

1.1. Introduction

The use of bridges built with adjacent precast, prestressed concrete box girders has been favored by several state Departments of Transportation, including the Pennsylvania Department of Transportation (PennDOT), due to the efficiency of their construction and the elimination of deck formwork (Miller et al. 1999). Box beams are typically connected by shear keys with some type of transverse reinforcement (mild or prestressed) and are typically grouted. Although the structural performance of such bridges has been successful, a common problem that has been observed is shear key grout failure at early stages, as shown in Figure 1.1. In many cases this cracking has resulted in water leakage, which could lead to corrosion problems on both the mild and prestressed reinforcement (Lall et al. 1998; Hawkin and Fuentes 2003). The Pennsylvania Department of Transportation is interested in evaluating improved design, construction, and repair practices that have the potential to reduce shear key grout failure in PennDOT's precast box beam bridges.

Figure 1.1 Shear key cracking during construction (Koller 2008)

This chapter presents a comprehensive state-of-the-practice assessment on the performance of connection details of adjacent precast box beams. Relevant information includes design and structural performance, grouting materials and techniques, construction specifications and practices, durability studies, maintenance techniques, and repair solutions. Sources consulted for the development of this report included the following databases: Compendex, Web of Science, Transportation Research Information System (TRIS), Transportation Research Board (TRB), Transportation Research in Progress (TRIP), National Technical Information System (NTIS), American Society of Civil Engineers (ASCE), Precast/Prestressed Concrete Institute (PCI), American Concrete Institute (ACI), as well as state DOT databases. In addition, various state Department of Transportation web sites were surveyed and technical literature on grouting materials was gathered from manufacturers.

This chapter is presented in six sections. The objective and organization of this report is presented in Section 1, Introduction. Section 2 provides background information on several aspects related to the connection details of adjacent precast box beams. Historical background on shear key details is also included in this section. Section 3 presents design issues that can affect the behavior of shear keys: shear key configuration, bearing details, and transverse reinforcement details. Section 4 discusses different types of grouting materials that have been used in shear keys. Section 5 presents a summary of construction practices reported in the literature surveyed. Section 6 presents a summary of the information gathered in this report, highlighting which parameters have been found to initiate cracking in shear keys and which design and construction practices have the potential to reduce shear key grout failure.

1.2. Background Information

Adjacent precast concrete box beams are connected by shear keys. One structural advantage of the adjacent box girder bridge is that it has a very low distribution factor; therefore, each box beam shares a small portion of the total loads induced by vehicles. This results in a shallower bridge, which is more cost efficient and aesthetically appealing. In order for the low distribution factor to accurately represent the behavior of this type of bridge, shear key must fully transfer the load between two adjacent girders (Greuel et al. 2000). Based on the 2008 *AASHTO LRFD Bridge Design Specification* (AASHTO 2008), the shear key component can be designed as either a hinge or a moment transfer connection. AASHTO Article 5.14.4.3 gives some brief guidelines on shear key design: "… Precast longitudinal components may be joined together by a shear key not less than 7.0 inch in depth. For the purpose of analysis, the longitudinal shear transfer joints shall be modeled as hinges. The joint shall be filled with nonshrinking grout with a minimum compressive strength of 5.0 ksi at 24 hours…" There is no specific guideline on the detailing of the shear key in the 2008 *AASHTO LRFD Bridge Design Specification*.

Design of the shear key appears to be left to the regional engineering offices (districts). While the origin for many of the "typical shear key details" currently used by DOT districts is unclear, it is usually based on a combination of AASHTO/PCI general guidelines and local practices. Issues regarding shear key cracking started to gain attention in the 1980s (Nottingham, 1995). Studies were conducted to identify the source of cracking and to identify solutions to this problem (Yamane et al. 1994, Gulyas et al. 1995, Huckelbridge et al. 1995, El-Remaily et al. 1996, and Miller et al. 1999). Different materials and construction practices were also tested in the field and under laboratory conditions (Gulyas et al. 1995, Miller et al. 1999, and Issa et al. 2003). In the early applications of adjacent box beam bridges, a low-strength, cement-based grout was used to grout the joint (Nottingham 1995). In the 1990s, non-shrinkage grout or cast-in-place concrete were commonly used as grouting materials (Gulyas 1995). Currently, epoxy-based grout is also being considered as a grouting material that could improve shear key performance because of its good bond strength to concrete.

A preliminary survey of PennDOT's state of practice indicates that typical shear key connections are designed with a partial depth and that a non-shrink grout is specified (Macioce et al. 2007; PennDOT 2007). The use of epoxy grouts has been successfully implemented by one district

(District 1); however there is no Departmental specification on these materials (such as PennDOT Bulletin 15).

1.3. Design Issues

1.3.1 Shear Key Configurations

There is not a standard shear key configuration used by all state Departments of Transportation. Instead, each state DOT uses a set of "typical shear key details." Typical AASHTO/PCI box beam cross sections, shown in Figure 1.2 (PCI 1997), indicate a shear key located at the top tier of the box girder. Based on the literature surveyed, three configuration parameters may affect the performance of shear keys: geometry, location, and grout depth.

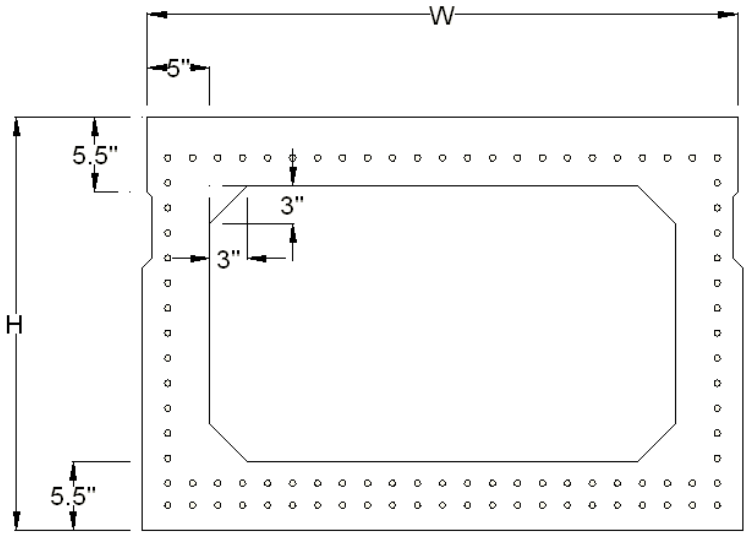

Figure 1.2 Typical AASHTO/PCI standard box beam cross-section (PCI, 1997)

Specific dimensions of the keyway as well as the gap distance between each box beam constitute the geometry of the shear key. The magnitude of the stresses at locations can be affected by variations on these parameters.

Only one study has been found that examines the effect of the geometry of the shear key. Dong et al. (2007) analytically compared the performance of the three types of shear key geometries using the finite element method. Their results indicated that joint A in Figure 1.3 performed better than the other two configurations: at the same load level, joints B and C had stresses at the top portion of the shear key exceeding the tensile strength of the grouting materials, whereas joint A showed principal stresses below that threshold. The analytical models used in this study showed the sensitivity of the shear key geometry on the magnitude of the stresses developed in this region. Different shear key grouting depths were also evaluated; it was found that full-depth shear keys behave better by reducing the number of locations where cracking

could occur. When the same load was applied to the FE models, a full-depth shear key developed lower stress levels compared to a partial-depth shear key.

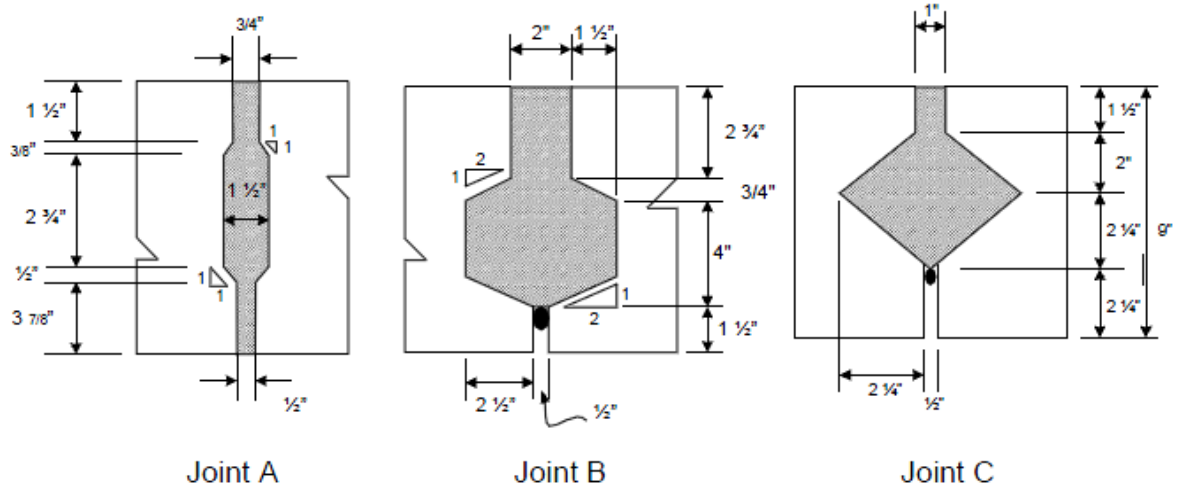

Figure 1.3 Different shear key geometries (Dong et al. 2007)

In a study by Huckelbridge et al. in 1995, the finite element method was used to evaluate the stress state of the shear key when a truck tire rolled over the center of the box beam. He found that under the standard AASHTO HS-25 truck load, the corners of the box beam bent inward toward the centerline of the box beam. The tensile stress associated with the strain eventually led to cracking of the shear key at the top portion. It can be concluded that the vertical location of the shear key has the potential to affect the performance of the system. In order to maintain the load transfer efficiency of the shear key, a mid-depth location between two adjacent box beams is recommended by other researchers (Miller et al. 1999).

Another study conducted by Kim et al. (2008) indicated that mid-depth shear key can control the relative deflection of two adjacent box beams when the bridge is loaded. They found that the top tier and bottom tier shear keys have a relative larger deflection as compared to the mid-depth shear configuration.

Grouting practices significantly affect the structural behavior of shear key. Two types of shear key grouting depth are used: partial depth and full depth. In a partial-depth shear key, the grout only covers a portion of the total height of the box girder. It usually coincides with the size of the shear key when it is located on the top tier of the box girder, as shown Figure 1.4 a). Full-depth shear keys have the entire space between two girders grouted, as shown in Figure 1.4 b).

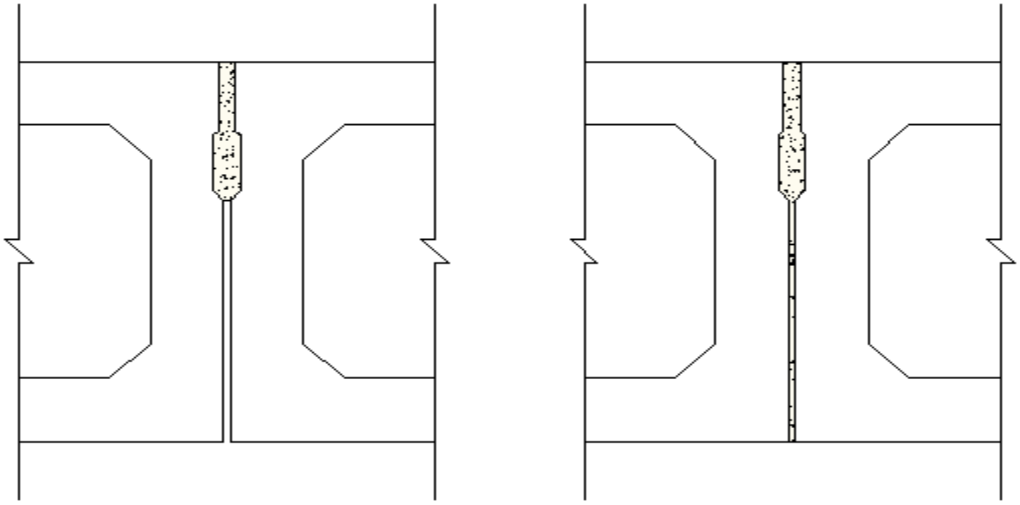

Figure 1.4 a) partial depth shear key b) full depth shear key

A study was conducted by the New York State Department of Transportation in 1996 to evaluate the performance of the full-depth shear key configuration in adjacent box girder bridges (Lall et al., 1998). Inspections were performed to 91 box girder bridges with full-depth shear keys, built after 1992. The results from this study were compared to the results from a previous study conducted on box girder bridges using a partial-depth shear key (Tang 1992). Shear key with longitudinal cracking was found on 21 (23%) of the 91 inspected bridges with full-depth shear key. In contrast, 54% of the bridges with partial depth shear key were found to have longitudinal cracking. Moreover, only 47 out of a total of 874 full-depth shear keys were associated with deck cracking. Therefore, it was concluded that full-depth shear keys significantly reduced shear key cracking. Figure 1.5 shows the categorized frequency of longitudinal deck cracking observed in this study.

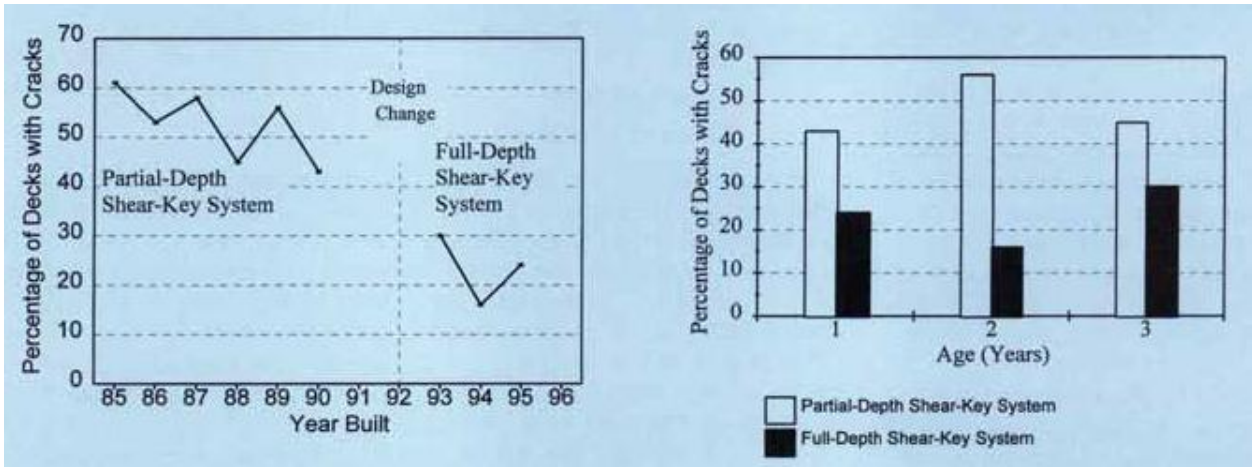

a) b)

Figure 1.5 Frequency of Longitudinal Deck Cracking a) by year built b) by age at time of inspection (Lall et al. 1998)

Based on this literature review, at least two DOTs have used full-depth shear key configurations (Michigan State DOT and New York State DOT). According to the shear key details defined in BC-775M Standard Miscellaneous Prestress Details provided by PennDOT (Figure 1.6), PennDOT uses a partial depth shear key configuration (PennDOT 2007). Several sources found in this literature survey also indicated that the full-depth shear key is a possible solution to the shear key cracking problem (Lall et al. 1998; Badwan and Liang 2007a, 2007b; Dong 2007; Hanna et al. 2007; Scott and Tremblay 2007; Attanayake and Aktan 2008, 2009).

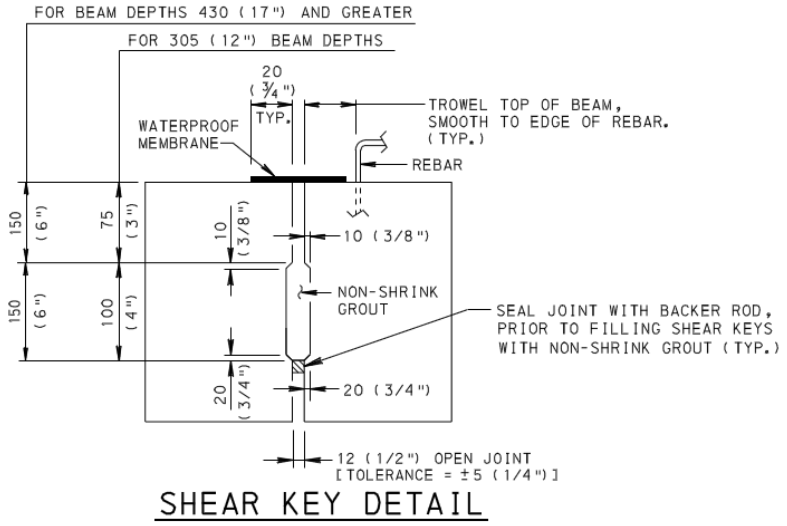

Figure 1.6 PennDOT partial-depth shear key details (PennDOT 2007)

1.3.2 Bearing Details

Bearing pads seem to be another contributor to shear key cracking. Two sources have noted the effects of bearing pad details on the relative deflection between girders. In a reflective cracking history graph provided by William Koller from PennDOT (2008), it is clear that shear key cracking is initiating near the two ends of the box beams and propagating toward the mid span. Miller et al.'s full-scale testing of a box beam bridge (1999) showed a similar crack pattern is observed, as seen in Figure 1.7.

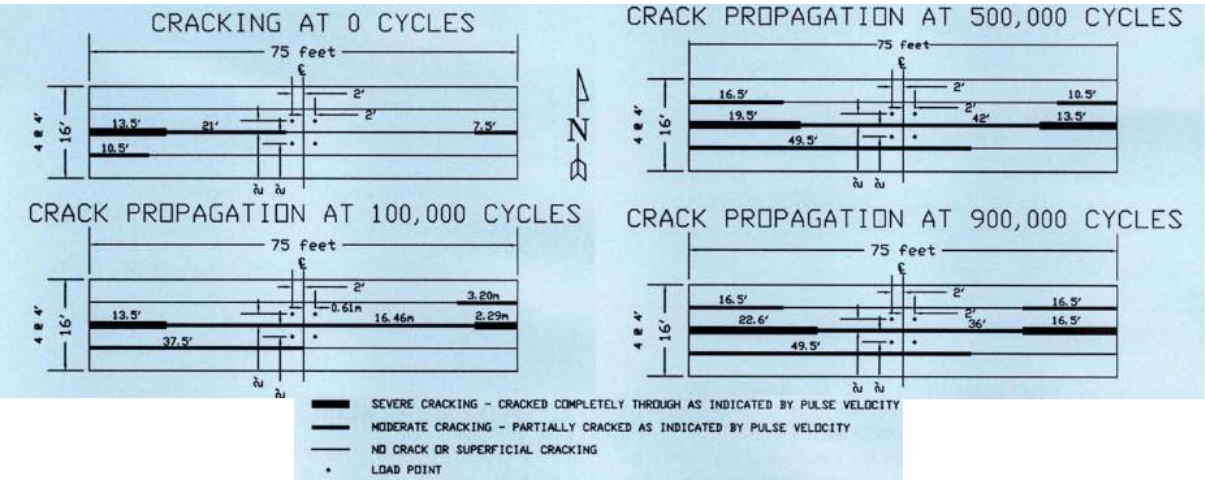

Figure 1.7 Shear key cracking propagation in the full-scale testing (Miller et al. 1999)

The New York State DOT requires the bearing pad to be at least half the width of the box beam. However, at least one study (Lall et al. 1998) has suggested that one half width of box beam is not adequate to provide lateral stability because the box beam can rotate along its longitudinal axis without restriction from such a short bearing pad. Therefore, the study proposed two alternative bearing pad details, as shown in Figure 1.8. The first alternative gives the box beam more restriction to rotate. The second alternative is to reduce the relative deflection between the two adjacent box beams as the bearing pad deforms. More in-depth analysis is necessary to verify the effectiveness of the two alternatives.

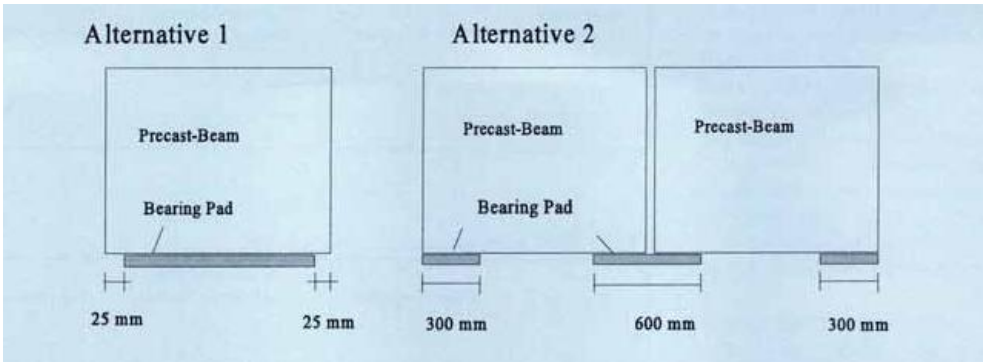

Figure 1.8 Bearing pad alternatives (Lall et al. 1998)

1.3.3 Transverse Reinforcement Details

Concept and Current Practices

Shear key alone cannot fully transfer the loads, between adjacent box beams, induced by moving vehicles. Transverse reinforcement is used to create a normal compressive force in the transverse direction. Adequate design of this type of reinforcement is essential in controlling relative deflections and providing adequate transfer of shear force and moment. Figure 1.9 shows a typical cross-sectional view of a box beam bridge with transverse post-tensioning reinforcement. Typical transverse reinforcement used in precast box bridges consists of

unbonded or bonded post-tensioning tendons/bars and non-prestressed (bonded or unbonded) reinforcement. Based on PennDOT BC-775M Standard Miscellaneous Prestress Details, PennDOT uses unbonded post-tensioning tendons (1/2″ ϕ), with 30 kips of jacking force.

The AASHTO LRFD Bridge Design Specifications (2007) specify that "precast longitudinal components may be joined together by transverse post-tensioning cast-in-place closure joints, a structural overlay, or a combination thereof…These joints are intended to provide full continuity and monolithic behavior of the deck. Article 5.14.4.3.3 requires a transverse prestress of at least 0.25 ksi on a compressive depth of at least 7.0 inches."

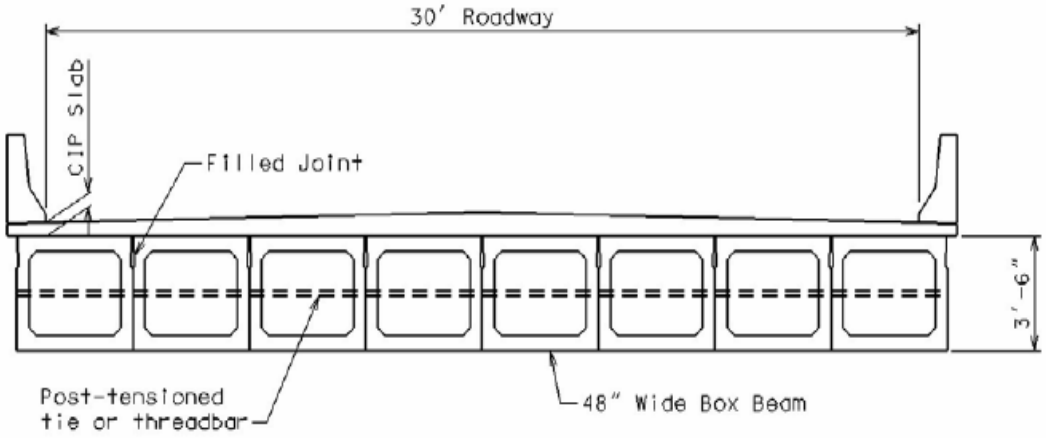

Figure 1.9 Transverse post-tensioning details (Hanna et al. 2007)

Transverse reinforcement details can affect the behavior of the shear key. Depending on the location and effective force induced by the transverse reinforcement, shear keys could behave as a hinge or a moment-transfer connection. Ontario Bridge Design Code assumes a complete transfer of shear force between girders and ignores the flexural rigidity of the shear key. Therefore, this bridge design code requires a structural slab with a minimum thickness of 5.9 inches. Some DOTs design a shear key to carry both shear and flexure. For example, Michigan DOT combines the use of a structural slab, a full-depth shear key and two layers of transverse post-tensioning tendons to develop a moment-resisting connection (Hanna et al. 2007).

A study was conducted in 1994 by Yamane et al. to evaluate the behavior of multi-box beam bridges in Japan. It was found that Japanese bridges typically had heavy transverse post-tensioning reinforcement at different elevations. Also, cast-in-place concrete is used to grout the full-depth shear keys instead of normal grout. In order to pour concrete, the Japanese box girder bridge has a wider (2-in wide minimum) and deeper shear key, allowing the coarse aggregate to disperse uniformly. The concrete mixture used for this grouting application has a much higher strength than the normal grouting material. This study suggested that the use of these design and construction practices reduced shear key cracking significantly. A similar design approach has been taken in South Korea (Kim et al. 2008): heavy transverse post-tensioning, combined with a mid-depth shear key fully filled with cast-in-place concrete; see

Figure 1.10. Detailed analysis and full-scale testing have been performed by Kim et al. (2008) to verify the effectiveness of this practice.

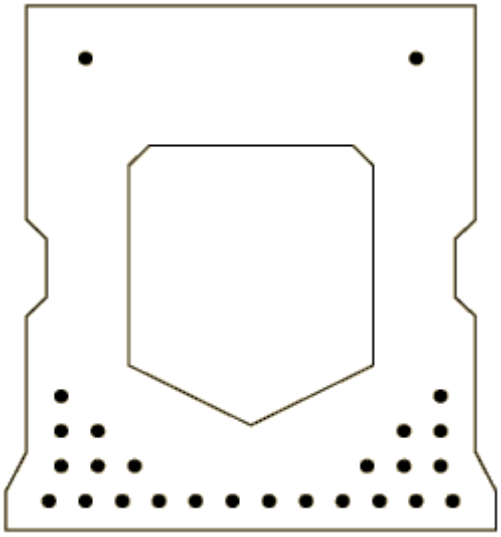

Figure 1.10 Typical Box Beam in South Korea (Kim et al. 2008)

Post-tensioning design and details

Many state DOTs recognize the benefit of transverse post-tensioning and specify large, transverse post-tensioning reinforcement to an adjacent box girder bridge. However, shear key cracking is still being reported. According to a recent study conducted by the Michigan DOT (Attanayake and Aktan 2008, 2009), shear key cracking is caused by inadequate transverse post-tensioning reinforcement. The 2003 PCI Bridge Design Manual requires the post-tensioning force to be "adequate" to limit the differential deflection under 0.02 inches. "The (prescriptive) method assumes those post-tensioned transverse diaphragms are the primary mechanism for the distribution of the wheel loads across the bridge" (Hanna et al. 2007). The diaphragm bonds the box girders into one unit so that relative deflection is minimized. Using grouted full-depth shear keys and post-tensioning tendons can mimic the same diaphragm mechanism. Hanna et al. concluded that more refined models of the bridge and better analysis tools need to be developed to determine the amount of the transverse post-tensioning tendons and their spacing.

Hanna et al. (2007) studied the different factors that are crucial to the calculation of post-tensioned tendon force using grillage analysis: A series of longitudinal beam elements along the center line of box girder is used to represent the girders; transverse beam elements at quarter points of the span are used to represent the transverse reinforcement. Connections between elements are assigned to resist shear, bending, and torsion to represent the full-depth shear key behavior. To prevent possible cracking, the concrete allowable stress limit is set as tension equal to 0 and compression equal to $0.6f'_c$. They identified the bridge width as the most influential parameter in calculating the post-tensioning force. Figure 1.11 shows two charts that relate bridge width to the amount of post-tensioning force required. Figure 1.11a) refers to the

2004 PCI Bridge Design Manual chart with AASHTO HS25 truck for calculating post-tensioning force. Figure 1.11b) is the proposed chart from the grillage analysis. It shows that the required post-tensioning force, based on their analysis, is significantly greater (more than 50%) than what's required by the 2004 PCI Bridge Design Manual.

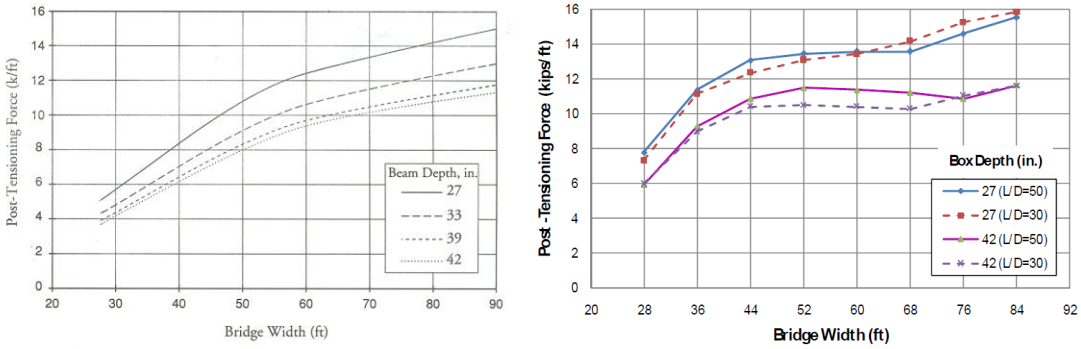

Figure 1.11 a) PCI BDM post-tension force design chart
b) Proposed post-tensioning force design chart (Hanna et al. 2007)

This study also considered the effect of skew angle (Hanna et al. 2007). Figure 1.12 shows the relationship between required post-tensioning force and skew angle. It shows that the differences in the post-tensioning force between different skew angles are small and can be neglected except when shallow girder is used.

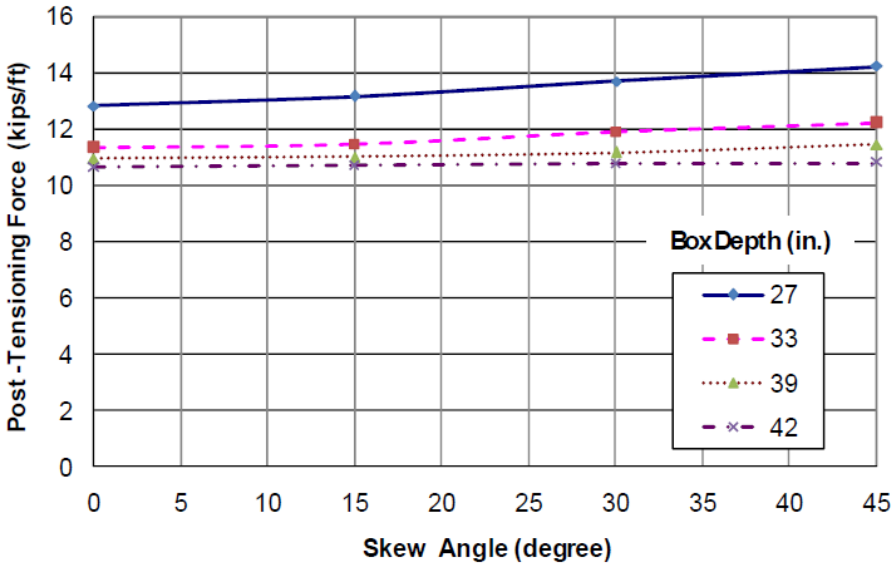

Figure 1.12 Required post-tensioning force vs. skew angle of bridge (Hanna et al. 2007)

Attanayake and Aktan (2008, 2009) also used a grillage analysis to calculate the amount of the transverse post-tensioning required to keep box girders behaving as one unit. They proposed a new modified grillage analysis method to solve the shear key cracking problems. This proposed analytical tool gives a more accurate prediction of the amount of reinforcement required to prevent shear key cracking. Figure 1.13 shows the overall procedure of the analysis tool.

According to the authors, bridges constructed in the State of Michigan State that were designed using this methodology have performed very well and cracking has been reduced significantly.

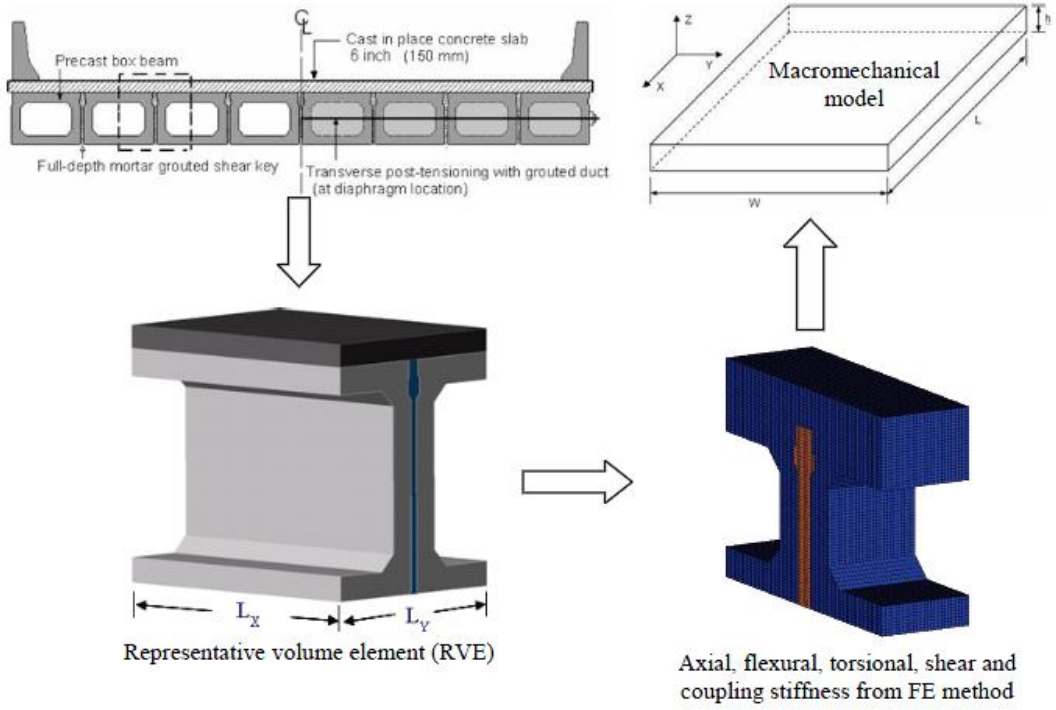

Figure 1.13 Macromodeling of an adjacent box girder bridge superstructure system (Attanayake and Aktan, 2009)

Non-post-tensioned connection details

Even though transverse post-tensioning is an effective practice to reduce the shear key cracking problem, it has disadvantages. For example, it is difficult to conduct post-tensioning on a skewed bridge. Hanna et al. (2007) proposed two non-post-tensioning connection details to prevent cracking of the shear key and eliminate the problems associated with post-tensioning and shear keys in general. The first alternative requires significant changes to the geometry of the box beam; therefore, it will not be shown in this report. The second alternative is shown in Figure 1.14. The specific details of this alternative are still under development at the University of Nebraska-Lincoln.

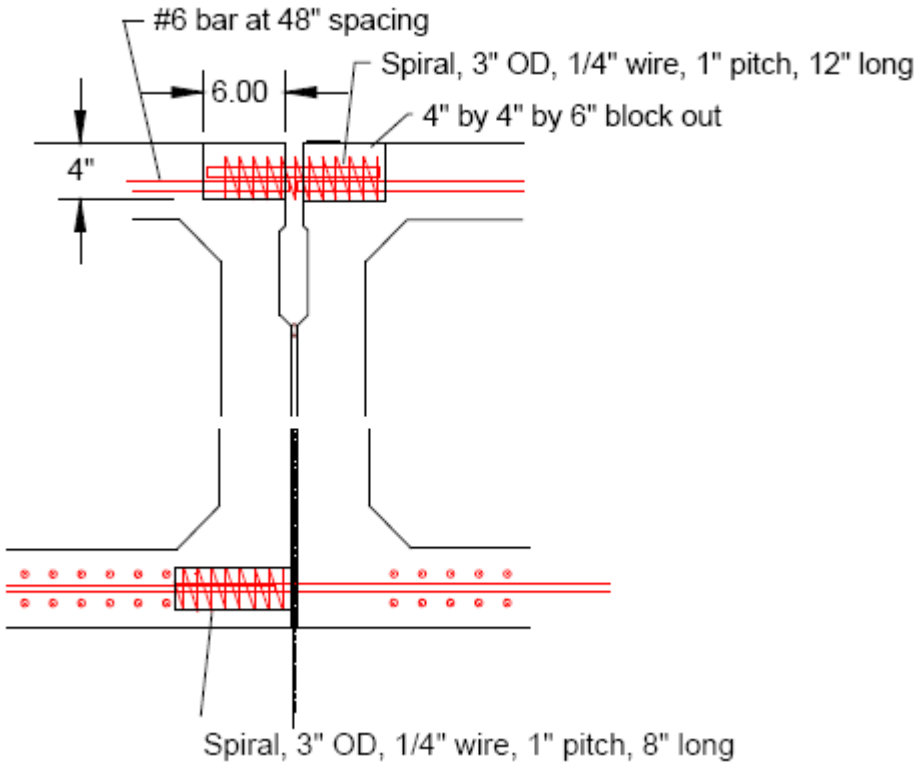

Figure 1.14 Alternative non-post-tensioning details of box beam shear key (Hanna et al. 2007)

1.4. Grouting Materials

Joints between box beams are filled with grouting material to transfer vertical shear and bending stresses induced by moving vehicles. Mechanical properties (e.g., stiffness, ductility, tensile strength, and shrinkage) of grouting materials as well as transverse shortening of concrete box beams may affect longitudinal cracking.

Nottingham (1995) pointed out that a high-quality, low-shrinkage, impermeable, high-bond, high early-strength grout with good workability and low working temperature feature should be used to fill the joint. Gulyas et al. (1995) found that the closest material with these qualities was magnesium ammonium phosphate grout extended with pea gravel (Set 45 Hot Weather). They conducted a follow-up study to compare Set 45 Hot Weather grout and a commonly used non-shrinkage grout. The results showed that the Set 45 Hot Weather developed higher bond strength when compared with the non-shrinkage grout. The composite shear, tensile, and compressive strength of Set 45 Hot Weather were also significantly higher than the conventional non-shrinkage grout. Another study conducted by Ohio DOT also confirmed the performance of Set 45 Hot Weather Grout by conducting full-scale testing of an adjacent box girder bridge. The study also recommended that high bond strength is essential to grout materials. The author suggested the evaluation of epoxy-based grout as a future research objective (Miller et al. 1999). West Virginia DOT in 1996 investigated several bridge failures and topping cracking problems. As a result of this investigation, the West Virginia DOT changed its practice to using workable epoxy as grouting material. Epoxy grout has the advantage in bond

strength as compared to other types of grouting materials. Some construction practices are also recommended by this study (El-Remaily et al. 1996). In a study done by Hlavacs et al. (1997), strain gages were placed inside shear keys to evaluate the effect of temperature at this location. The study found that the magnitude of the thermal strains was greater than those induced by truck loading. A grout material with similar coefficient of thermal expansion to concrete could remediate this problem.

Test methods have been developed to study the effects of grouting materials on the shear key performance in small-scale specimens. Issa et al. (2003) investigated the effect of three different grouting materials. They proposed and tested three composite testing methods for obtaining relevant properties of the shear key grout materials, specifically shear, tensile, and compressive strength. Figure 1.15 shows photographs of the three test methods developed: a) direct shear test, b) direct tensile test, and c) flexural test.

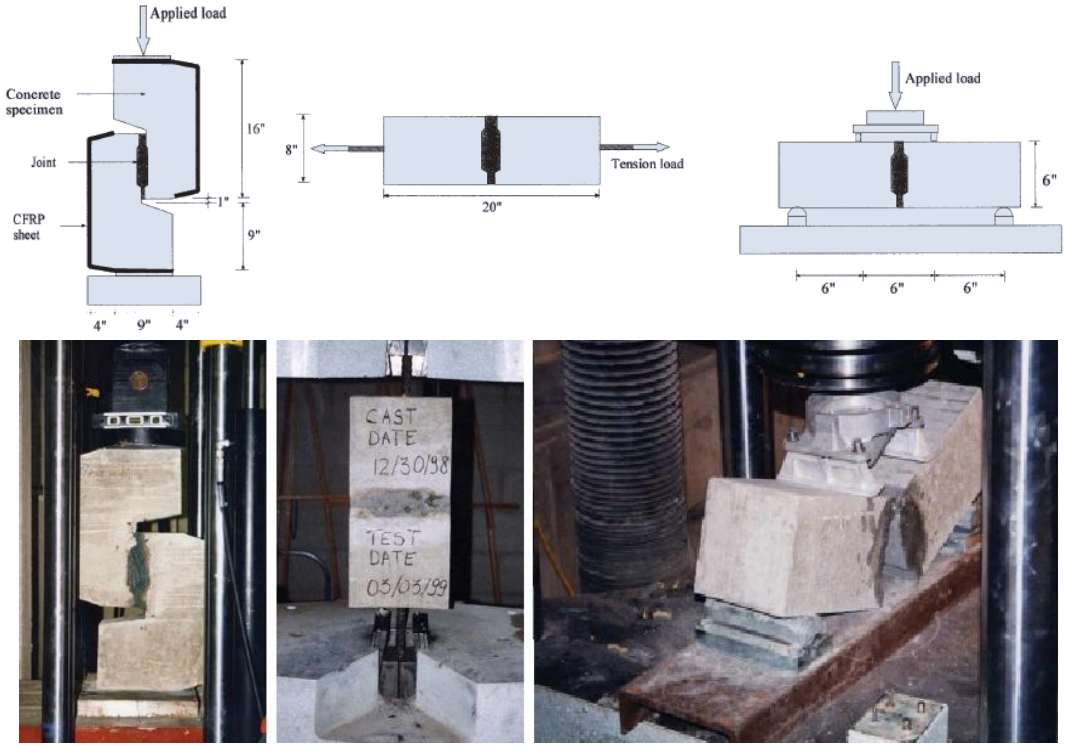

Figure 1.15 Composite testing methods: a) direct shear test b) direct tensile test c) flexural test (Issa et al. 2003)

In the 1990s the most commonly used grout materials by state DOTs were Set 45, Set 45 Hot Weather, and Set Grout. By performing the above tests to three grout materials and polymer concrete, they concluded that the shear, tensile, and compressive strength of the polymer concrete evaluated was the highest among all three grouting materials; see Table 1.1. It also showed the value of shrinkage and permeability among the grout materials. Set Grout performed relatively well compared to the Set 45 series. It was noted that the cracks in the polymer concrete specimen initiated in the concrete box beam away from the joint, an indication that the fracture strength of the polymer concrete was larger than that of the

concrete beam. The finite element method was also used in this study. The material properties of grout, obtained from the experiments, were used in a finite element model of the box beam system to determine the critical stress locations.

Table 1.1 Mechanical properties of grouting materials (after Issa et al. 2003)

Type of Material	Compressive Strength (psi)	Shear Stress (psi)	Tensile Stress (psi)	Flexural Stress (psi)	Permeability
Set 45	5820	301.1 - 354.1	175.9 - 219.0	266.6 - 284.3	very low
Set 45 Hot Weather (Non-shrink Grout)	5658	285.3 - 305.9	198.4 - 214.6	446.5 - 531.4	very low
Set Grout	7700	330.1 - 401.5	197.0 - 246.3	601.4 - 633.9	moderate
Polymer Concrete	10810	667.1 - 748.4	256.0 - 330.1	685.6 - 849.7	negligible

Currently, PennDOT District 1 is experimenting with epoxy-based grout in eight precast box bridges. Their district standard specification for epoxy-based grout has a list of four commercially available products. One of the epoxy-based grouts used in their pilot study is Masterflow 648 CP. Figure 1.16 shows a field application of this grout on a PennDOT bridge in District 1 (Koller 2008). This epoxy-based grout is made of three components: two epoxy resins and aggregates. The advantage of this type of grout material is that it has excellent resistance to creep, high compressive strength (good even at high temperatures), high modulus of elasticity, and excellent resistance to cracking. It also has good adhesion to concrete. Its working time is 50-60 minutes at 32 °C, 90-120 minutes at 21 °C, and 120-150 minutes at 10 °C. The compressive strength of this grout is 14.5 ksi at 40 °C. and its average tensile strength is 2,000 psi.

Figure 1.16 Photograph of the field application of an epoxy-based grout (Koller 2008)

Another material that can be used to grout the shear key is fiber-reinforced concrete. It is apparent that the main cause of cracking is tensile stress. Fibers can be added to grout to control cracks. So far, based on the literature review, there has not been any research done on fiber-reinforced concrete in terms of shear key application. However, it could be a possible solution to this problem.

1.5. Construction Practices

Construction practice is the most important factor in preventing shear keys from cracking. Based on the literature review, the following construction practices are recommended:

1) Use prepackaged grout mix to obtain high-quality joints with more consistency.
2) Sand blast the surface of the shear key to ensure better bonding of grouting material onto the concrete surface of box beams.
3) Use seal block to prevent grout leaking down from the shear key. Figure 1.17 illustrates the potential problems.

Figure 1.17 Grouting material leaking from the joint during the construction (Koller 2008)

4) Use a waterproof membrane between box beams and deck to prevent water leakage into the shear key. However, this seems ineffective based on Koller's own experience (2008). The membrane breaks during its service life. The cause could be relative deflection between box beams.
5) Use wide bearing pads and locate them at the two ends of the box beam to prevent rocking of the box beam. Two adjacent beams may share one bearing pad for deflection compatibility.

1.6. Summary

Although the structural performance of adjacent precast-concrete box beam bridges has been successful, shear key grout failure at early stages could lead to corrosion problems on both the mild and prestressed reinforcement as well as possible reduction of load transfer between adjacent box beams. Based on the findings of the literature survey documented in this report, the following list indicates the most likely sources for shear key cracking:

- Partial grouting depth and top tier shear key location (related to shear key geometry),
- Bearing details that induce relative beam deflection,
- Insufficient transverse post-tensioning reinforcement, and
- Inadequate strength and shrinkage incompatibility of grouting materials.

The following list presents several design and construction practices, among others, that have the potential to reduce shear key cracking:

- Use of a better shear key configuration (for example, a full grouting depth with shear key at midheight),
- Increase of bearing pad width to limit rotation of the box beam and create compatibility between two adjacent box beams,
- Performance-based design of the transverse reinforcement, and
- Use of a grouting material that meets the requirements of strength, compatibility, and impermeability needed for optimum performance of the shear key connection.

Chapter 2. Laboratory Evaluation of Selected Connection Modifications

2.1. Introduction

The Penn State research team conducted a comprehensive state-of-the-practice assessment on the performance of connection details of adjacent precast box beams, described in Chapter 1 of this report. Relevant information included design and structural performance, grouting materials and techniques, construction specifications and practices, durability studies, maintenance techniques, and repair solutions.

Based on the findings from the literature review, several parameters were identified as potential solutions for reducing shear key cracking. PennDOT's technical advisor, in discussion with the Penn State research team, agreed to further exploration of the following alternatives:

1) Shear key configuration: full-depth grouted shear key; geometry and location of the shear key.
2) Grouting material: Fiber-reinforced mortar and epoxy-based grout.
3) Transverse post-tensioning: Post-tensioning reinforcement details (location of tendons; level of prestress force)
4) Bearing pad details

This chapter presents results from the laboratory evaluation of the different grouting materials and selected connection modifications. Analytical results will be presented in the following chapters. This chapter is organized in three main sections. Section 1 presents an introduction. Section 2 describes the mix proportion, preparation, and characterization of the concrete and three different grouting materials. Section 3 describes the results from the experimental test of shear key connections in shear and flexure.

All experiments described in this report were performed at the Civil Infrastructure Testing and Evaluation Laboratory (CITEL) at Penn State.

2.2. Material Characterization

2.2.1. Concrete

The concrete mixture used in this project was a PennDOT-approved, self-consolidated mixture provided by Newcrete Products, a division of New Enterprise Stone & Lime Co. Inc. This concrete mixture is used in the company's Roaring Springs precast plant to cast precast box beams for PennDOT bridges. This type of concrete has shown to have satisfactory workability and relatively high strength comparing with conventional concrete. Specimens for material characterization and shear key connection testing were cast using this mixture. All of the laboratory specimens were fabricated at the Roaring Spring precast plant during production of precast box beams. Figure 2.1 shows photographs of precast box beams during casting at this

facility. Table 2.1 shows the concrete mixture composition (information provided by Newcrete Products). Material characterization was conducted to obtain concrete compressive and tensile strengths over time as well as fracture energy. These tests were conducted at CITEL.

Figure 2.1 Casting of precast box girders using self-consolidation concrete
(Newcrete Products, a division of New Enterprise Stone & Lime Co. Inc., Roaring Springs)

Table 2.1 Mix proportion for self-consolidation concrete used in this project

Material	Type	Specific Gravity	Weight (lb/ft^3)
Cement	3	3.15	23.1
Pozzolan	GGBFS	2.90	7.7
Coarse aggregate	#67	2.82	62.6
Fine aggregate	A	2.79	48.1
Water	-	1.00	8.6
Air entraining admixture	Vinsol Resin	-	1.2 (oz/ ft^3)
Water reducer	High range	-	6.1 (oz/ ft^3)
Viscosity modifying admixture	-	-	0.7 (oz/ ft^3)
Set retarding admixture	-	-	0.3 (oz/ ft^3)

Compressive strength

Concrete compressive strength was determined at 3, 7, and 28 curing days. Tests were performed following ASTM C 39. This test method consists of applying a compressive axial load to molded cylinders (6-in diameter x 12-in height) at a loading rate of 35±7 psi/sec until failure occurs. The compressive strength of the specimen is calculated by dividing the maximum load obtained during the test by the cross-sectional area of the specimen (ASTM C 39, 2005). Figure 2.2 shows photographs of the cylindrical specimen fitted in the testing machine before and after failure. Results from specimens were recorded and averaged (3 specimens per test) to obtain a representative compressive strength at a certain curing day.

(a)

(b)

Figure 2.2 Concrete compression test: (a) Equipment used (b) typical failure mode

The fracture pattern of a typical specimen is shown in Figure 2.2 (b). This failure mode is defined as Type 1 per ASTM C 39, which indicates that the specimen failed in an acceptable manner. Test results are listed in Table 2.2. As expected, the ultimate compressive strength of the concrete used for precast box beams is high. The strength development occurs during the first 3 days. It is designed for the release of strands during precast operations after the first 24 hours. The strength reaches a plateau after 3 days.

Table 2.2 Test results of concrete compressive strength

Curing Day	Specimen 1 (psi)	Specimen 2 (psi)	Specimen 3 (psi)	Average Strength (psi)
3	9535	9324	8818	**9226**
7	10609	10437	10380	**10475**
28	12300	10569	11118	**11329**

Splitting tensile strength

The concrete splitting tensile strength was tested at 28 days in accordance with ASTM C 496. This test method consists of applying a splitting compressive force along the length of a cylindrical concrete specimen (4-in diameter x 8-in height) at a loading rate of 100-200 psi/sec until failure occurs. This loading induces tensile stresses on the plane containing the applied load and relatively high compressive stresses in the area immediately around the applied load. Thin plywood bearing strips (0.25-in width and 8-in length) were used to distribute the load applied along the length of the cylinder. The maximum load sustained by the specimen is divided by a geometric factor to obtain the splitting tensile strength (ASTM C 496, 2004). Figure 2.3 shows the cylindrical specimen with bearing strips fitted in the testing machine. Three

cylinders were used for each test. Results were recorded and then averaged to obtain the ultimate splitting tensile strength.

Figure 2.3 Splitting tensile test of a concrete specimen;
photograph on the right shows typical failure mode

Failure occurred when a crack propagated from the mid place to the support region, as shown in Figure 2.3 (right). Test results are shown in Table 2.3. The ultimate splitting tensile strength of concrete is less than 10% of its compressive strength, which is typical of high-strength concrete mixtures.

Table 2.3 Test results of concrete splitting tensile strength

Specimen No.	Maximum Load (lb)	Splitting Tensile Strength (psi)
1	40250	801
2	36290	722
3	35250	701
Average tensile strength (psi)		**741**

Fracture toughness

The fracture energy of plain concrete was measured by determining its fracture toughness in accordance with a draft ASTM standard proposed by the American Concrete Institute, Technical Committee 446 Fracture Mechanics (ACI 446, 2007). Three beam specimens (6 in x 6 in x 22 in) were cast for this test. The preparation of the beam specimens for testing included creating a notch, grinding of the load bearing areas, and attachment of a clip-on gage to measure and control crack opening. The notch was cut in the middle of the beam. The depth of the notch was 1/3 of the total thickness of the beam (2-in deep). Two steel beams with knife edges were attached on each side of the notch to hold a clip-on gage.

A steel frame with two Linear Variance Displacement Transducers (LVDTs) and two concrete blocks for weight compensation were used; see Figure 2.4. A clip-on gage was attached to the

sides of the bottom notch. A sketch of the specimen and test loading is shown in Figure 2.4. Figure 2.5 shows photographs of the test setup and concrete fracture surfaces.

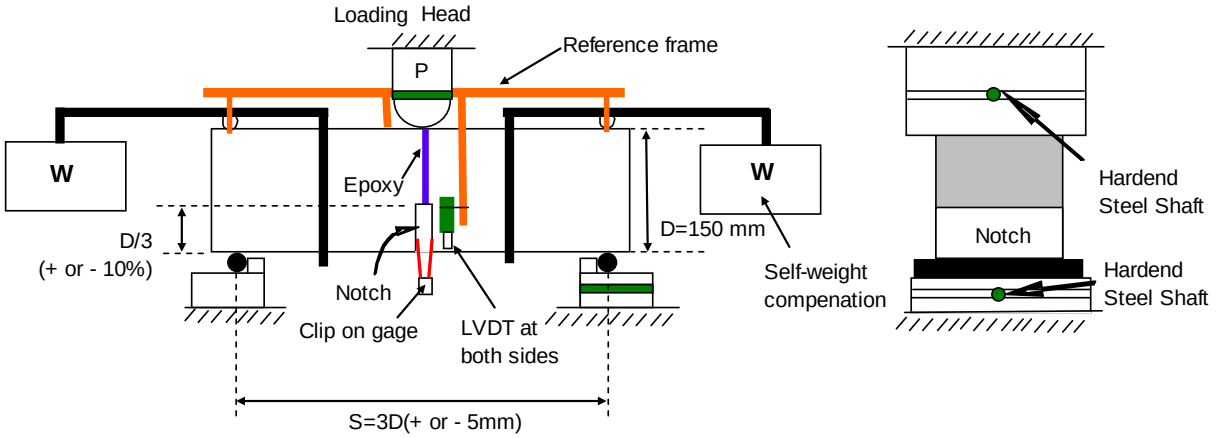

Figure 2.4 Sketch of a loading apparatus

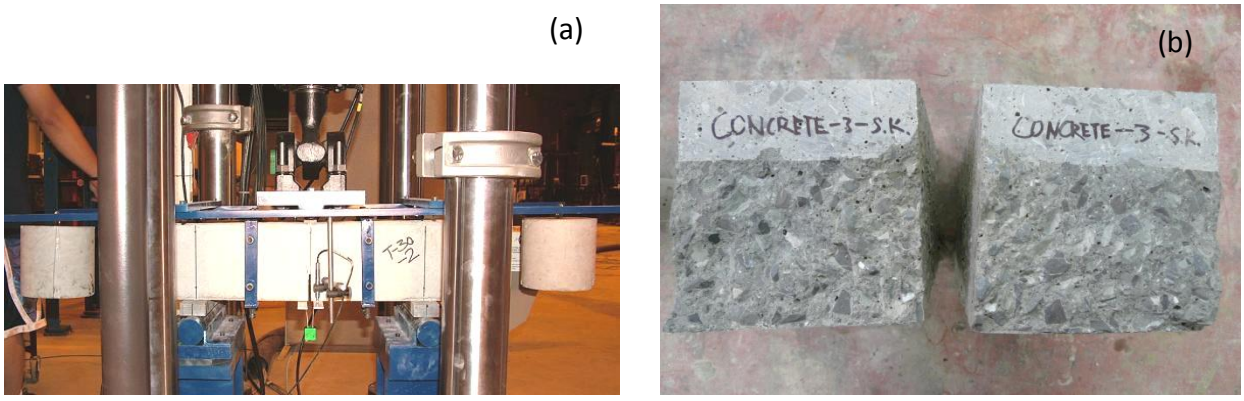

Figure 2.5 Photographs of fracture test: (a) test setup and (b) fractured specimens

The test was conducted after 21 days of casting using crack mouth opening displacement (CMOD) control with a loading rate of 0.01 mm/minute. The peak load was reached in 3-5 minutes. During the test, measurements of load, deformation, and crack opening were recorded. Failure occurred by a crack initiated at the notch and propagated upward very slowly until it reached the top surface. Figure 2.5 (b) shows the fracture surfaces of a typical failed specimen after the test. Load-CMOD curves for the three tested specimens are shown in Figure 2.6. For each specimen, the measured work of fracture was computed as the area enclosed between the positive part of the curve and the x-axis. More detailed information about how to calculate the fracture toughness based on the experimental data can be found in the draft ASTM Test Standard “Fracture Toughness Testing of Concrete” reported by ACI Committee 446 (2007). The mean fracture energy was then determined as the average of the fracture energy of individual specimens. The results are shown in Table 2.4.

Table 2.4 Concrete Fracture Toughness

Specimen	Fracture Energy (N/m)
1	169
2	148
3	157
Average (N/m)	**158**

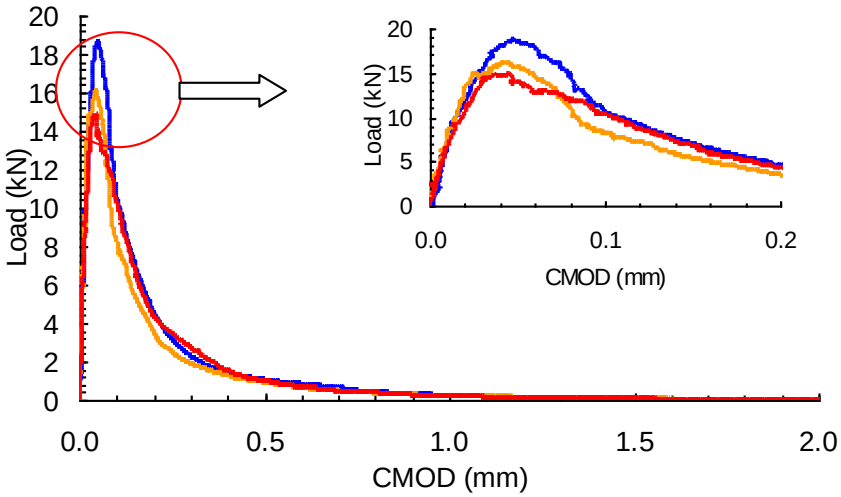

Figure 2.6 Load-CMOD curves of plain concrete (three specimens tested)

2.2.2 Grouting Materials

Two types of grouting materials were evaluated: an epoxy grout (commercial name: FIVE STAR DP Epoxy Grout) and a cementitious (cement-based) grout. The two grout products were selected based on their suitability to be used as grout for the shear key region of adjacent boxes beams. The cementitious grout was selected from a list of PennDOT-approved grouts (PennDOT Bulletin 15, 2004). Initially, a FIVE STAR cementitious grout (commercial name: FIVE STAR GROUT) was used; however, material characterization results indicated strengths well below the reported data by the manufacturer, see Table 2.5. The company was notified of this situation and agreed to repeat these tests at its laboratories. In the meantime, it was decided that a different type of cementitious grout would be used (commercial name: BASF Masterflow 713).

Table 2.5 Results of Compressive strengths of FIVE STAR GROUT

Curing Day	Reported data by the manufacturer (psi)	Results of the first batch obtained at CITEL (psi)	Results of the second batch obtained at CITEL (psi)
3	3500	1500	1462
7	5000	1880	1575
28	6500	1881	1705

FIVE STAR DP Epoxy Grout is a three-component system consisting of resin (component A), hardener (component B), and aggregate. As recommended by the manufacturer, a mix proportion of 3.78 lb of component A + 1.14 lb of component B + 45 lb of aggregate was used to obtain 0.4 ft^3 of grout for the epoxy specimens. Masterflow 713 is a cement-based grout with specially graded mineral aggregates. To achieve an appropriate workability, 55 lb of grout material was mixed with 11.25 lb of water to obtain 0.52 $ft^3$of grout for the cement specimens. Compressive strength, splitting tensile strength, flexural strength, modulus of elasticity, linear shrinkage, and coefficient of thermal expansion were evaluated for each grouting material. In addition, properties of a fiber-reinforced cement mixture were also investigated. BASF Masterflow 713 mixture was combined with an enhanced fibrillated polypropylene fiber (MasterFiber F100, also manufactured by BASF). The fiber dosage was 2.7 g/1 kg of cement material, which corresponds to a volume fraction of 0.5%. Material properties were determined at the same age of testing of the shear key specimens.

Compressive strength

Concrete compressive strength of the epoxy and cementitious grouts was determined at 3, 7, and 28 curing days. Tests were performed following ASTM C 579 Test C. Cylindrical specimens (2-in diameter and 4-in height) were cast for this test. Six specimens were used for each test. The compressive strength was determined by averaging the results of six specimens. The testing procedure was the same as that for the compressive strength test of concrete described previously, except with a different loading rate (50-100 psi/sec).

Results for both cementitious grout and epoxy grout are listed in Table 2.6. The numbers in parentheses are provided by the manufacturer in the product specifications. Results are very consistent with these expected values. The change of the compressive strength over curing time is plotted in Figure 2.7. It can be seen that epoxy grout has much higher compressive strength than cementitious grout. The compressive strength of epoxy doesn't change value after 3 days, which suggests that the epoxy is cured by the third day. In comparison, the slower curing process of the cement is reflected in the changes of compressive strength of the cementitious grout over time.

The compressive strength of fiber-reinforced cementitious grout was determined on the 7^{th} curing day. Its average compressive strength is 4,606 psi, which is slightly higher than the compressive strength of cementitious grout on the same curing day. It was observed that when the specimen failed in compression, fiber bridging prevented a total splitting failure, as was observed with the cementitious and epoxy grouts. The specimen after the failure is shown in Figure 2.8.

Table 2.6 Grouting materials compressive strengths

Curing Day	Epoxy Grout (psi)	Cementitious Grout (psi)
3	10089 (9000)	3701 (3200)
7	10036	4474 (4500) 4606*
28	10072	5,47 (7000)

*grout with fibers

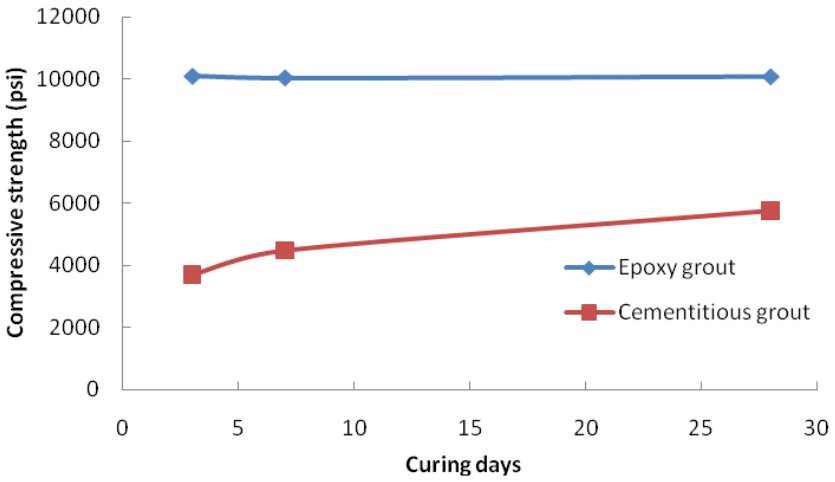

Figure 2.7 Compressive strength of grouting materials over curing time

Figure 2.8 Fiber-reinforced cementitious grout after compression failure

Splitting tensile strength

The splitting tensile strengths of epoxy and cementitious grouts were tested at 3, 7, and 28 curing days by following ASTM C 496. Cylindrical specimens (2-in diameter and 4-in height) were cast for this test. Six specimens were used for each test. The splitting tensile strength was determined by averaging the results of the six specimens. The test procedure was the same as that for the splitting tensile test of concrete described in the previous section.

The failure mode of both grout materials was splitting tension, as shown in Figure 2.9. The specimen was split into two half parts along the bearing strips. Localized cracks were also found in the region near the bearing strips. Test results are summarized in Table 2.7. It can be found that the tensile strength of epoxy grout is much higher than that of cementitious grout. Although the compressive strength of cementitious grout increases over the curing time, no such increase was found for the splitting tensile strength.

The tensile strength of fiber-reinforced cementitious grout was also determined on the 7th curing day. Its average tensile strength was 601 psi. Compared with the tensile strength of cementitious grout without fiber, the addition of fiber increases the tensile strength by 15%. It

was observed that fibers bridged the main crack, preventing a split failure of the specimen (shown in Figure 2.9c), as opposed to the failure mode exhibited by the non-fiber grout specimens.

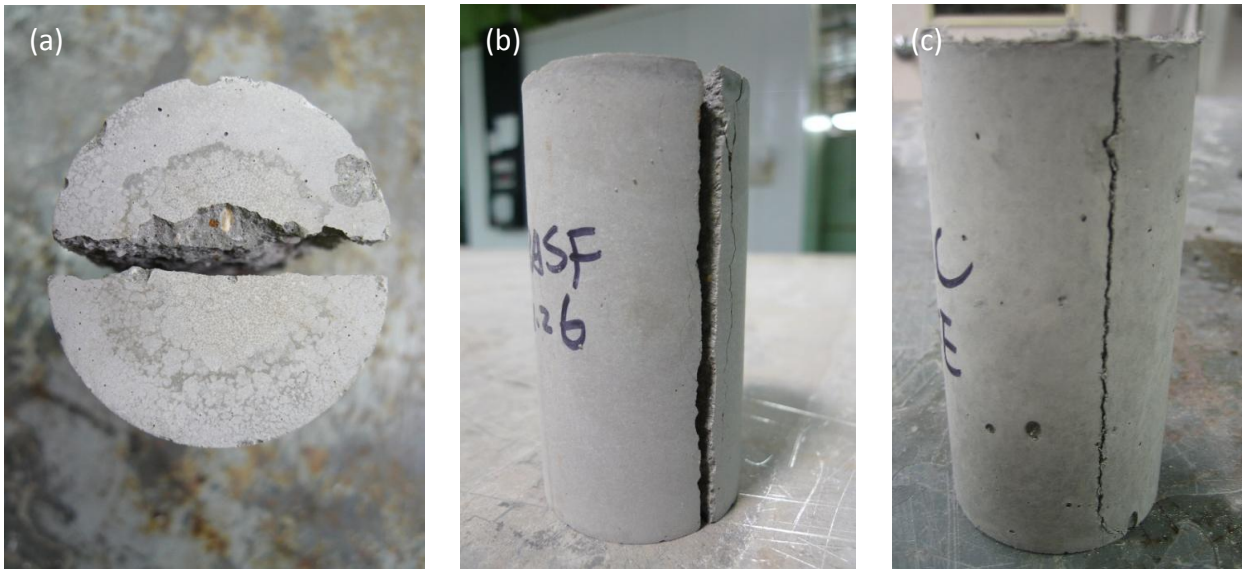

Figure 2.9 Cementitious grout specimen after the splitting tensile test: (a) top view of the specimen, (b) side view of the specimen, (c) side view of the specimen with fibers

Table 2.7 Results for splitting tensile strength test of grouting materials

Curing Day	Epoxy Grout (psi)	Cementitious Grout (psi)
3	1377	509
7	1325	522
28	1397	583

Flexural strength

Flexural strengths of epoxy and cementitious grout were tested at 3, 7, and 28 curing days in accordance with ASTM C 580 Method A. Six bar specimens were made for each test. The dimensions of the bar specimen were 1-by-1-in area x 12-in length. The specimen geometry was measured, before testing, to the nearest 0.001 in using a micrometer. Specimens were tested in 3-point bending with the load being applied by means of a loading nose midway between the supports (ASTM C 580, 2008). The span length between the two supports was 8 in. A sketch and photograph of the flexural test setup is shown in Figure 2.10. The load was applied to the specimen at the head speed of 0.107 in/min. Load-deflection data were recorded. The flexural strength was calculated from the maximum load. Results are presented in Table 2.8. The manufacturer's expected strength at 3 days is presented in parenthesis. It can be observed that similar to other mechanical properties, the epoxy grout has a higher flexural strength than the cementitious grout. Figure 2.11 shows a photograph of the fracture surfaces of the cementitious grout (left) and the epoxy grout (right).

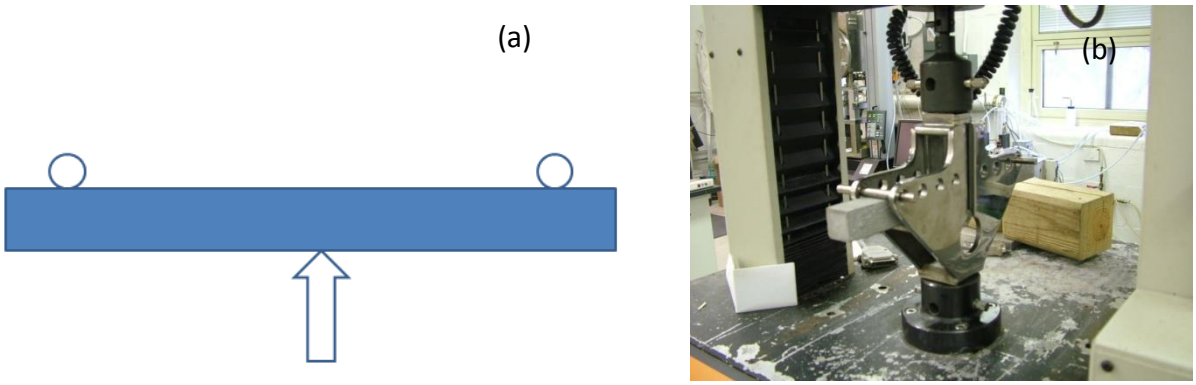

Figure 2.10 Flexure test: (a) sketch of the test set-up, (b) photograph of testing equipment


Figure 2.11 Fracture surfaces of the cementitious grout (left) and the epoxy grout (right)

Table 2.8 Result for flexural strength test of grouting materials

Curing Day	Epoxy Grout (psi)	Cementitious Grout (psi)
3	4197 (4000)	704
7	4407	1122 [1141*]
28	5599	1046

* grout with fibers

The flexural strength of the fiber-reinforced cementitious grout was determined on the 7th curing day. This result is also presented in Table 2.8 (1,141 psi). Figure 2.12 shows a photograph of the fiber-reinforced specimen after the testing. It can be observed that a large amount of micro fibers are bridging the main crack. Figure 2.13 shows the load versus machine displacement response of a typical fiber-reinforced cementitious grout in flexure. The

appearance of the second peak indicates that the fibers could provide some residual strength to the beam specimen after the peak flexural capacity is reached.

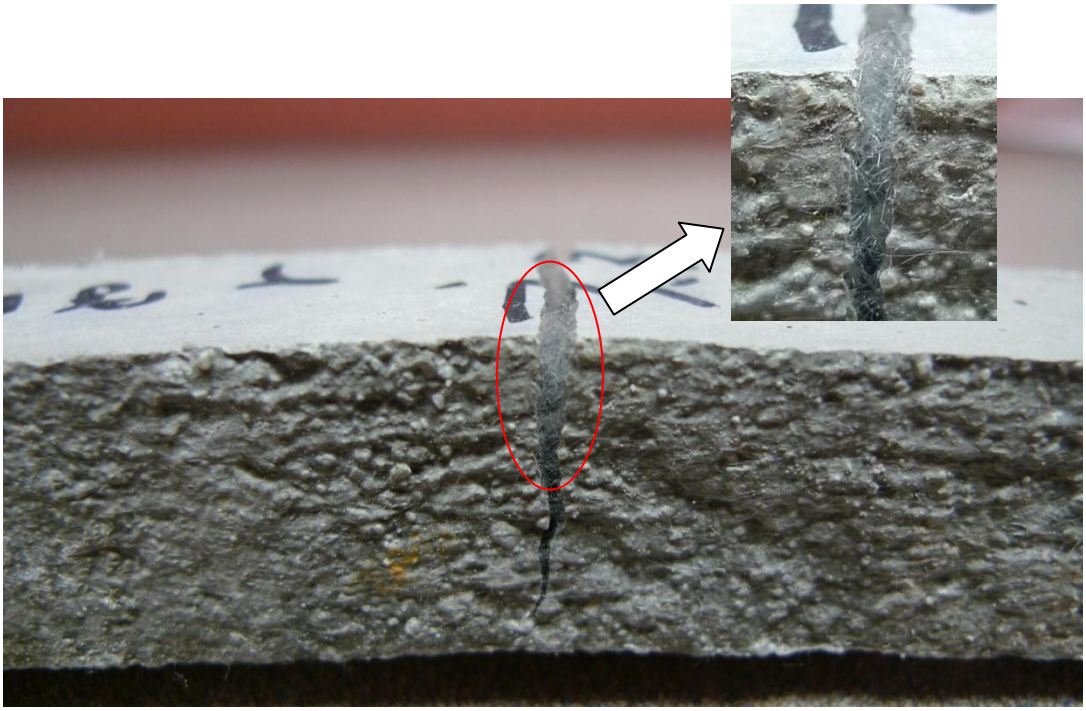

Figure 2.12 A flexural crack in a fiber-reinforced grout specimen

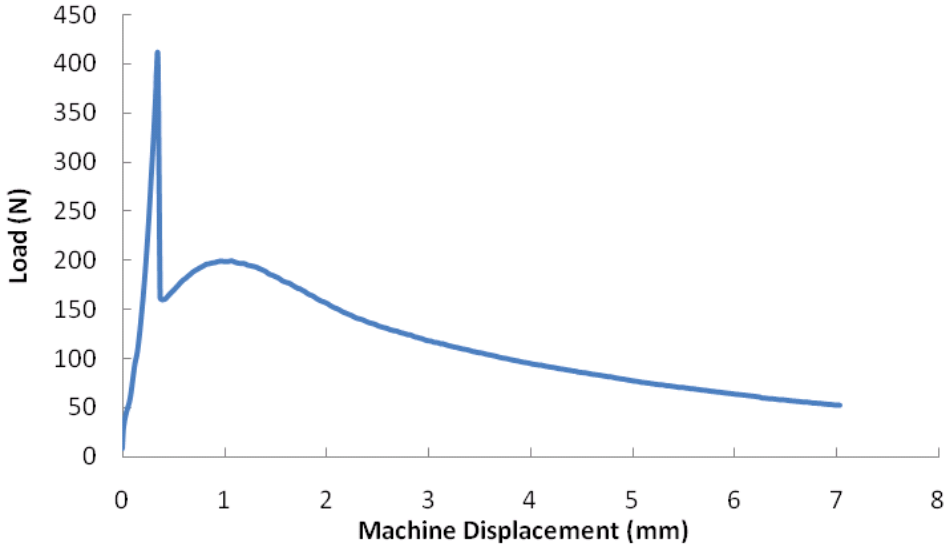

Figure 2.13 Load-machine displacement curve for a fiber-reinforced cementitious grout specimen

Modulus of elasticity

Moduli of elasticity for both grouting materials were determined by the further analysis on the load-machine displacement curve obtained from the flexural strength test. An example of the load-machine displacement curve for an epoxy grout specimen is shown in Figure 2.14. A tangent line (the red line in Figure 2.14) was drawn in the initial portion of the load-deflection curve to derive the modulus of elasticity (ASTM C 580, 2008).

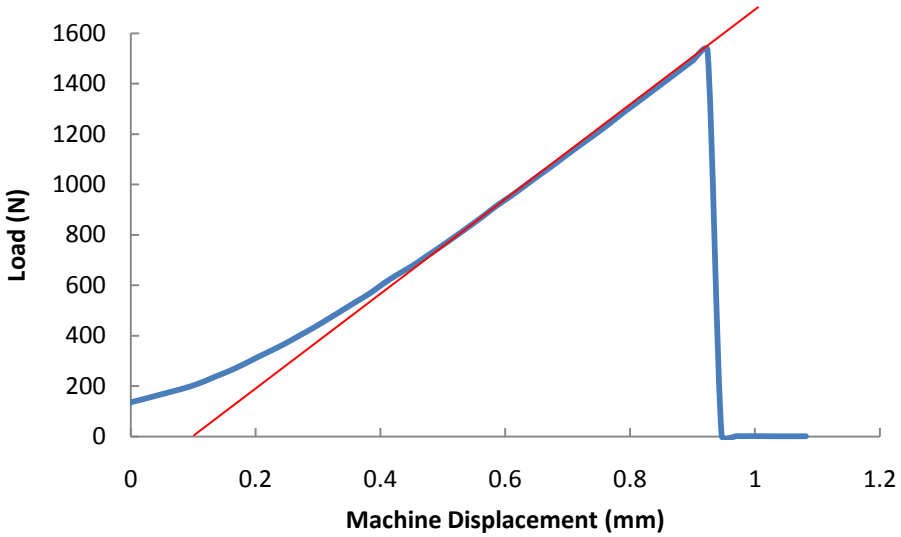

Figure 2.14 Load-machine displacement curve for an epoxy grout specimen at 3 curing days

The moduli of elasticity for both epoxy and cementitious grout are shown in Table 2.9. It is evident that the epoxy grout's higher modulus of elasticity than cementitious grout is a reflection of how small deformations can be expected from this material. Both grouting materials exhibit moduli that increase over time. The modulus of elasticity of the fiber-reinforced cementitious grout on the 7th curing day was determined as 1.12E+6 psi, which suggests that the addition of the fibers in the cementitious grout increases its stiffness.

Table 2.9 Modulus of elasticity of grouting materials

Curing Day	Epoxy Grout (psi)	Cementitious Grout (psi)
3	1.35E+6	5.71E+5
7	1.46E+6	8.37E+5 [*1.12E+6]
28	1.74E+6	8.28E+5

* grout with fibers

Linear shrinkage

The linear shrinkage of the epoxy and cementitious grout during setting was measured in accordance with ASTM C 531. Beam specimens (1-by-1-in square area and 12-in length) with two measuring studs in each end were cast for this test. Figure 2.15 shows photographs of specimens from both grouting materials as well as the test setup used. After demolding, the initial length of the bar was determined by inserting it in the length comparator (as shown in the right photograph). After 3 and 7 days of curing (moisture curing for cementitious grout and dry curing for epoxy grout), the length of the bar was measured again and recorded respectively. The linear shrinkage was calculated as follows:

$$\text{Percent shrinkage} = [(L_0\text{-}L)/L_0] \times 100$$

where:

L_0 = original length, in, and

L = length as measured at a certain curing day, in.

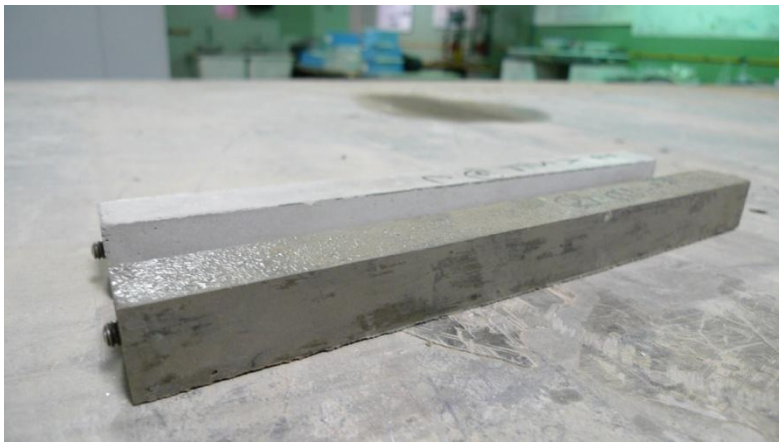

Figure 2.15 Photographs of the test setup and specimens used to determine linear shrinkage

Results are presented in Table 2.10. A positive (+) sign is used to indicate that a material expands, a negative sign (-) to indicate contraction. It was found that the cementitious grout expanded while the epoxy grout shrank. The fiber-reinforced cementitious grout expanded less than the cementitious grout without fibers. This is because the fibers added into the grout do not expand during the hydration of cement.

Table 2.10 Result summary of the linear shrinkage for grouting materials

Curing Day	Epoxy Grout (%)	Cementitious Grout (%)	Fiber-reinforced Cementitious Grout (%)
3	-1.33E-3	+5E-4	+2.1E-4
7	-5.33E-3	+2.4E-4	+2.5E-4

Coefficient of thermal expansion

Coefficients of thermal expansion for grouting materials were determined by following ASTM C 531. The specimens were the same ones previously used for the shrinkage determination (see Figure 2.12). The length of each bar at 20 °C was measured with the length comparator. Then the bars were placed in an oven heated to 100 °C. After 1 day, the bars were quickly removed from the oven and measured with the length comparator. After cooling to 20 °C, the specimens were checked again to determine if they returned to their original lengths. If not, the above procedure was repeated. The coefficient of thermal expansion was calculated as follows:

$$C = (Z - Y - W)/T(W - X)$$

where:
Z = length of bar, including studs, at elevated temperature, mm,
Y = length of stud expansion, mm,
W = length of bar, including studs, at lower temperature, mm,
T = temperature change, °C,
X = length of the two studs at lower temperature, mm.

The results of coefficient of thermal expansion are shown in Table 2.11. Manufacturer's reported data for the epoxy grout are presented in parenthesis. It can be observed that the coefficient of thermal expansion of the epoxy grout is larger than that of the cementitious grout, which indicates that the epoxy grout would have a larger expansion than the cementitious grout at the same temperature increment. When fibers are added, the coefficient of thermal expansion becomes even smaller, which may be attributed to the higher thermal resistance of the fiber to thermal expansion.

Table 2.11 Results of coefficient of thermal expansion for grouting materials ((mm/mm)/°C)

Grouting Material	Average Value	Specimen 1	Specimen 2	Specimen 3	Specimen 4
Epoxy grout	2.92E-05 (3.2E-5)	2.93E-05	2.92E-05	2.86E-05	2.98E-05
Cementitious grout	6.0E-06	6.06E-06	5.57E-06	6.35E-06	6.01E-06
Fiber-reinforced cementitious grout	2.19E-06	2.74E-06	1.87E-06	1.95E-06	2.21E-06

2.2.3 Concrete-grout Interface

Bond strength between grout and concrete

The bond strength between epoxy and concrete was tested in accordance with ASTM C 882. The bond strength was determined by using epoxy grout to bond together two slanted sections of 4-in-by-8-in concrete cylinder. Each section was cut from the concrete cylinder at a 30-degree angle from a vertical axis (ASTM C 882, 2005). Figure 2.16 shows photographs of the bond specimen and typical failure mode. After 28 days of curing, the bonded specimens were tested in compression. Capping was done in accordance with ASTM C 39. Six specimens were prepared and tested to obtain the bond strength. The peak load was recorded for each test. Specimens failed near the concrete side of the interface between epoxy and concrete, which is

attributed to epoxy grout's higher strength. Bond strength was calculated by dividing the load carried by the specimen at failure by the bonded surface area (25.13 in^2). The average bond strength between epoxy grout and concrete is 5,019 psi.

Figure 2.16 Photograph of typical concrete-epoxy bond strength specimen and fracture surface

Splitting tensile strength of the concrete-grout interface

The splitting tensile strength of concrete-grout interface was determined by using the same cylindrical specimens for plain concrete (see section 2.1.2). Concrete cylinders at least 28 days old were cut in half along their longitudinal axis using a wet diamond saw. The cut surfaces were prepared using sandblasting to remove loose material and to expose the concrete aggregates. After specimen preparation, each specimen's halves were bonded back using grouting material (epoxy or cement-based). Following curing of the grouting material, the specimen's edges were ground in order to avoid uneven application of the load during testing. The testing of specimens was conducted by following ASTM C 496 with a loading rate of 50 psi/sec. More detailed information about this test can be found in Coronado and Lopez (2008).

The splitting tensile strengths of three grouting material interfaces are listed in Table 2.12. It was found that the splitting tensile strength of the concrete-epoxy grout interface is the highest among all three grouting material interfaces, which in turn is very close to the splitting tensile strength of plain concrete. Fiber-reinforced cementitious grout (FRC grout) has a higher interfacial splitting tensile strength than cementitious grout. During testing, two types of cracks were observed. For the epoxy grout specimen, the main crack occurred within the concrete as shown in Figure 2.17a. For the cement and FRC specimens, the crack was found to propagate along the concrete-grout "true" interface as shown in Figure 2.17b.

Table 2.12 Interfacial splitting tensile strength results

Grouting Material	Epoxy Grout	Cementitious Grout	FRC Grout
Splitting tensile strength (psi)	732	100	331

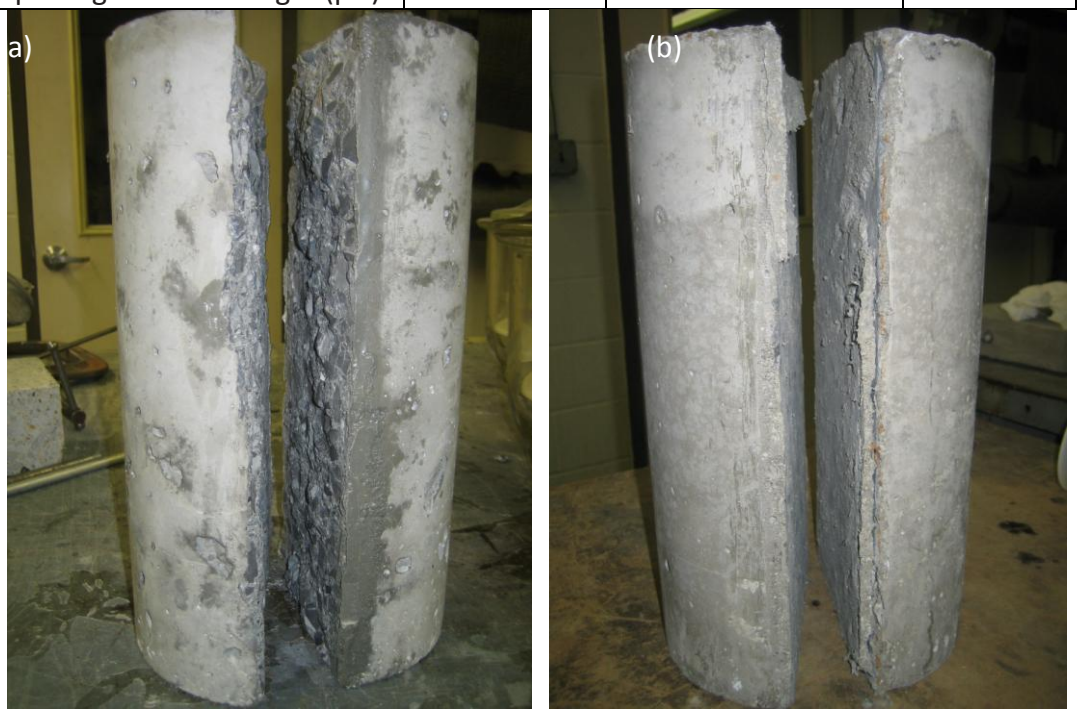

Figure 2.17 Failure mode of the splitting tensile test for (a) concrete-epoxy grout specimen (b) concrete-cementitious grout specimen

Fracture toughness of the concrete- grout interface

The fracture toughness of the concrete-grout interface was characterized by using the same specimen geometry for plain concrete (see section 2.1.3). A concrete beam was cut in half using a wet saw and glued back together using epoxy grout. A notch was created (2-in deep), as shown in Figure 2.18. The test was conducted using a CMOD control (rate of 0.01 mm/min). For the two concrete-epoxy specimens tested, it was observed that the crack propagated along the interface, which indicates that the interface has a smaller (weak) fracture energy than the plain concrete. Fracture surfaces of the epoxy-bonded specimen are shown in Figure 2.18.

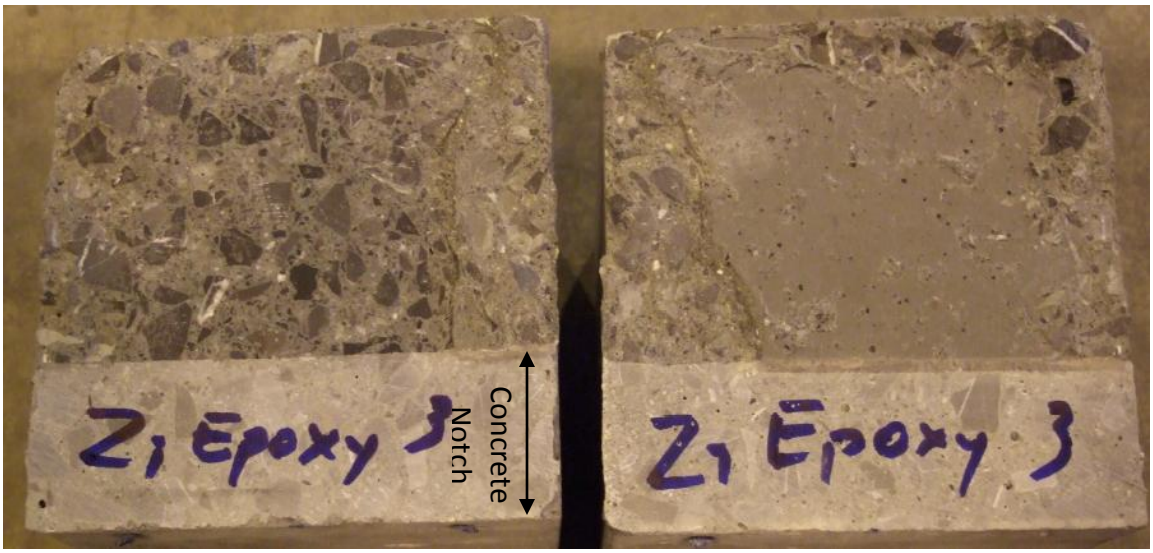

Figure 2.18 Fracture surfaces of the epoxy bonded specimen

Figure 2.19 shows a comparison of the load-CMOD curves for plain concrete, concrete-epoxy, concrete-cementitious grout, and concrete-FRC grout interfaces. The fracture energy of concrete-epoxy grout interface was calculated to have an average value of 116.5 N/m, which is 26% less than the fracture energy of the plain concrete obtained previously. The specimens used to characterize the concrete-cement-based interface (one specimen was tested per interface) had even smaller fracture energies. The fracture energy of the concrete-cementitious grout interface was calculated to be 8.9 N/m, and the fracture energy of concrete-FRC grout was determined to be 49.3 N/m. Table 2.13 presents these fracture energy values. It can be found that the addition of fiber appears to enhance the bond strength of the interface, leading to an increase of fracture energy. A larger experimental database is needed to confirm this finding. However, it must be pointed out that the fracture energy for both concrete-cementitious and FRC grout are significantly smaller (on the order of 8% and 42%, respectively) than the fracture energy of epoxy-concrete interface.

Table 2.13 Fracture energy results of concrete-grout interface specimens

Interface	Concrete-Epoxy Grout	Concrete-Cementitious Grout	Concrete-FRC Grout
Fracture energy (N/m)	116.5	8.9	49.3

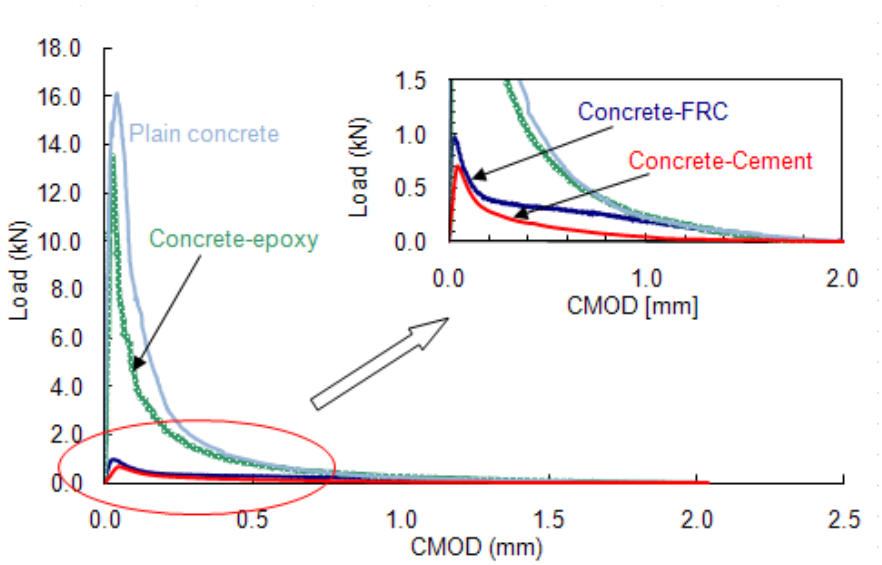

Figure 2.19 Load-CMOD curves for plain concrete and concrete-grout interfaces

2.3. Experimental Tests of Shear Key Connections

2.3.1 Overview

According to the approved laboratory test plan, small-scale shear key connections were experimentally tested in order to: (1) compare the effectiveness of three different grouting materials: epoxy grout, cementitious grout, and fiber-reinforced cementitious grout; and (2) verify the validity of the finite element models developed in this project. Two types of tests were conducted: a shear test and a flexural test. It is expected that the shear test provides a good representation of the load-transfer mechanism of the shear key between two adjacent box beams. One flexure test was also conducted with the strongest grouting material to assess the behavior of this connection under possible flexure loading. This report presents results from these experimental tests. Numerical analyses of these shear key connections as well as a box-beam bridge, using grillage analysis and finite element analysis, will be presented in the following chapters.

2.3.2 Specimen Fabrication

As indicated in Section 2.2, shear key specimens and material characterization specimens were cast at the Newcrete Precast Concrete Plant in Roaring Springs, Pennsylvania. The concrete mixture used was described previously. The current standard PennDOT-approved shear key geometry was used for the design of the shear key specimens (PennDOT, 2007), see Figure 2.20.

Each set of shear key specimens was made of two halves, as shown in Figure 2.20. Each half geometry was a 17-in-deep, 8-in-wide, and approximately 5-in-long, rectangular concrete block

with one face containing the shear key geometry. A layer of steel mesh reinforcement (W4xW4) was used inside the concrete block to prevent cracking during construction. The two halves of the shear key specimen were bound together at a later time using the different grouting materials. Newcrete fabricated the molds for these specimens, using the same materials for its standard precast box beams. Specimens were cast along with other precast box beams during regular operating hours. After casting, the shear key faces were sandblasted at the precast plant. Surface preparation was found to significantly affect the bonding between the grouting materials and the concrete box beam surfaces (see Section 2.3.4.4).

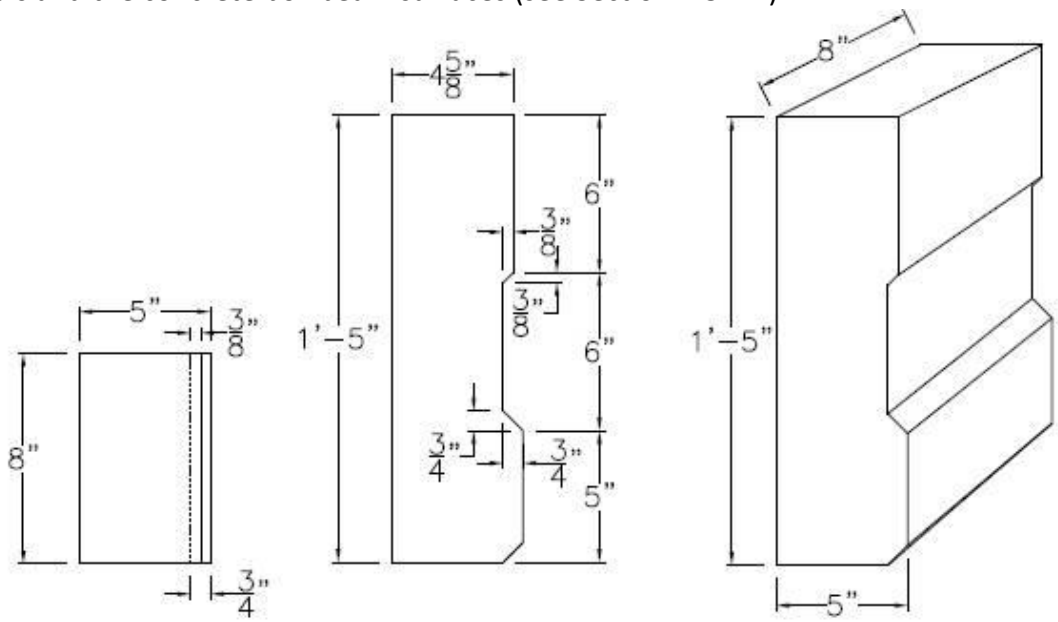

a) Specimen geometry

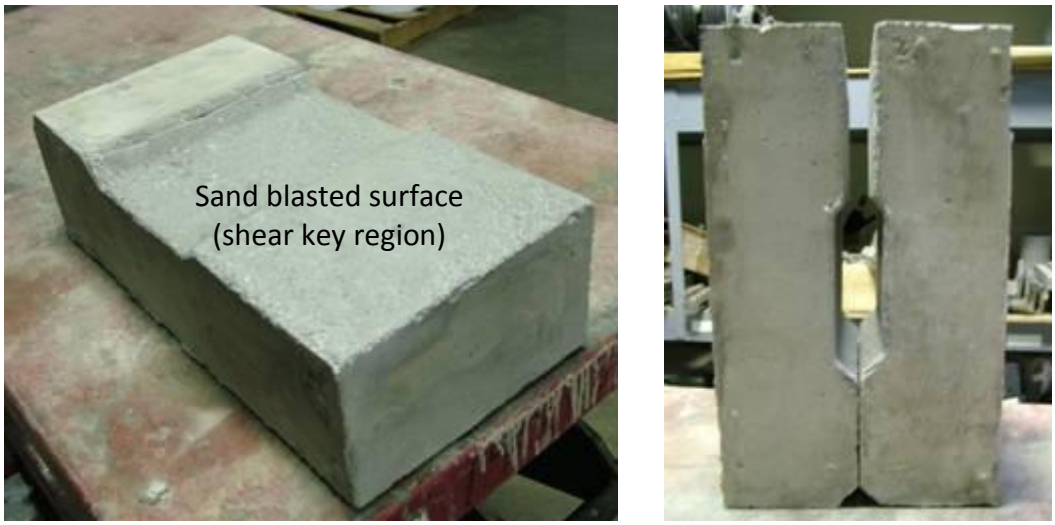

b) photographs of shear key modifications

Figure 2.20 Shear key specimens as cast at the Newcrete precast plant

The shear key specimen geometry was modified before grouting to better fit the shear and flexure test set-ups (which will be described in Section 2.3.5). A wet diamond saw was used to

cut a 1.5-in-by-2-in notch at the corner of each half shear key specimen. The purpose of this modification was to create a bearing plane for the steel angle plates in order to hold the specimen in place during flexure and shear tests. The new geometry of the shear key specimens is shown in Figure 2.21. The accuracy of the cut on the notch was found to be of importance during the experimental tests, as grooves and imperfections in this region can lead to premature failures.

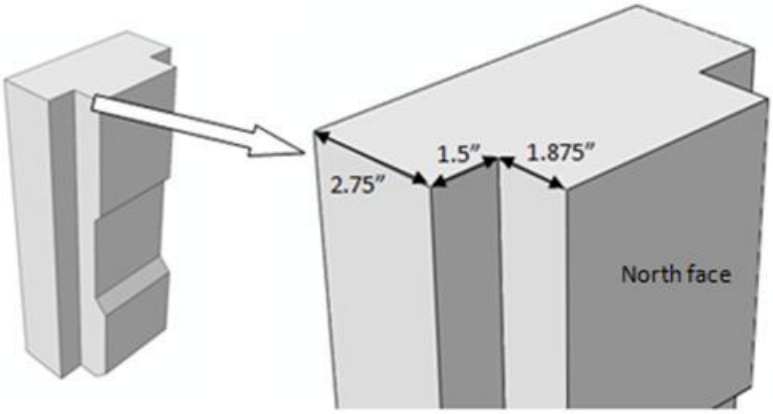

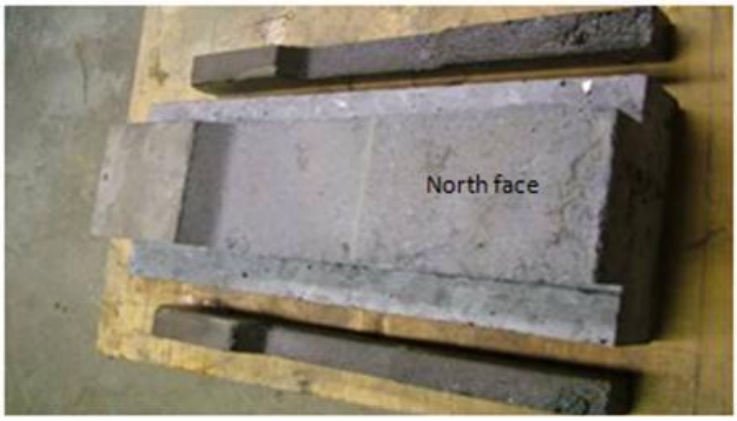

a) Modified shear key specimen geometry

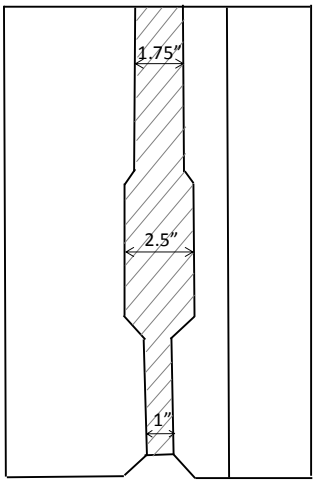

b) Shear key specimen used for the shear test

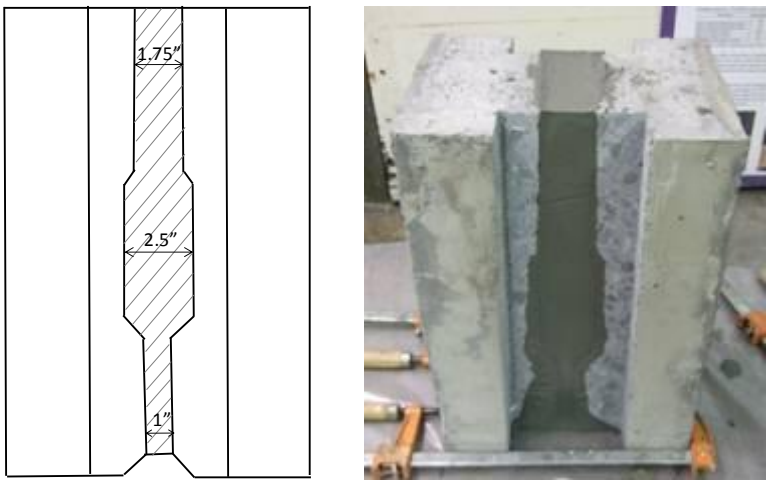

c) Shear key specimen used for the flexure test

Figure 2.21 Shear key specimens (epoxy grout shown in all photographs)

2.3.3 Test Setup Fabrication

The setup to conduct shear and flexure tests was designed to induce shear or flexure stresses in the region near the shear key. Even though a shear key between two adjacent concrete box beams is expected to be subjected to a combination of flexure and shear (and to a certain extent torsion), isolating the shear and flexure effects may provide a more clear insight on the performance of the different types of grouting materials. Design of the test set-up was done by the Penn State research team at CITEL. Parts made of grade 50 steel were ordered from a steel manufacturer, and construction and assemblage was done at CITEL. The setup was designed so that it can be used in both the flexure and the shear tests with minimal changes. Figure 2.22 shows the different components of the test setup. It consists of four main parts: (1) angle plate, (2) 2.5-in-thick steel plate with a bottom bearing plate, (3) top plate, and (4) W16x67 beam.

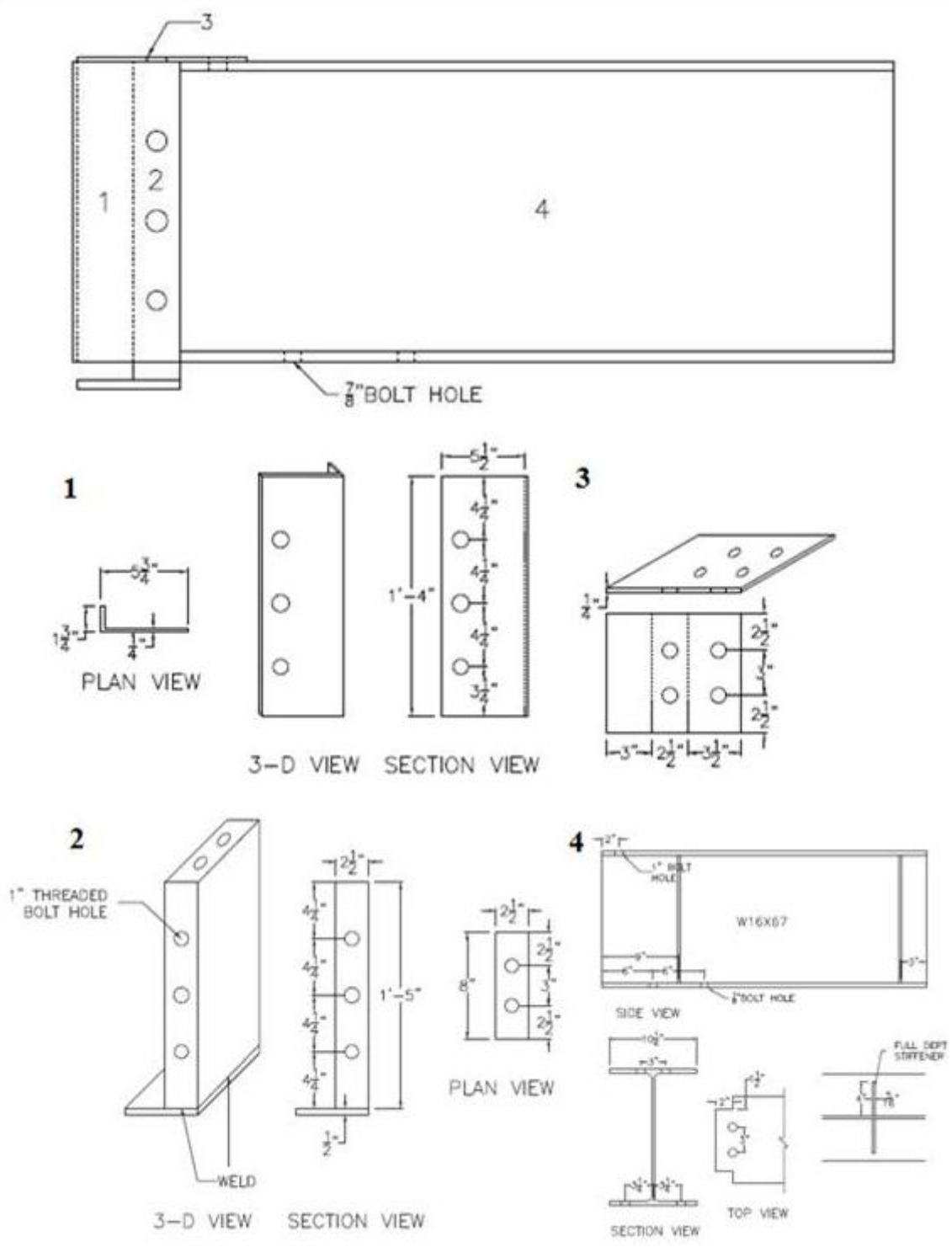

Figure 2.22 Test setup components

The W16x67 steel beam was welded onto the 2.5-in-thick steel plate to fully transfer the load during the test using high-strength weld. The angle plates and the top plates were installed after the specimen was placed on top of the bottom bearing plate. The edges of the specimens were grinded down to fit inside the angle plates and top plate. Steel sockets were bolted to the 2.5-in-thick plate using 1-in-diameter A325 bolts.

2.3.4 Shear Test

Test configuration

The test setup was designed to create a state of shear stresses in the shear key region. A concentrated load (coming from the actuator) provides a downward movement to one side of the shear key connection, while the other side is prevented from movement and rotation. A sketch of this test configuration is shown in Figure 2.23 (a). Figures 2.23 (b) and (c) show a drawing and photograph of the shear test configuration used at CITEL.

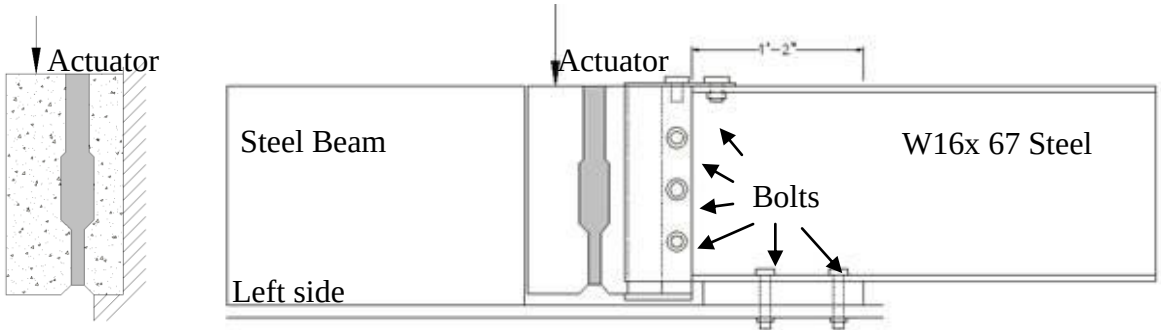

a) Sketch of the test configuration b) Drawing of the shear test configuration

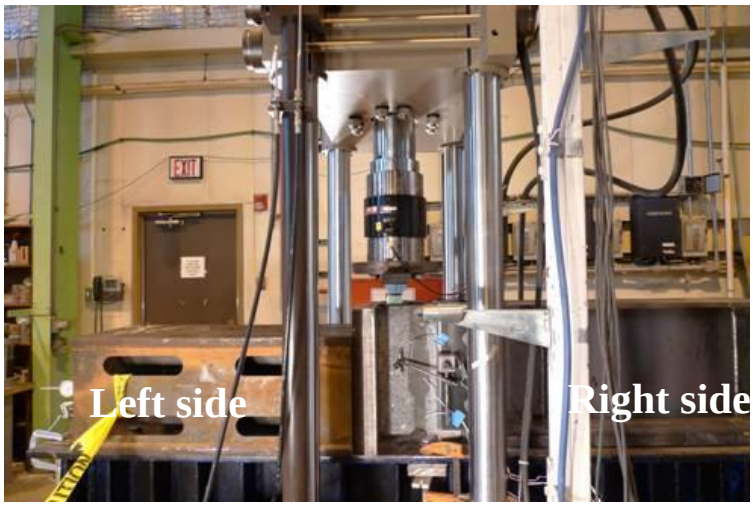

c) Photograph of the shear test configuration

Figure 2.23 Shear test configuration

The right end of the setup was fixed to the platform of the universal testing machine with bolts placed at the bottom flange of the steel beam. Steel shims were placed under the thick vertical steel plate where the structural bolts go to prevent any vertical deflection of the support during the shear test. The far right end of the beam was clamped down to prevent uplifting. After the specimen was installed into the test setup, another steel beam with similar depth as the concrete specimen was placed at the free end of the shear key specimen. It served an important function in the shear test, which was to restrain the lateral movement of the shear key specimen during the test. Note that lateral movement allows for the development of negative moment at the top surface of the shear key specimen, which can cause (1) flexure behavior of the specimen and (2) local failure of the specimen near the angle plate, as discussed in Section 2.3.4.3.

Load from the machine actuator was applied at the free end of the shear key specimen. An elastomeric bearing pad and steel bearing plate were used to avoid crushing of concrete. The loading rate was set to be 0.276 in/min.

Instrumentation

To correlate the experimental results with the finite element model, deflection and strain measurements were required. LVDTs (shown in Figure 2.24 as white arrows) and a string pot were used to measure deflection at various locations on the shear key specimen. Quarter bridge strain gages (Model KFG-10-120-C1-11L3M3R) were also installed to measure the strain history of certain points on the specimen during the loading. Figure 2.24 shows the location of the different transducers used for this type of test. Note that the long LVDT is attached to the steel socket to measure the relative deflection of the shear key specimen with respect to the test setup.

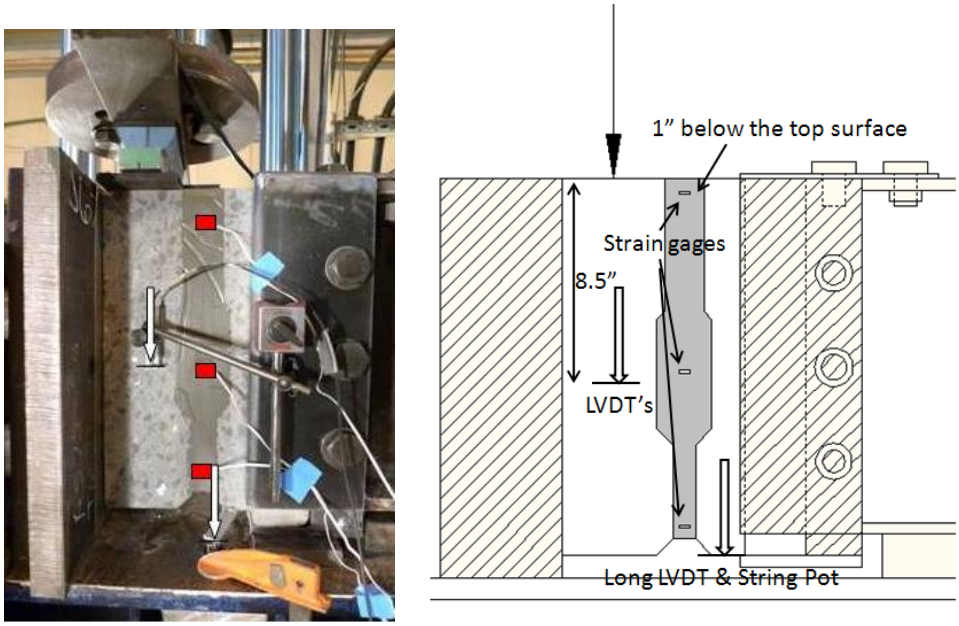

a) photograph of shear key specimen b) instrumentation setup

Figure 2.24 Instrumentation on the shear test specimen

Shear test of specimen with epoxy grout

Observations

After the test was initiated, the loading head displaced downward at a rate of 0.276 in/min. No visual crack was observed at the early stages of the shear test. The first visible crack was observed at 20 kips. It was located at the bottom of the specimen over the steel support. It is denoted as crack 1 in Figure 2.25. The location of this crack indicates a high level of stress near the support area. As the load level reached 68 kips, a crack opened at top of the concrete side of shear key specimen (crack labeled as 2 in Figure 2.25). It was caused by the stress concentration from the pressure of angle plates. As the load increased, wide shear cracks started to form, as seen in Figure 2.25 (labeled as 3), and the specimen eventually failed in a brittle manner at 89 kips.

The observed crack pattern indicates that the presence of the epoxy grout "strengthens" the shear key region. Therefore, initial cracks form on the outer boundaries of this region (cracks 1 and 2). After the regions with high stress concentration crack, shear cracks start to form across the concrete-shear key region. The presence of the epoxy was found to create higher energy at failure, characterized by noise and a sudden load drop when the crack crossed the concrete-epoxy interface into the pure epoxy region (crack 3, middle).

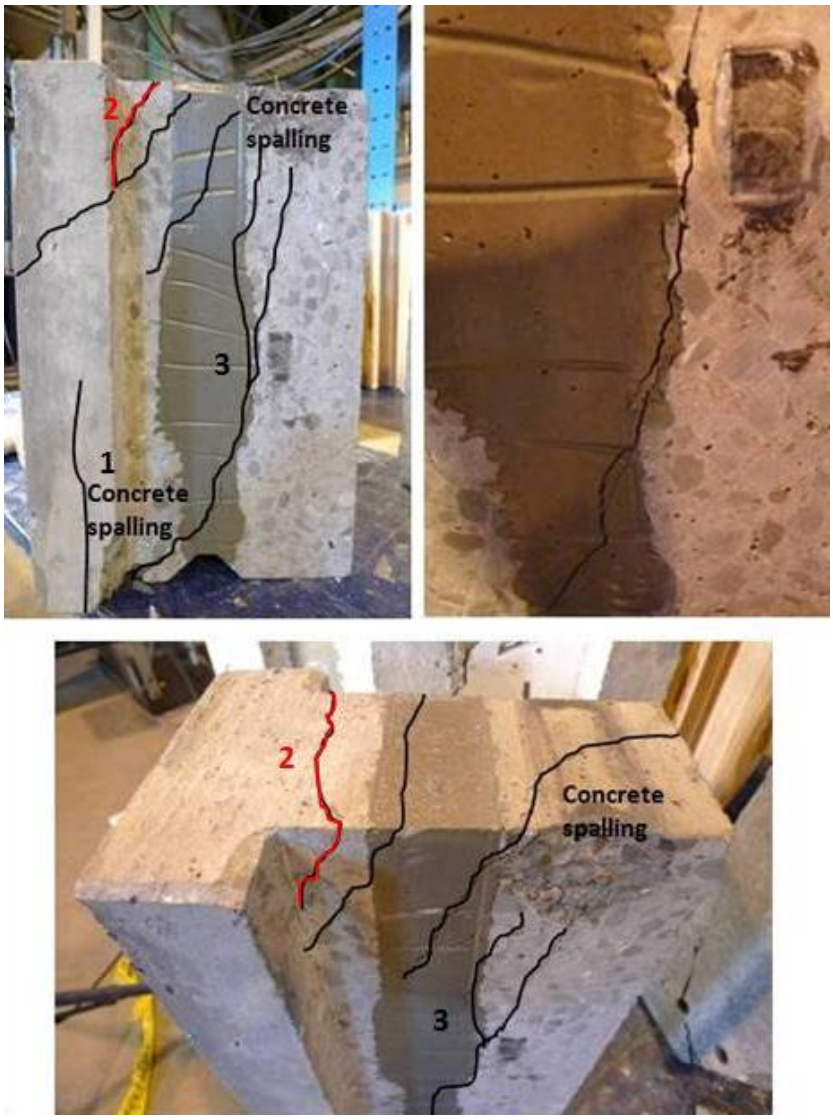

Figure 2.25 Crack patterns of a typical epoxy-based grout shear key specimen tested in shear

Test results

Figure 2.26 shows the transducer displacement data versus load level. All transducers show a relatively flexible response up to 20 kips of loading. This was expected, as it is attributed to test rig deformation as well specimen deformation at the early loading stage. LVDT1 and LVDT2 were placed on the concrete side at the specimen mid-height. The string-pot and the long LVDT were placed at the bottom of the concrete specimen, near the support. The displacements registered by these two transducers were therefore smaller than the ones registered by LVDT1 and LVDT2, as observed in Figure 2.26. The initially observed cracks in the vicinity of a load level of 20 kips are reflected in the graph by small "jumps" on the load-displacement curves. After the load reaches 65 kips, a crack on the top concrete side, described as "crack 2" in the previous section, induces larger deformations in the specimen, as reflected by the larger

change on the horizontal axis of the plotted curves. The specimen reached the maximum load of 89 kips, at which point the wide shear cracks were formed through the shear key region.

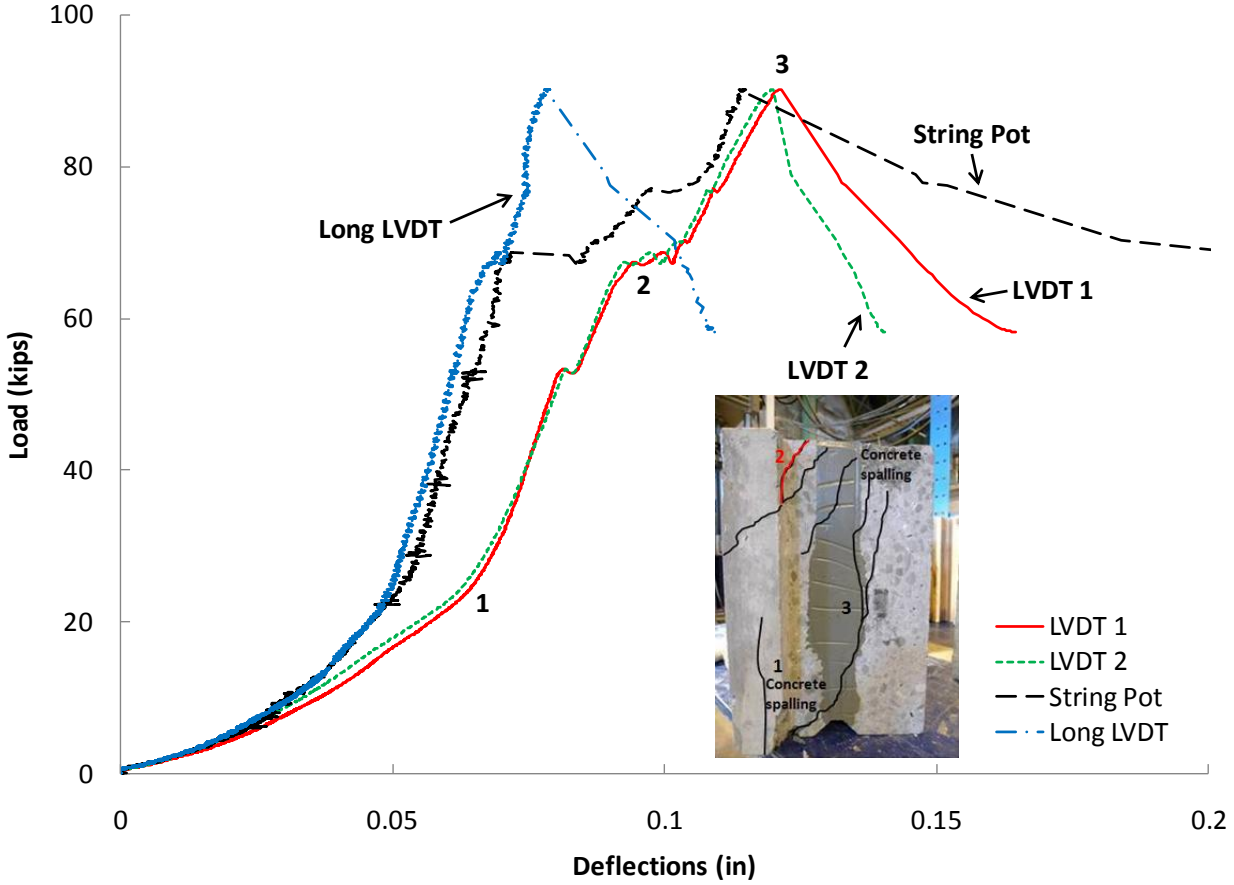

Figure 2.26 Load-deflection of the epoxy-based grout shear key specimen tested in shear

Strain gage data are also plotted against the load level in Figure 2.27. For a load level less than 40 kips, all three strain gages show linear response, reflecting the linear elastic response of the epoxy and surrounding concrete. At higher load levels, changes in the strain response are a reflection of cracks occurring on the concrete, and ultimately epoxy shear key failure. Large cracks occurring on the top concrete region, near the 68-kips load level, caused a drop in the magnitude of the strain in the surrounding shear key region, as reflected by the "top" strain gage. Changes of deformation on the concrete side of the specimen were also registered by the "bottom" strain gage.

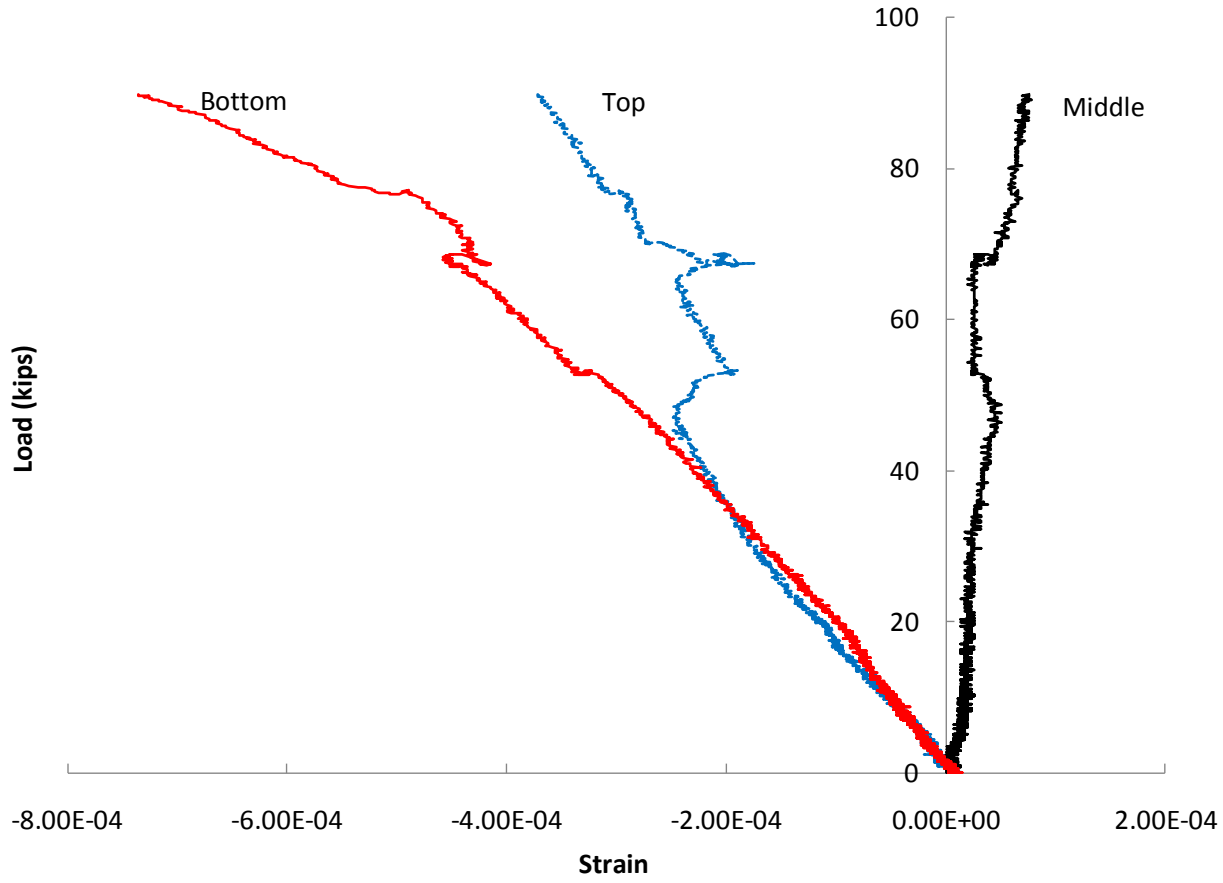

Figure 2.27 Load-strain curves of the epoxy-based grout shear key specimen

Shear test of specimens with cementitious grout

Two shear key specimens were fabricated using a cementitious grout for the shear key region. They were tested under the shear test configuration. Both specimens showed a major crack propagating between the interface of the concrete and the shear key. This is an indication of the weaker bond between the concrete and cementitious grout as opposed to the concrete-epoxy bond behavior exhibited by the epoxy grout specimen. Both cementitious grout specimens also exhibited residual strength after the major crack occurred, provided by the mechanical interlock of the shear key geometry (this phenomenon will be described in more detail next). It was interesting to note that surface preparation for the concrete shear key region has the potential to significantly affect the strength of the concrete-cementitious grout interface. Specimen 2 had a lower failure load than specimen 1. Among several possible causes for this difference, it was found that both specimens exhibited differences in their sand-blasted surfaces.

Specimen 1 observations

In this test, the major crack occurred at the interface between the concrete and the cementitious grout at a load level of 38.1 kips. It initiated at the bottom of the shear key region (crack 1) and propagated in a sudden manner along the interface (crack 2), as shown in Figure 2.28 (a). The bond failure between the concrete and the cementitious grout was the controlling failure mechanism. Crushing of the cementitious shear key grout was observed after the major bond crack occurred, see Figure 2.28 (b). This type of concrete bearing failure along with the relative slip between the two surfaces creates a residual strength of the connection, which is more ductile than the failure mode observed by the epoxy-based grout specimen.

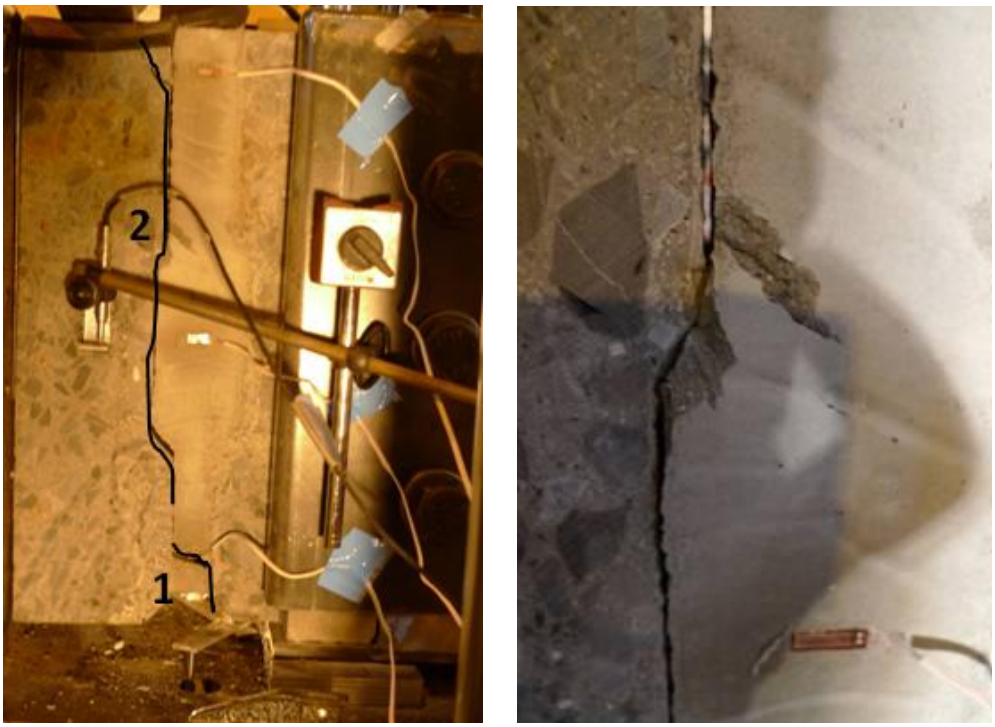

(a) cracks along the shear key interface (b) bearing failure between two surfaces

Figure 2.28 Crack patterns of a typical cementitious-grout shear key specimen tested in shear

Test results

Figure 2.29 shows the transducer displacement data versus load level. All transducers showed initially a relatively flexible response up to 20 kips of loading. This can be attributed to test rig deformation as well as specimen deformation at the early loading stage. As the load level increased, small cracks developed along the bottom portion of the shear key interface. When the load level reached 38.1 kips, a horizontal crack on the cementitious grout occurred, creating a second drop of load, as shown in all load-deflection curves. Transducers placed at the bottom of the specimen (long LVDT and string pot) showed larger deformations, due to their proximity to these cracks, than LVDT1 and LVDT2. The propagation of the crack along the entire shear key interface caused a significant drop in the load capacity. Figure 2.29 shows that the residual

strength developed reached a plateau around 30 kips. Figure 2.30 shows the regions where crushing, bearing, and slip damage occurred at the shear key interface.

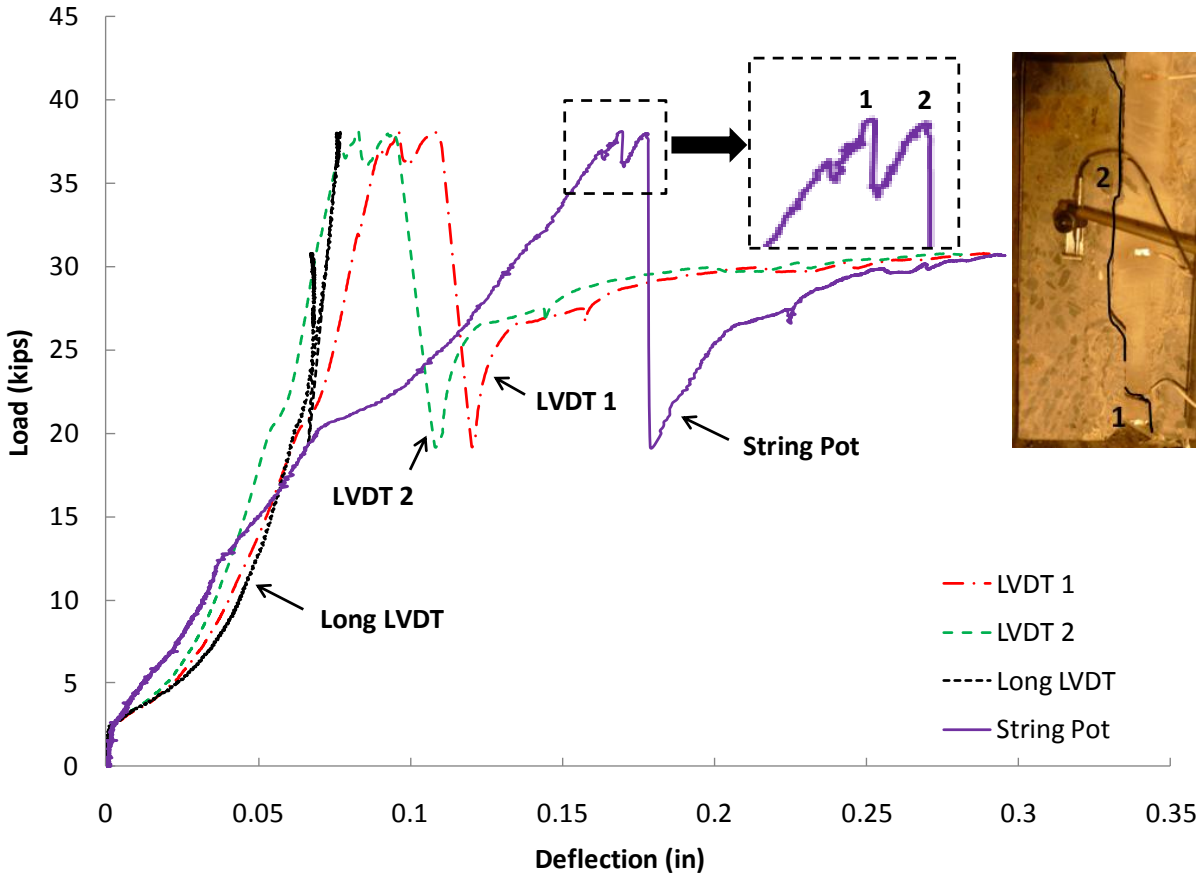

Figure 2.29 Load-deflection of the cementitious grout shear key specimen tested in shear

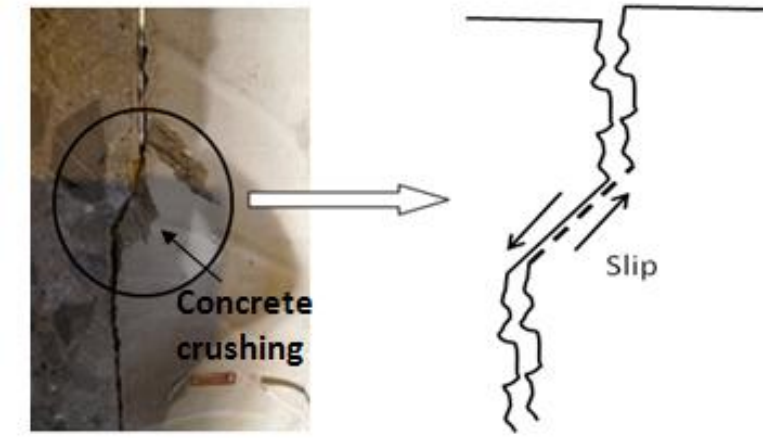

Figure 2.30 Bearing and slip failure mechanisms at the shear key interface

Specimen 2 observations

The crack pattern of the second cementitious grout specimen was similar to the one observed with the first specimen. The first crack originated at the bottom of the shear key interface (crack 1 shown in Figure 2.31), then propagated through the shear key to join a second crack along the shear key interface (shown as crack 2 in Figure 2.31). After this main crack pattern occurred, bearing and slip were observed between the two crack surfaces of the specimen.

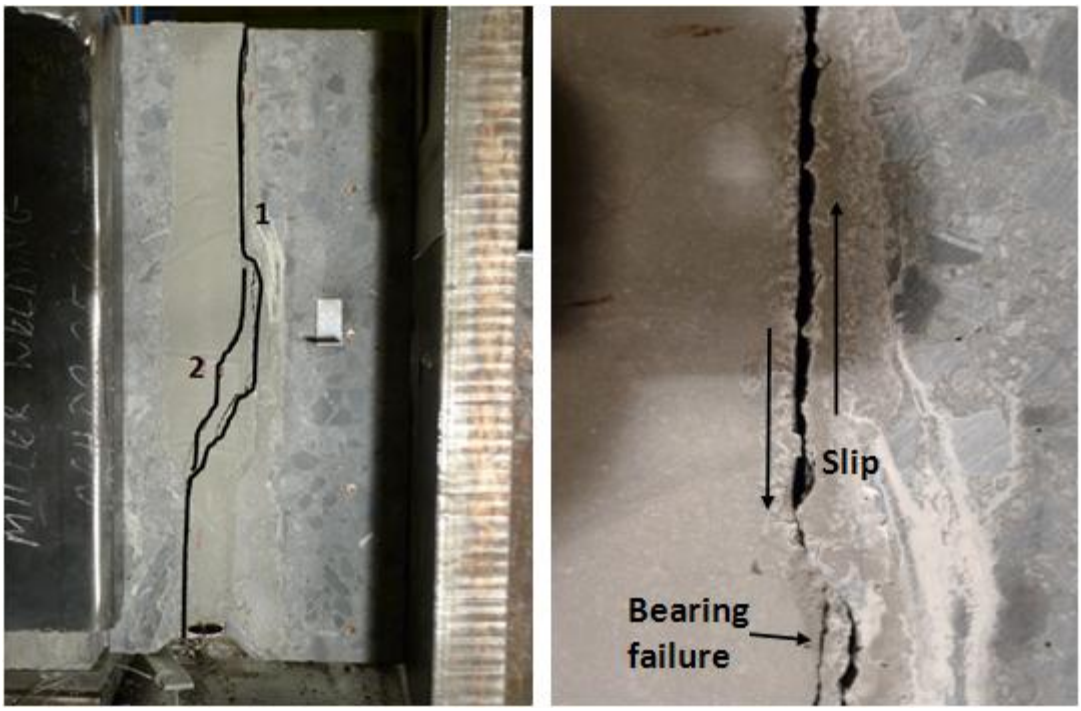

Figure 2.31 Photographs of the crack pattern observed in the second cementitious grout specimen

Test results

The failure load of the second cementitious grout specimen was 23.1 kips, which was significantly less than the strength of the first specimen. Several possible factors such as confinement effect, surface preparation, and differences in specimen fabrication could have contributed to this difference. However, it was found that the specimen was also able to provide a residual strength after the major crack pattern developed. Figure 2.32 shows that all displacement transducers had similar deformation rates up to a load level of 17 kips, where LVDT1 and LVDT2, placed at the specimen mid-height, showed larger deformations. It was expected that the onset of cracking along the shear key interface creates a larger relative displacement between the two sides of the concrete specimen.

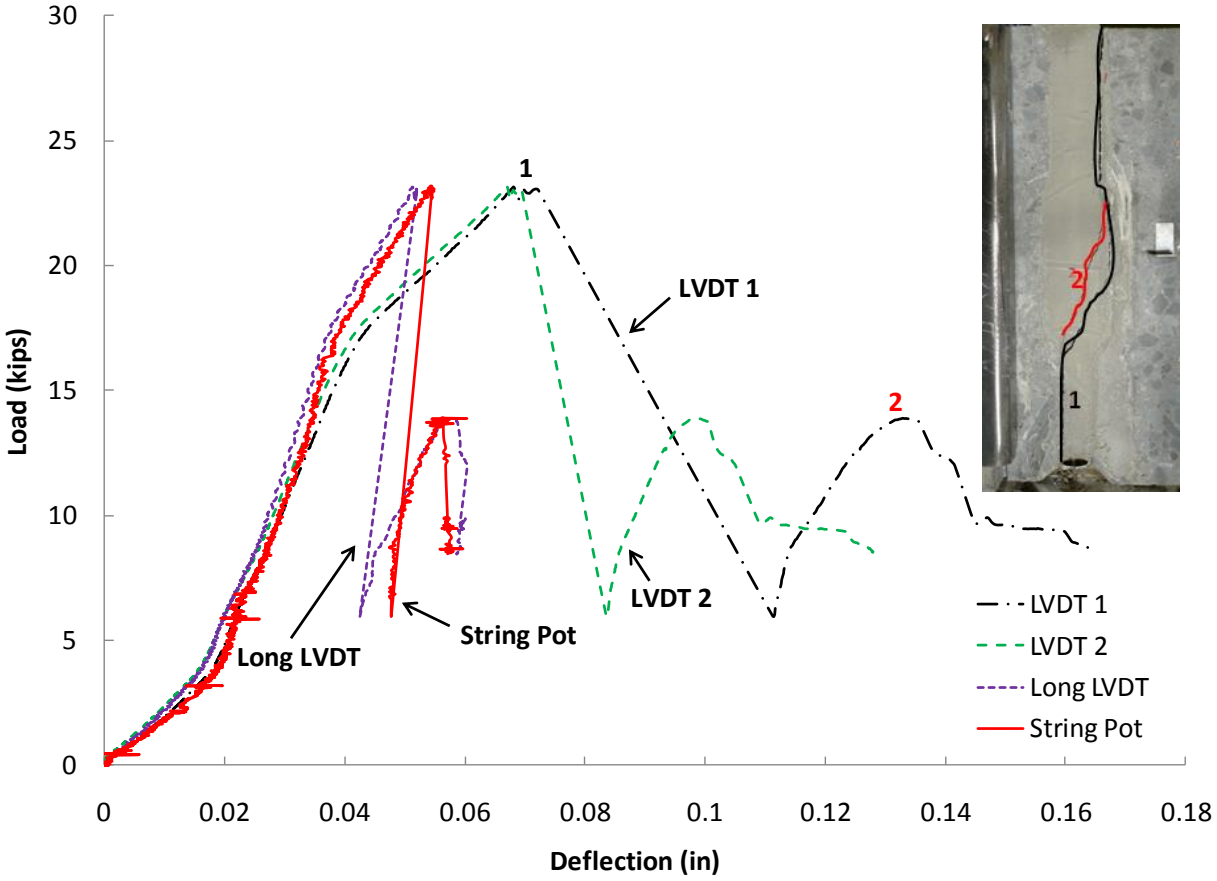

Figure 2.32 Load deflection plot of the second cementitious grout specimen

After the shear test was conducted, the fractured surfaces of the shear key specimens were examined. The first cementitious grout shear key specimen, which failed at 38.1 kips, had a more roughened, sand-blasted surface, as shown in Figure 2.33, with a larger amount of coarse aggregates exposed from the cement paste. By contrast, the blasted surface of the second specimen, which failed at 23.1 kips, showed a smoother surface. It can be concluded that surface preparation, reflected by the roughness of the sand-blasted shear key surfaces, can increase the bonding strength of the grout and the concrete, which in turn can result in a higher load-bearing capacity of the system.

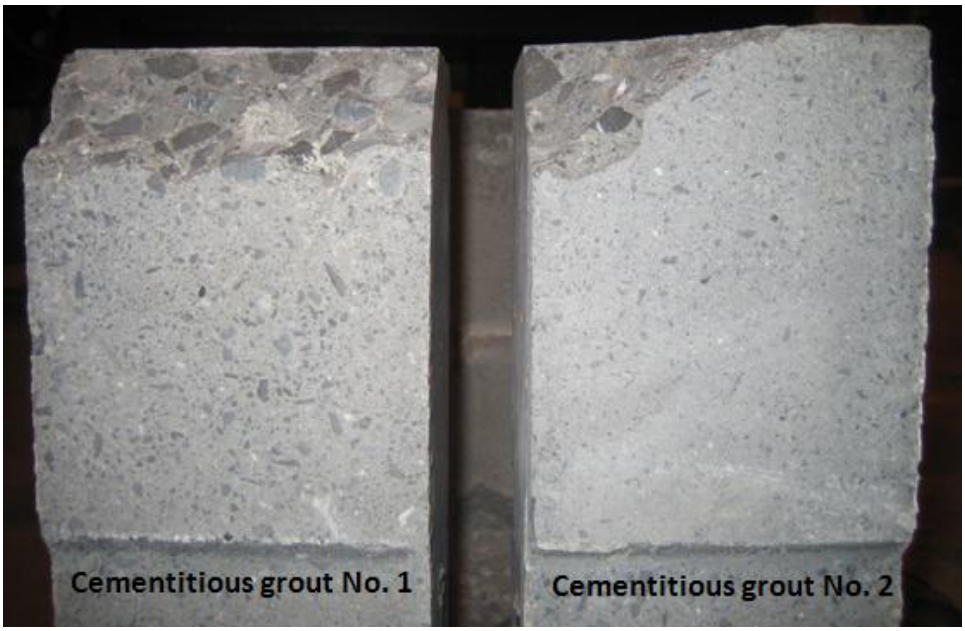

Figure 2.33 Differences in sand-blasted surfaces between two cementitious grout shear key specimens

Shear test of specimen with fiber-reinforced cementitious grout

Observations

The failure mode for this specimen was similar to the one observed in the cementitious grout specimens. The interface between the concrete and the fiber-reinforced cementitious grout constitutes a weak plane where cracks develop. Figure 2.34 shows a photograph of this type of major crack (crack marked as "1"). A significant load drop accompanies this crack propagation. A secondary crack occurred at a later time, joining the tip of crack 1 with the support region (crack 2). This crack propagated through concrete with a second load drop.

Figure 2.34 Failure of fiber-reinforced cementitious grout specimen

Test results

Figure 2.35 shows the load-deflection curves for the fiber-reinforced cementitious grout specimen. As in previous shear tests, after an initial adjustment of the test setup, increases in deflection accompanied increases in the load level. When the load level reached 35.8 kips, the first major crack occurred along the shear key interface (on the fix-support side of the test specimen). The load dropped approximately 10 kips and started increasing again. The load was able to reach 47.3 kips before the second crack propagated through the concrete at the bottom of the specimen. Data from the string pot showed larger deformations than the long LVDT, indicating a possible slip between the attachment used for this transducer and the concrete surface. LVDT1 and the long LVDT had similar deformation rates during the testing.

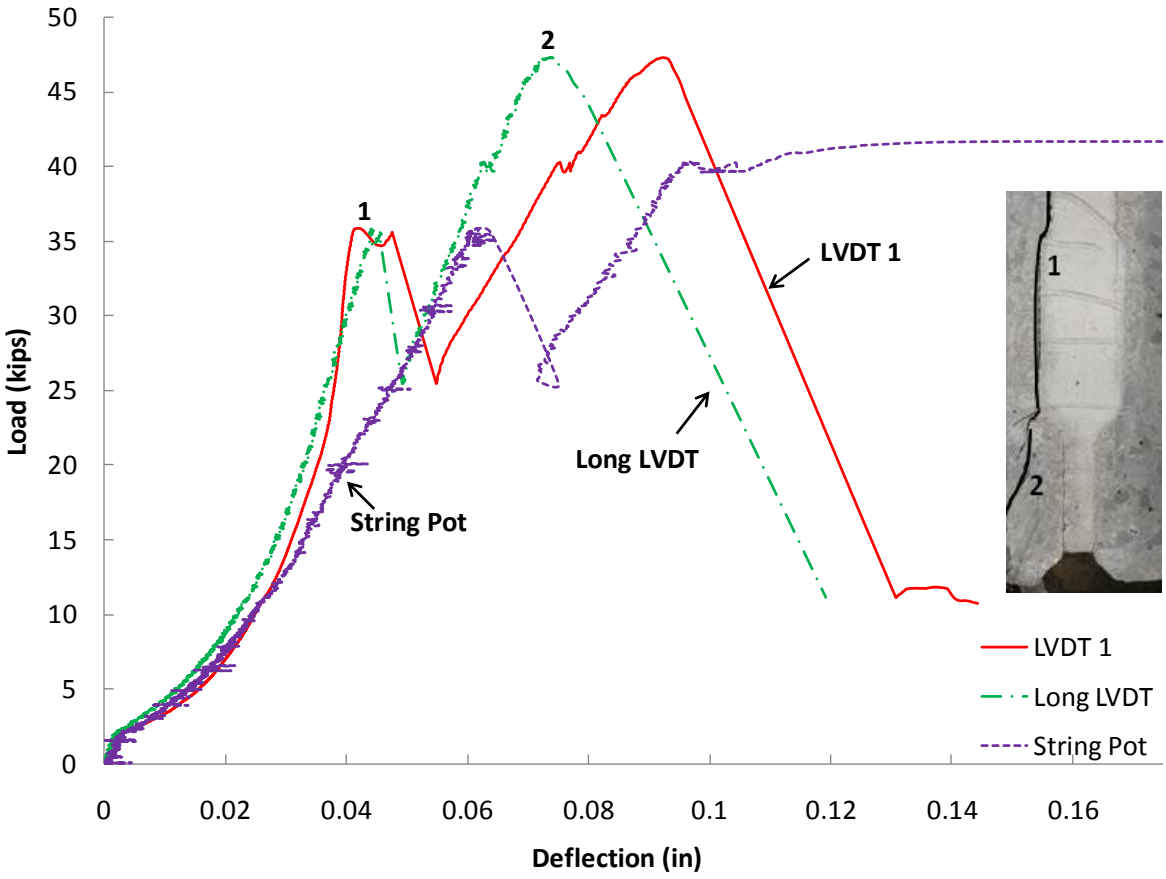

Figure 2.35 Load deflection plot of the fiber-reinforced cementitious grout specimen

Summary of test results

Three types of grouting materials were evaluated: epoxy grout, cementitious grout, and fiber-reinforced cementitious grout. Two shear tests were conducted with a cementitious grout; one test was conducted with the epoxy grout and one with the fiber-reinforced cementitious grout. Test results are presented in Table 2.14. The specimen with the epoxy grout had the highest strength. The cementitious specimens had a lower strength. The specimen with the fiber-reinforced cementitious grout had a strength comparable to the specimen without fibers. A second cementitious grout specimen exhibited lower strength than the first specimen, perhaps influenced by surface preparation. Table 2.15 summarizes the main findings of this type of testing.

Table 2.14 Shear test summary

Material Type	Failure Load (kips)	Residual Strength (kips)	Shear Stress at Failure (psi)
Epoxy-based grout	89.4	-	1009
1st cementitious grout	38.1	30.8	476
2nd cementitious grout	23.1	13.8	231
Fiber-reinforced cementitious grout	35.8	47.3	638

Table 2.15 Summary of the findings of the shear test

Material Type	Failure Characteristics	Laboratory Findings
Epoxy grout	• The failure mode of the shear key specimen was shear failure. • No debonding at the interface was observed. • Presence of epoxy led to initial cracks originating on the concrete. • Shear cracks developed through concrete and epoxy as if the specimen were isotropic, indicating a strong bond between these two materials.	• The epoxy grout was stronger than the concrete. The concrete always failed prior to any failure in the grout region. • The epoxy grout and concrete had excellent bond strength; therefore an epoxy grouted shear key can provide a good transfer of load between adjacent box beams. • When the epoxy grout fails, the failure pattern does not follow the shear key interface; thus it does not provide residual strength. It is possible that the shear key geometry is irrelevant to the performance of adjacent box beams when using epoxy grout.
Cementitious grout	• Main cracks propagated along the shear key interface through a debonding failure. • The cement-based grout and concrete interface are a weak bond plane. • Fractured shear key surfaces exhibited residual strength due to the bearing failure and slip mechanisms.	• The cementitious grout and concrete had a weaker bond strength compared to the epoxy grout specimens. • The shear key geometry can provide residual strength post cracking. • Shear key surface preparation can significantly affect the shear key strength.
Fiber-reinforced cementitious grout	• Similar failure mode to cementitious grout.	• Similar to cementitious grout.

2.3.5 Flexure Test

Test configuration

The flexure test is a four-point bending test as shown in Figure 2.36. Two of the steel beams used for the shear test (shown in Figure 2.23) are used in this setup. The shear key specimen is placed in between the two steel beams and fixed in position using the steel sockets. The combined beam is supported on two ends with roller supports. Load is applied through a spreader beam and two small rollers, which are restrained from rolling laterally. Steel stiffeners were fabricated at the loading and support locations to prevent a potential local failure of the steel beam. The spreader beam was fixed to the loading head for safety.

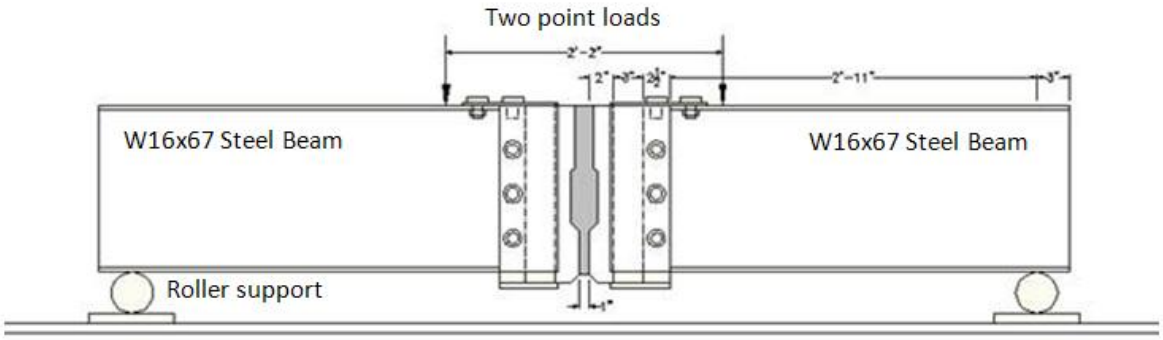

Figure 2.36 Flexure test setup

Instrumentation

To obtain the load, deflection and strain data in the shear key region, two LVDTs were installed at the top of the mid span, and two strain gages were installed at top and bottom of the mid-span section, as shown in Figure 2.37.

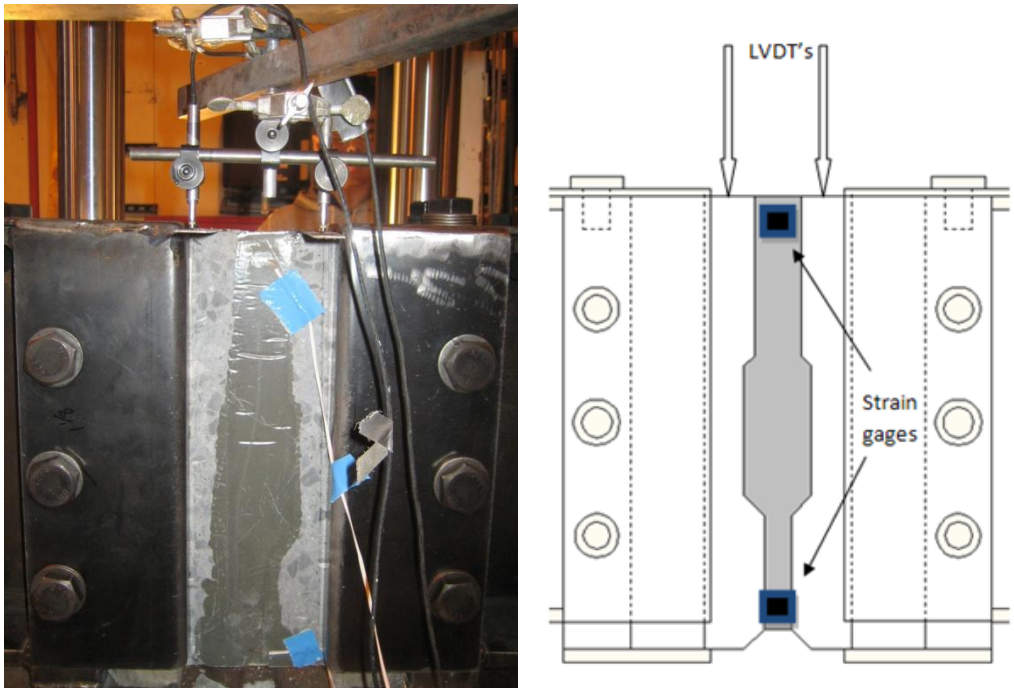

a) photograph of shear key specimen in flexure b) instrumentation setup

Figure 2.37 Instrumentation details of the flexure test setup

Flexure test of the epoxy grout specimen

Observation

The failure mode of the flexure test specimen was localized failure of the concrete flanges. The mid-span region containing the epoxy shear key proved to be stronger than the notched region near the concrete flanges. Stress concentration due to grooves and imperfections triggered crack initiation and led to localized shear failure of the concrete flanges at the bottom of the specimen. It appears that the strength and stiffness of the epoxy shear key was significantly larger than the surrounding concrete. Therefore, flexure failure on the epoxy material is not likely to occur. Instead, localized failures in concrete will triggered the main failure mechanism. They will originate at the bottom of the specimen where tension stresses are larger.

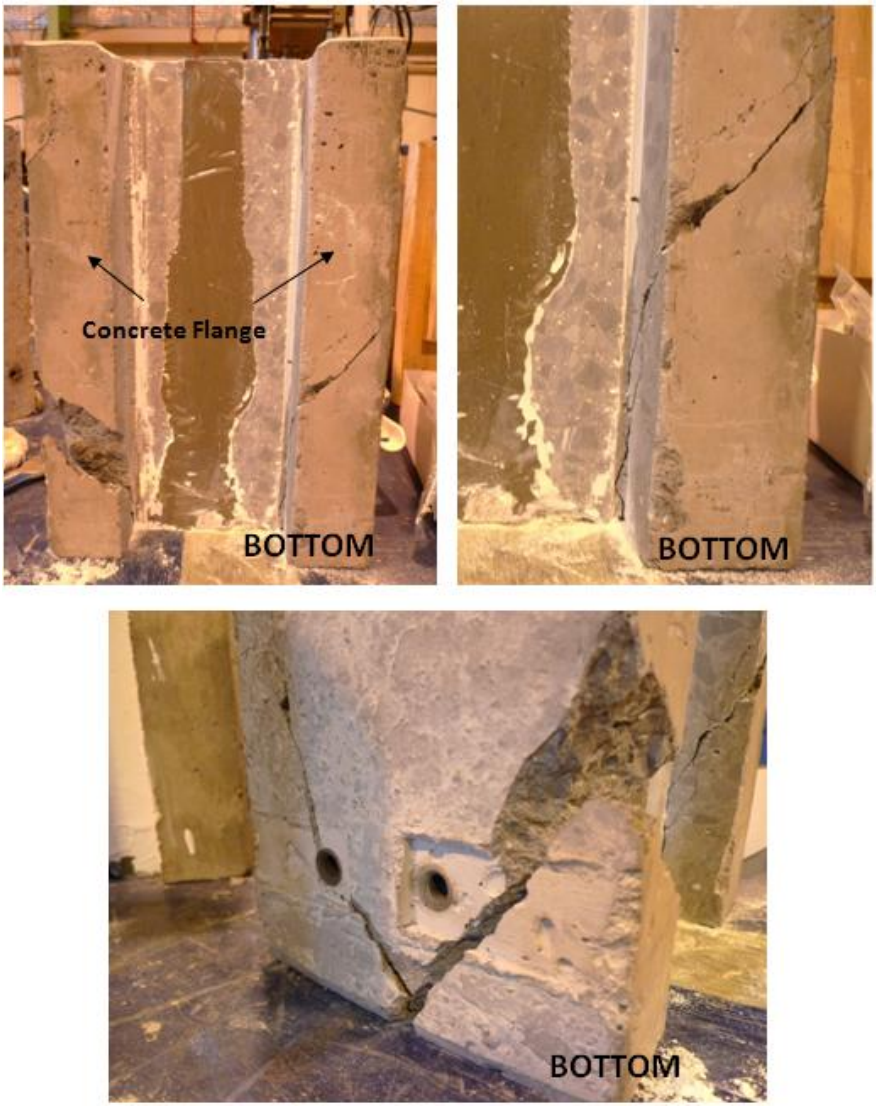

Figure 2.38 Failure mode of the epoxy grout specimen tested in flexure

Figure 2.39 shows the load deflection data recorded from the two LVDTs and load cell. The initial portion of the test involved adjustment of the test setup, and although it was not recorded, its loading magnitude was noted (1 kip). The same loading rate was used as in the shear tests (0.276 in/min). Concrete cracks are reflected in these curves by load drops. As expected, the deflection readings from the two LVDTs follow the same trend. After several cracks developed at both ends of the shear key specimen, differences in deformation between both sides were registered. Table 2.16 shows the equivalent bending stress at mid span for the first and second load drops at 3 kips and 4.2 kips. It can be seen that the magnitude of these stresses is two orders of magnitude lower than the splitting tensile strength of the epoxy grout. The strains at the mid span were too small to be recorded by the strain gages.

Table 2.16 Equivalent bending stress at mid span at different load levels

Load Level	Equivalent Bending Stress (psi)
3 kips	17.8
4.2 kips	24.9

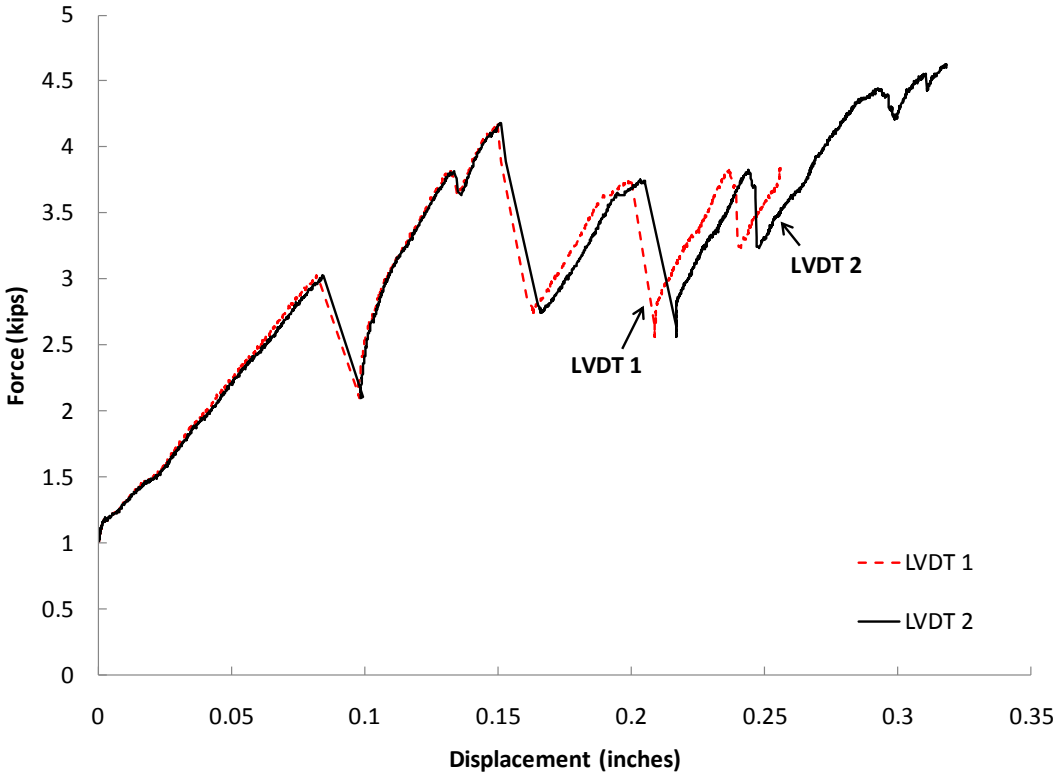

Figure 2.39 Load deflection plot of the epoxy grout in flexure test

Chapter 3. Grillage Analysis

3.1 Introduction

A grillage analysis was conducted to determine the load effects around the shear key region. Results, including moment and shear forces obtained from the grillage analysis, were used in the next phase of the analysis, in which finite element analysis of an isolated shear key model was conducted; these FE analyses will be described in the next chapter. The grillage converts the bridge deck structure into a network of rigidly connected beams (e.g., a network of skeletal members rigidly connected to each other at discrete nodes). Each element is given an equivalent bending and torsional rigidity to represent the portion of the deck that it replaces. Bending and torsional stiffnesses in every region of the slab are assumed to be concentrated in the nearest equivalent grillage beam.

A simply-supported, prototype bridge with the following characteristics was chosen for the grillage analysis (see Fig. 3.1).

- Span length: 80 ft
- 12 box beams (AASHTO Standard BII-48) with 11 shear keys
- 1-inch-thick shear key; this geometry matches the experimental tests described in Chapter 2.
- Composite deck with 5.5-in concrete overlay and typical PennDOT barrier (BD601m specifications)

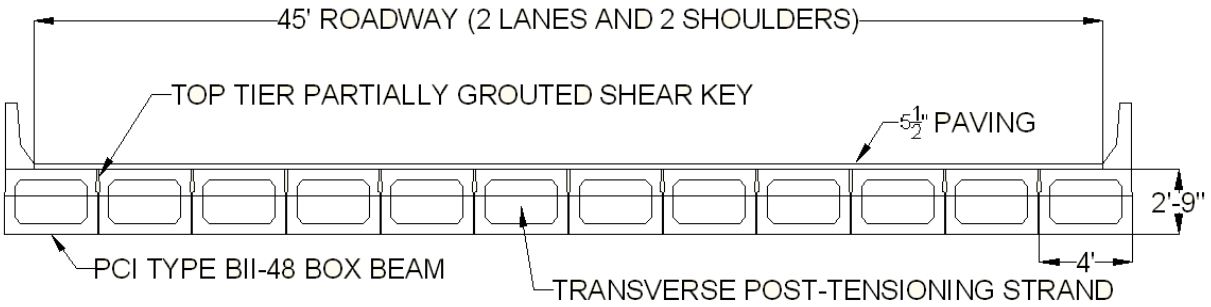

Figure 3.1 Cross-section of the bridge superstructure

3.2 Loads

Two load types were considered in this study – dead load and live load. Dead load consisted of the self weight of box beams, concrete topping, and barriers of the bridge superstructure. Live load consisted of truck load and lane load per AASHTO LRFD specifications. The truck load was an HS25 design truck, which consists of three axles of 10 kips, 40 kips, and 40 kips, as shown in Figure 3.2a. While the distance between the 40-kip and 10-kip axle loading can vary from 14 ft to 30 ft, a 14-ft spacing was chosen, as it produces the maximum load effect in a simply supported beam. Another type of AASHTO live load was the design lane load of 0.64 kips per

linear foot, as shown in Figure 3.2b. PennDOT's P-82 truck overload (Fig. 3.2c) was also considered in the grillage analysis.

The AASHTO bridge design guide Service I load combination (AASHTO *LRFD Bridge Design Specification* 2008) was considered for this grillage analysis. Multiple presence factor and dynamic impact factor were incorporated into the load cases.

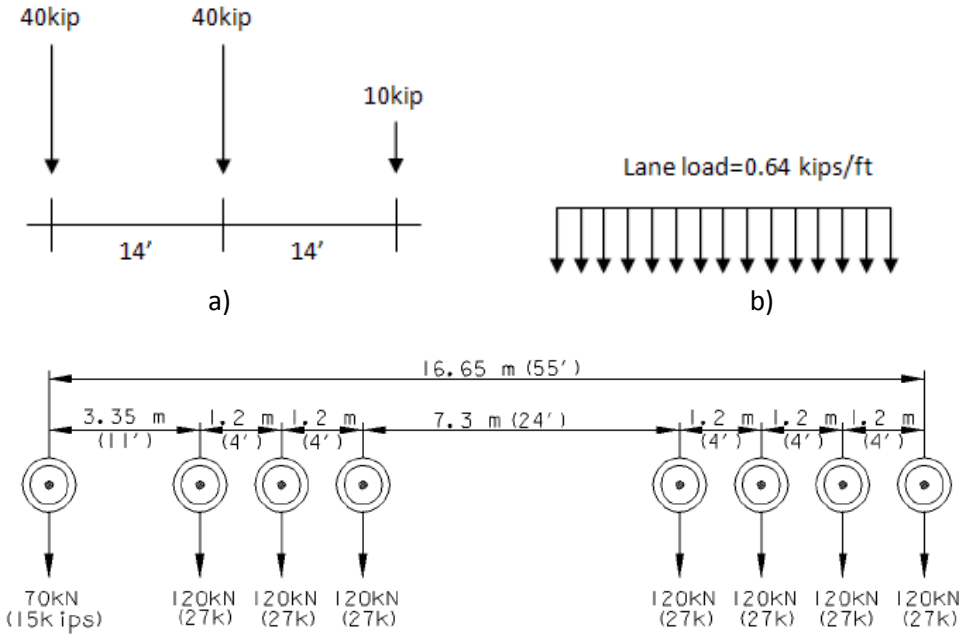

Figure 3.2 Live loads: a) AASHTO HS25 design truck; b) AASHTO design lane load; c) PennDOT P-82 204-kip truck overload (PennDOT DM-4 2007)

3.3 Modeling Description

3.3.1 Grillage

In the grillage analysis the box beam system is treated as a grid system, as shown in Figure 3.3. Twelve longitudinal grid lines coincide with the center lines of box beams in Fig. 3.1. Each transverse member represents a portion of the box beam that acts as a transverse component, providing superstructure stiffness in the transverse direction. The bending and torsional characteristics of the box beam plus 5.5-in topping (assuming composite section) are assigned to these transverse members as well as longitudinal members. The two ends of the grid system are considered to be simply supported.

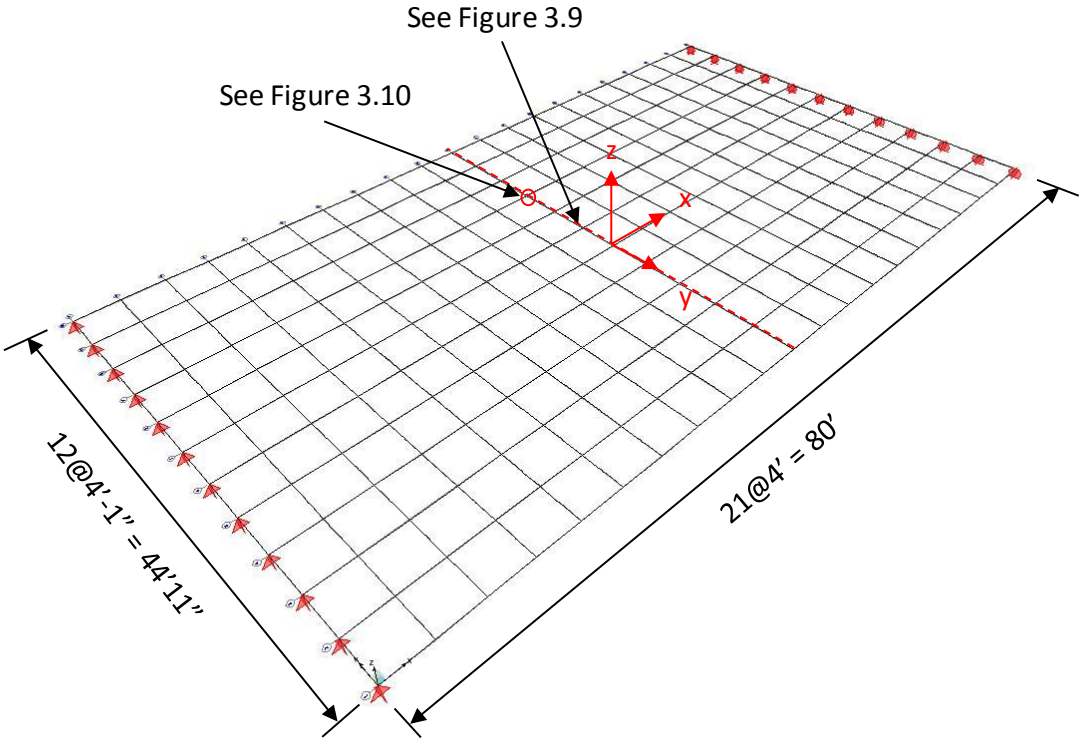

Figure 3.3 Grillage analysis model

The mesh size is determined based on grillage analysis conventions. The transverse beam spacing must be sufficiently small to accurately model the distribution of loads and assignment of the point loads. If the spacing is too large, the grillage model may not adequately capture the transverse stiffness inherent to box beam bridges. It is recommended that the spacing of the transverse members be similar to the spacing of the longitudinal member spacing to allow a uniform distribution of loads, as the adjacent box beam bridge superstructure acts like a continuous slab rather than discrete beams and cross bracings (Hambly 1991). Since the width of the box beam is 4 ft, the spacing between the longitudinal members is set to be 4 ft plus 1 in to account for the width of the shear key. The spacing of the transverse members is set to be 4 ft.

3.3.2 Material Properties and Member Section Properties

Sectional properties of the longitudinal members are assigned according to the AASHTO/PCI bridge design standard (AASHTO/PCI Bridge Design Manual 1997) for box beam sections. Figure 3.4 shows the cross section of longitudinal members. The stiffness contribution of the barriers on the edge beams is considered in terms of shear area. The barrier was transformed to an equivalent rectangular section to simplify the calculation of section properties (see Figure 3.4b). Its flexural stiffness is not considered because it will make the edge beams disproportionately stiff; in grillage analysis, such stiff edge beams will not undergo any deflection and, therefore,

will act as fixed supports on the two ends in the transverse direction (e.g., the bridge would appear to be supported on all four sides, which is incorrect). It should also be pointed out that these barriers are usually discontinuous, non-prestressed, and could be cracked. Therefore, they don't behave as elastic elements.

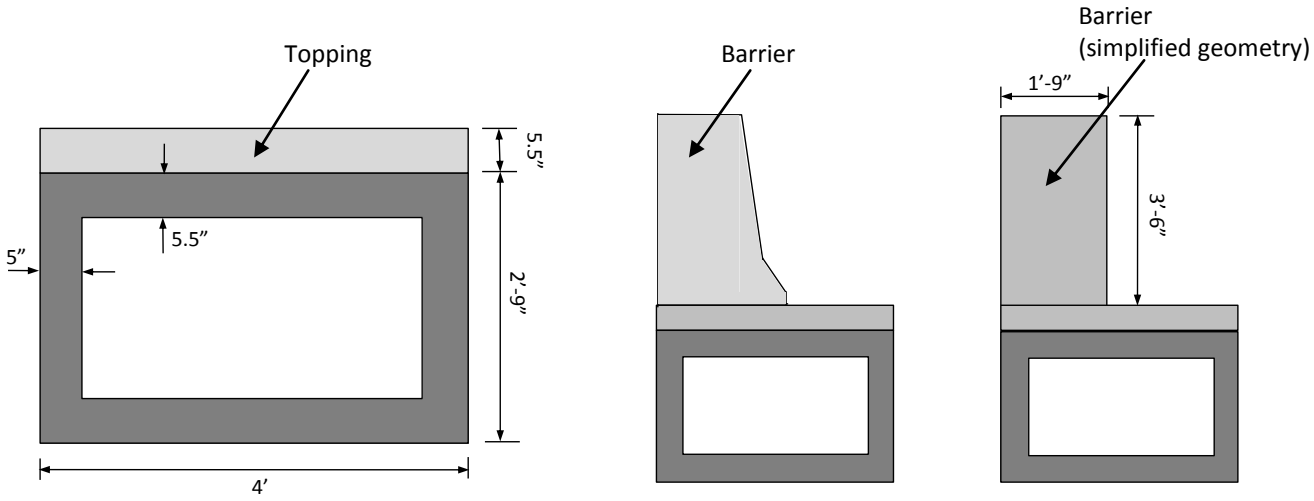

a) b)

Figure 3.4 Cross section of typical longitudinal members in the grillage analysis:
a) Interior box beam; b) Exterior box beam (as-is and simplified rectangular section)

The second moment of inertia of the section was calculated using conventional section analysis and assuming elastic behavior. Note that the center of gravity of the entire cross section was determined assuming that barriers are rigidly connected to the concrete overlay and box beams underneath, thus contributing to the torsional stiffness of the section. Therefore, the neural axis should be located above the mid-height of the box beams. The torsional stiffness of the cross-section was calculated based on equations developed by Marshall (1970). The torsional stiffness of a closed, thin-walled section subjected to torque can be expressed as follows:

$$J = \frac{4A_c^{\,2}}{\sum \frac{l}{t}} \qquad \text{(Eq. 3.1)}$$

where *Ac* is the area enclosed by the centerline of the box beam webs and flanges, *l* is the length of each segment of the box beams (web and flange), and *t* is their corresponding thickness. Marshall suggested the following expression to compute the torsional stiffness of bridge decks (since flange and/or web of box beams may be considered thick and open in torque). Equation 3.2 was used to calculate the torsional stiffness of the elements considered in this analysis. When using Eq. 3.2, the $\sum \frac{l}{t}$ is taken as the sum of length thickness ratio of all the segments constructing the box beam. Moreover, the webs are neglected because they are already accounted for as the shear area of the longitudinal beam.

$$J = J_o + J_c = \sum \frac{bt^3}{3} + \frac{4A_c^{\ 2}}{\sum \frac{l}{t}} \qquad \text{(Eq. 3.2)}$$

A 5.5-in composite deck system was placed on top of the box beams. The topping was made of 4,000 psi concrete, whereas the box beam was made of a higher-strength concrete. Material characterization determined the compressive strength at 28 days of the concrete specimens tested to be 11,300 psi, see Chapter 2. This value will be used in this grillage analysis to be consistent with the properties of the shear key sections tested in the laboratory. When calculating the stiffness of the composite box beam section, the top layer of deck is transformed based on the modulus ratio of the two concrete materials. Table 3.1 summarizes the sectional properties used in the analysis.

Table 3.1 Sectional properties of grillage elements

	Flexural Stiffness, I, (in^4)	Torsional Stiffness, J, (in^4)	Axial Cross-section Area, A, (in^2)	Shear Area, A_s, (in^2)
Members in longitudinal direction				
Interior box beams	162400	205000	919.5	330
Exterior box beams	162463	205000	1477	778
Members in transverse direction				
Two flanges	148587	205000	695	8.4
Web	229586	330585	1750	1584
Shear key	131072	307712	1536	1584
Intermediate diaphragm	159235	205000	959	396
Endspan diaphragm	177869	205000	1421	1089

The transverse members in the grid were modeled as shown in Figure 3.5. In between the longitudinal members, running along the x axis, a typical transverse member is divided into segments (see cross sections A-A to C-C). Each segment represents a part of the bridge cross-section in the transverse direction. The segment that represents the box beam with the top and bottom flanges in the transverse direction is shown as section A-A in Figure 3.5. Its flexural stiffness is calculated using the two flanges (with a void in-between). Table 3.1 shows this value for "two flanges." The torsional stiffness of this segment is assumed to be the same as that of longitudinal members (as typically done in grillage analysis; Hambly 1991). The segment corresponding to the web section of the box beam has a rectangular cross section, shown in section B-B of Figure 3.5. Section properties for the "web" are presented in Table 3-1. Similarly, the segment corresponding to the shear key also has a rectangular cross section. However its material properties are different (grout). Material properties obtained experimentally were

used for this segment. In addition, the shear key cross-section does not include the deck because the deck and shear key don't act as a composite section.

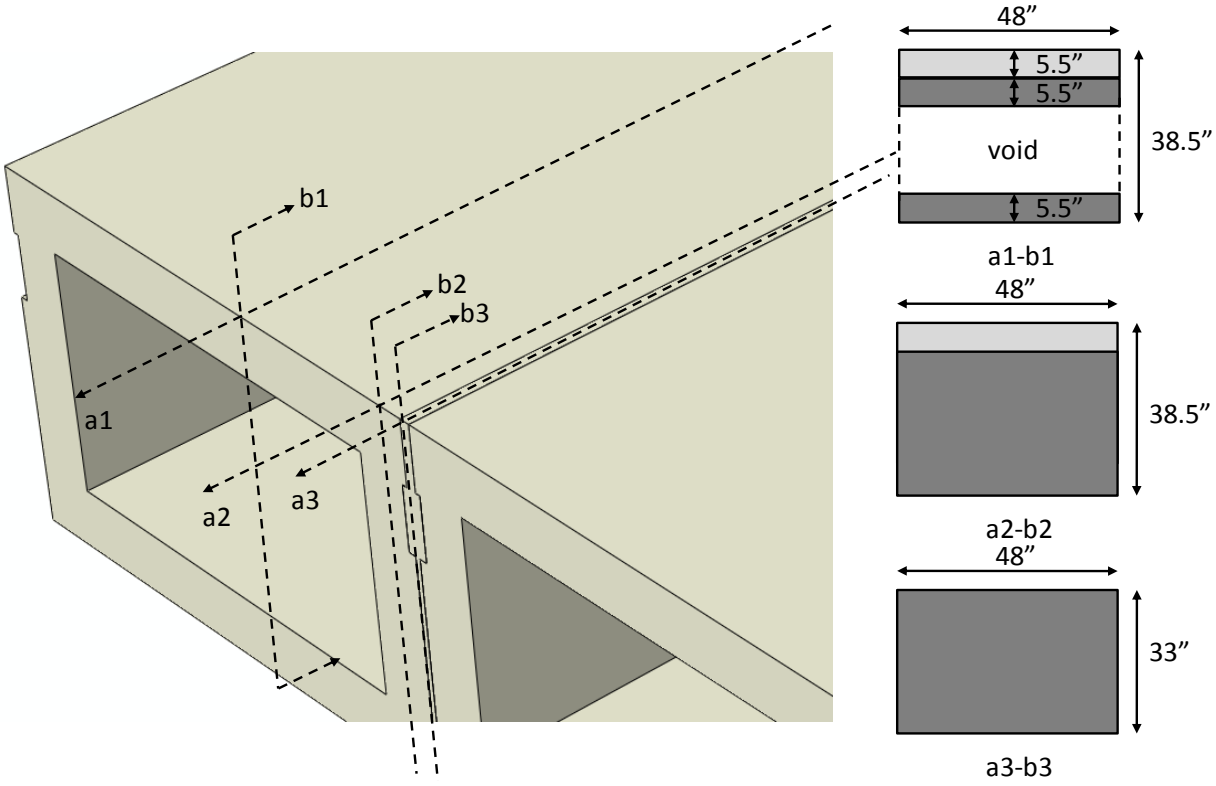

Figure 3.5 Cross sections of a typical transverse member in grillage analysis

The diaphragms inside the box beam were considered because their effect on the distribution of load is significant. The spacing and width of the diaphragms are based on PennDOT Bureau of Design standards BD651M. Figure 3.6 shows the location, dimensions, and cross section of a typical transverse diaphragm and diaphragm dimensions. Properties of transverse members with diaphragms are presented in Table 3-1. They are calculated based on the cross sections shown in Figure 3.6. The solid concrete section (no void between flanges) where the diaphragm is present is represented as a web. The axial cross section area, shear area, and flexural stiffness in the transverse direction are calculated following the procedure discussed previously. The torsional stiffness was assumed to be the same as that of a longitudinal interior box beam, if we neglect the web effect of the diaphragm.

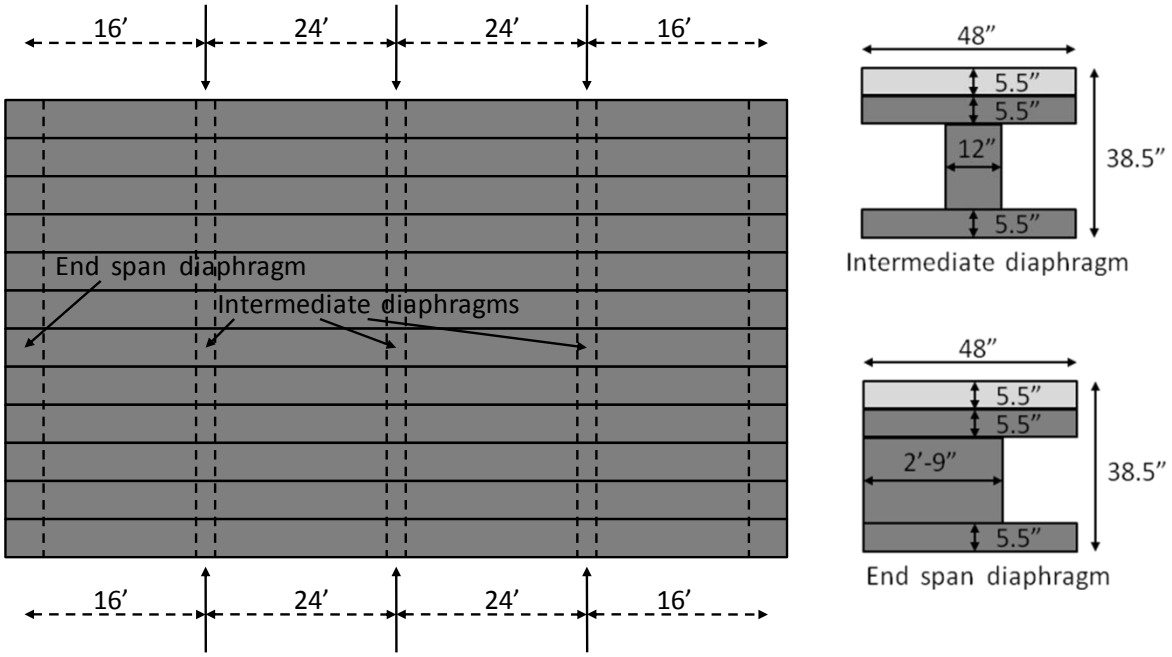

Figure 3.6 Cross section of typical transverse diaphragm members in grillage analysis

3.3.3. Load Combinations

One of the main objectives of conducting a grillage analysis was to determine the critical moment and shear forces in the shear key region that could be used in subsequent finite element analysis. To determine an appropriate range of bending moment and shear force in the transverse members, and thus shear key region, various load combinations and placement of live load were carefully considered. Seven different live load configurations expected to produce greater load effects were selected. They are summarized in Table 3.2, where uppercase letters represent AASHTO HS25 truck load and lowercase letters represent AASHTO design lane load or PennDOT P-82 at various locations of bridge deck, as illustrated in Figures 3.7 and 3.8.

The following loading cases were considered to produce maximum load effects: Case 1, an HS25 truck near the edge beam at the mid span of the bridge; Case 3, two HS trucks on opposite edges at the mid span of the bridge; Case 4; and Case 6, which adds the design lane load to the edge lane of the bridge. These four cases would likely produce the maximum negative moments in the transverse members, or shear keys, at the mid span. Case 2, an HS25 truck at the center of the bridge, and Case 5, an HS25 truck at the center of the bridge plus two design lane loads occupying the two interior lanes would produce the largest positive moment in the shear key at the mid span of the bridge. Last, the case in which a truck overload (P-82) is placed on the edge lane of the bridge (Case 7) was also investigated.

Table 3.2 Load cases considered in this study

Load Case No.	Live Load Configuration
1	D
2	E
3	D, F
4	D + a
5	E + b, c
6	D, F + a, d
7	PennDOT P-82 on edge beam

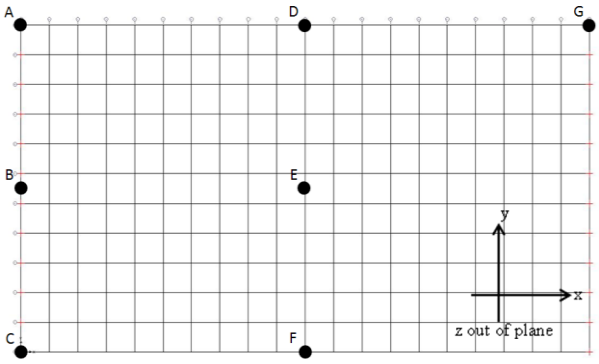

Figure 3.7 Locations to put the AASHTO HS25 design truck

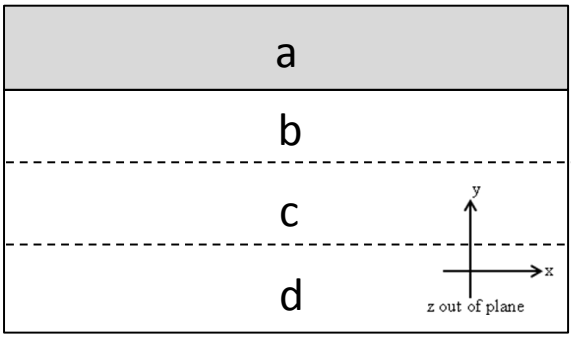

Figure 3.8 Locations to put the AASHTO design lane load (only lane load in location “a” is highlighted for clarity)

3.4 Results and Discussion

Bending moments and shear forces from the grillage analysis were examined. The longitudinal members carried larger bending moments compared to the transverse members, as expected. Figure 3.9 shows the bending moment on the transverse member across the mid span (see Figure 3-3) when the system was subjected to load case 7. The figure shows bending moments expressed in terms of the node location in the transverse direction from one end of the bridge to the other. Note that there is a discontinuity in moment magnitude where the transverse beam intersects with longitudinal beam members. This is expected, as the torsional moment of the longitudinal beam becomes part of the moment equilibrium about the global y-y axis, as shown in Fig. 3.9: the sum of bending moments on the transverse beam and torsional moments on the longitudinal beam equals zero. This check verifies the validity of the grillage model developed.

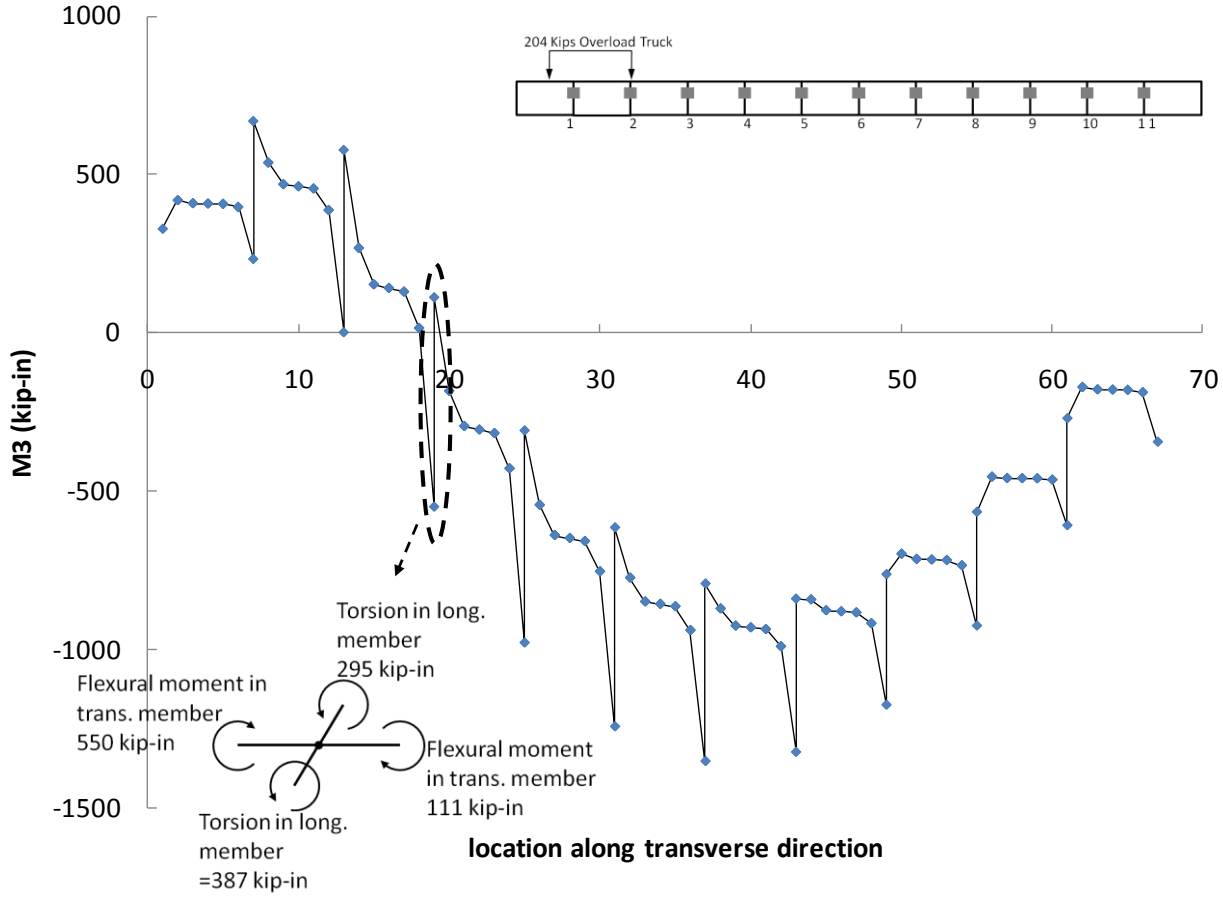

Figure 3.9 Transverse moment at the midspan, LC7

The transverse beam presents rigidity in discrete locations while in reality there is no physical beam in that direction. Therefore, the bending moments on the shear key region should be averaged out. Figure 3.10 shows the transverse moments in terms of shear key locations from

one end of cross section to another in x-axis; averages are also indicated. A similar procedure is applied when plotting the shear forces in the shear key.

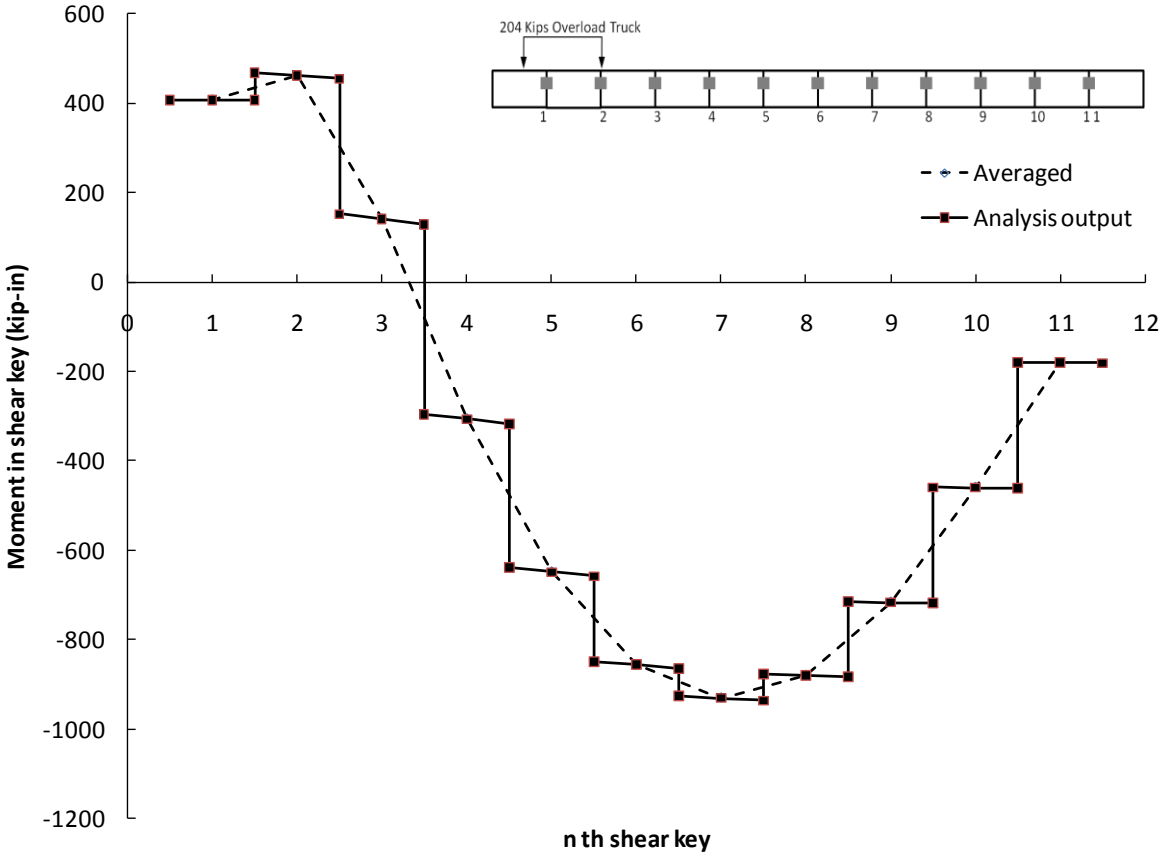

Figure 3.10 Transverse moments in shear key regions

The results of grillage analysis are summarized in Figures 3.11 and 3.12 where the average moment and shear force are plotted at each shear key location for all the load cases. It can be observed that two load cases, LC5 and LC2, create the largest maximum positive moments (which creates tension stresses at the bottom of the shear key) for shear key locations 3 through 10. The largest magnitude is found at mid span (shear key 6) under LC5, where a HS 25 truck at the center of the bridge plus two design lane loads occupy the two interior lanes. This result is tabulated in Table 3.3. For shear keys located near the exterior beam (1, 2, 10, 11), LC4 controls; however, its magnitude is four times smaller than the one obtained under LC5. The maximum negative moment, which creates tension stresses at the top of the shear key, was found to be created by LC6 (two HS trucks on opposite edges at the mid span of the bridge plus lane load) on shear key 6 (mid span). This result is tabulated in Table 3.3.

The maximum shear forces were found to be influenced by the position of the design truck. For each load case, the maximum shear force was located in the shear key closest to the position of the truck. The largest magnitude corresponds to LC4, where truck and lane loads were placed at the edge of the bridge.

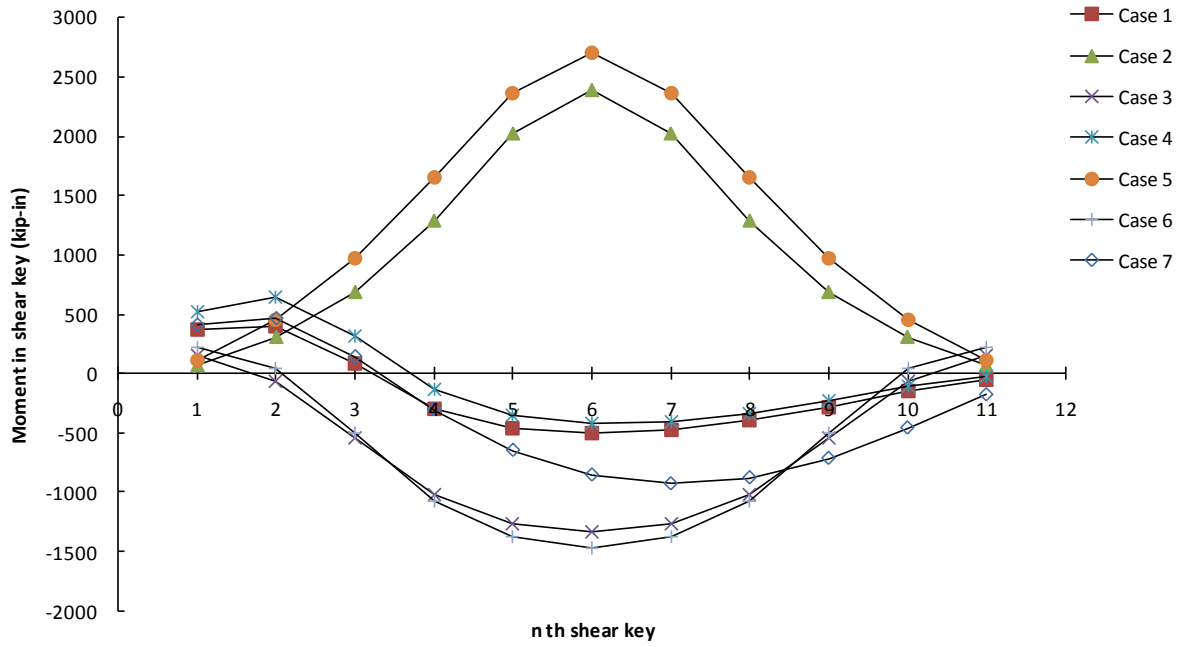

Figure 3.11 Average moment in shear keys for all load cases

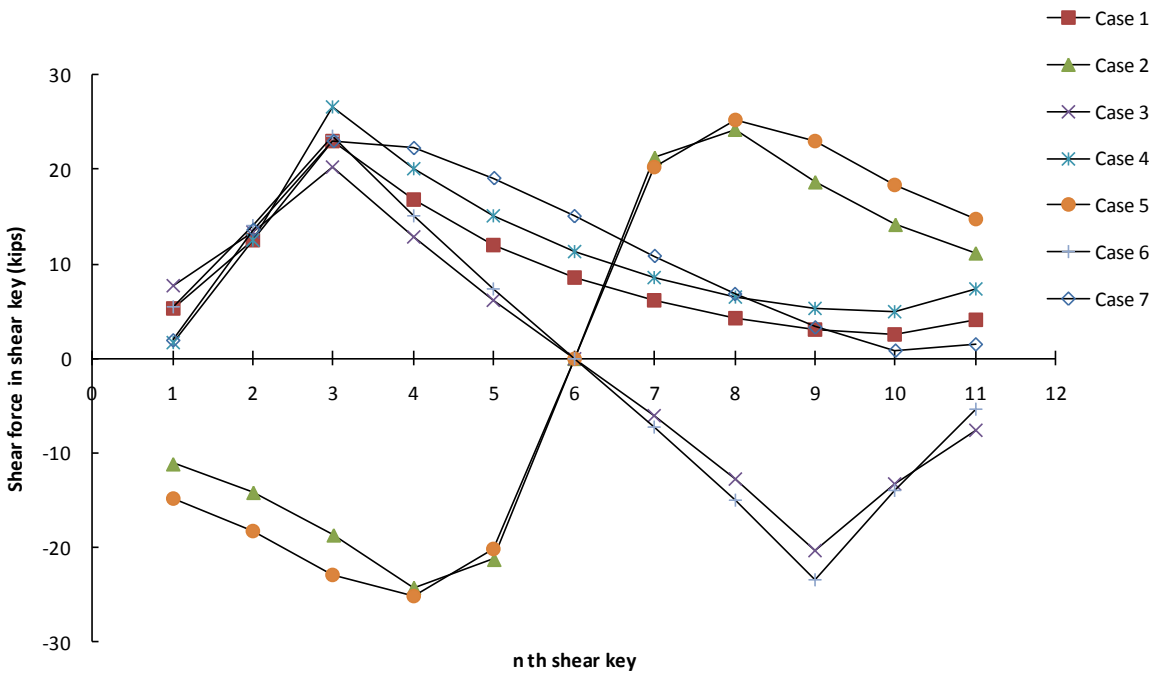

Figure 3.12 Average shear force in shear keys for all load cases

To summarize, the maximum load effects are determined as follows:

- Max positive moment = 2,701 kip-in, shear = 0 kips (load case 5), shear key 6 (midspan)
- Max negative moment = -1,470 kip-in, shear = 0kips (load case 6), shear key 6 (midspan)
- Max shear = 26.7 kips, moment = 306 kip-in (load case 4), shear key 3 (edge)

Table 3.3 Summary of the moments and shear force for all seven cases

Case Number	Maximum Moment (kip-in)	Location (nth Shear Key)	Maximum Shear Force (kip)	Location (nth Shear Key)
1	-508	6	23	3
2	2393	6	24.3	8
3	-1340	6	20.3	3
4	650	2	**26.7**	3
5	**2700**	6	25.3	8
6	**-1471**	6	23.5	3
7	-931	7	23	3

These three load cases will represent the behavior of shear keys at midspan and the edge of the bridge, thus providing an appropriate framework to explore the effects of connection modifications (geometry, material, transverse post-tensioning). Results from this analysis will be presented in the next chapter.

Chapter 4. Finite Element Analysis

4.1 Introduction

The purpose of the numerical models conducted in this study was to (1) validate the experimental shear tests conducted during the laboratory phase of the project, and (2) explore the effects of changes in the shear key configuration, grouting material, post-tensioning, and bearing pad positioning in the behavior of the shear key region between adjacent precast concrete box girders. A commercially available finite element software, ABAQUS (version 6.9), was used to build all numerical models. Material properties for the concrete, cementitious grout, epoxy grout, and interfaces obtained from the material characterization tests (see Chapter 2, section 2.2) were used in these models.

4.2. Modeling of the Shear Key Test

Results from the experimental shear tests of shear key specimens were presented in Chapter 2. Table 2.15 summarizes the principal findings from the shear test of epoxy and cementitious grouted specimens. Results from the numerical models developed in this section are compared with the experimental observations, in particular principal failure modes, crack sequence, and specimen strength levels. The purpose of this comparison was to gain insight into the capabilities of the developed finite element models to predict the occurrence of cracking or damage in the shear key region. This information was used to develop the numerical models of shear keys placed on adjacent concrete box girders, Section 4.3.

4.2.1 Geometry and Boundary Conditions

The configuration of the shear test is described in detail in Section 2.3.4 of Chapter 2, laboratory evaluation. A few important features of the test setup are highlighted in Figure 4.1, as they determined geometry and boundary conditions of the developed models. Figure 4.1a shows the dimensions of the shear key specimen and surrounding supports. The shear key specimen was placed into a steel socket (right side of the specimen), as shown in Figure 4.1b. The steel socket consisted of two angle plates gripping onto the shear key flange on each side of the specimen and one top plate to prevent vertical movement of the specimen. Its main purpose was to serve as a fixed support to the shear key specimen. On the free end of the specimen (left side of the specimen), a steel beam was placed to restrain the specimen movement in the horizontal direction. The load was applied as a downward point load by the hydraulic actuator onto a 2-in-wide steel plate (Figure 4.1a).

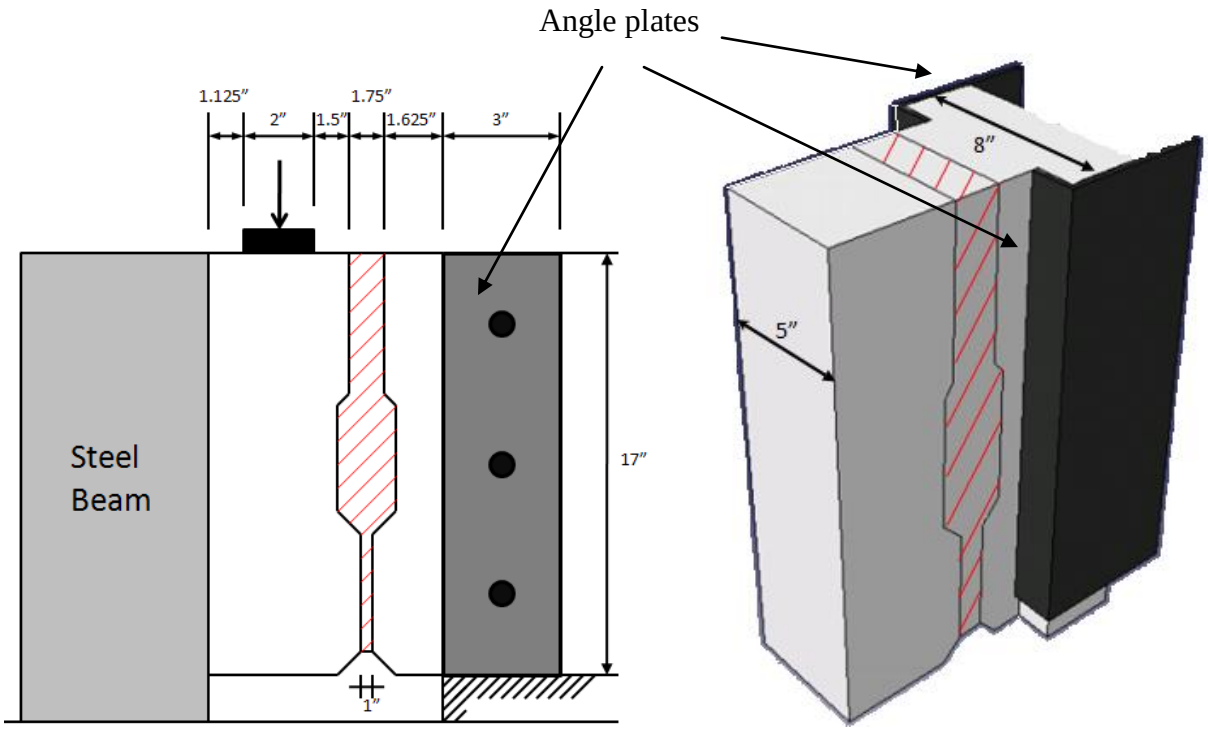

a) b)

Figure 4.1 a) Front view and b) 3-dimensional rendering of the experimental shear test

Using this information, a two-dimensional FE model was created using ABAQUS. The geometry of the model followed the actual dimension of the specimen tested. Specimen thickness was defined as 4.75 in (8 in was assumed for the concrete region inside the steel socket). Two boundary conditions were investigated to evaluate the support conditions in the experimental test setup. They are shown in Figure 4.2. The reaction provided by the steel beam on the left side of the specimen was modeled assuming a restraint of horizontal movement (u1 = 0). The support on the right side of the specimen required further study. Due to the possibility of localized slip or deformations between the concrete and the steel socket, two conditions were evaluated: the first model (see Figure 4.2a) assumes that the steel socket provides full restraint of displacement in the horizontal and vertical direction as well as in-plane rotation (therefore u1 = 0, u2 = 0, and u3 = 0); the second model (see Figure 4.2b) includes the possibility of deformation of the concrete, except in the contact regions with the steel plates. Results from these two models showed that the behavior of the shear key specimen was not significantly influenced by these two types of boundary conditions. Therefore, the first boundary condition, shown in Figure 4.2a, was used due to its simplicity for all models described in this section.

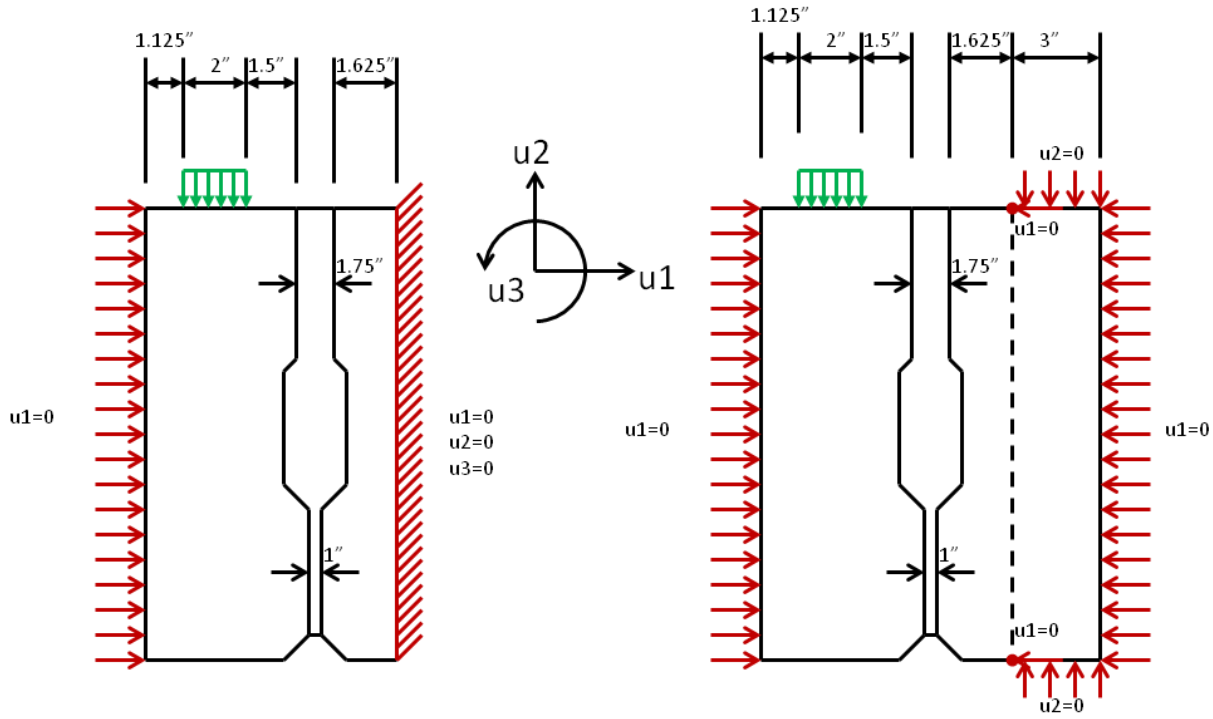

Figure 4.2 Two FE models of the shear test (boundary conditions differ)

4.2.2. Material Models

A plastic-damage model (available in ABAQUS) was used to predict the constitutive behavior of the concrete and grouting materials, epoxy and cementitious, as well as their respective interfaces. This approach assumes that compressive crushing and tensile cracking are the main failure mechanisms of these materials. Both of these phenomena are the result of microcracking. Tensile cracking and compressive crushing are interpreted as a local damage effect controlled by a yield function, which defines their onset and evolution. Particular details of the mathematical implementation of these ideas to model quasi-brittle materials are given by Lubliner et al. (1989) and Lee and Fenves (1998).

Input parameters required for this type of plastic-damage model are: compressive stress-strain relationship, elastic modulus, tensile strength, dilation angle, and fracture energy. Results from the material characterization described in Chapter 2 were used as input parameters. Details of this implementation are described next.

Compressive behavior: The stress-strain curve of the cementitious grout under uni-axial compression was assumed to follow a parabolic function, shown in Equation 4.1, as defined by Todeschini et al. (1964):

$$f_c = \frac{2f_c^{"}\left(\varepsilon/\varepsilon_0\right)}{1+\left(\varepsilon/\varepsilon_0\right)^2} \qquad \text{(Eq. 4.1)}$$

$$f_c^{"} = 0.9f_c'$$

$$\varepsilon_c = 1.71 f_c'/E_c$$

The compressive stress-strain relationship of the concrete and epoxy grout was calculated based on the formula developed by Thorenfeldt et al. (1987):

$$\frac{f_c}{f_c'} = \frac{n\left(\varepsilon_c/\varepsilon_0\right)}{n-1+\left(\varepsilon_c/\varepsilon_0\right)^{nk}} \qquad \text{(Eq. 4.2)}$$

$$n = 0.8 + \left(\frac{f_c'}{2500}\right)$$

$$k = 1$$

$$\varepsilon_0 = \frac{f_c'}{E_c}\left(\frac{n}{n-1}\right)$$

These functions have been proven to be appropriate for the modeling of concrete structures. It is expected that they can also represent the behavior of the epoxy and cementitious grout in compression. Figure 4.3 shows the compression stress-strain curves for epoxy, concrete, and cementitious grout. Table 4.1 shows the maximum compressive strength values for all the materials used in the numerical models.

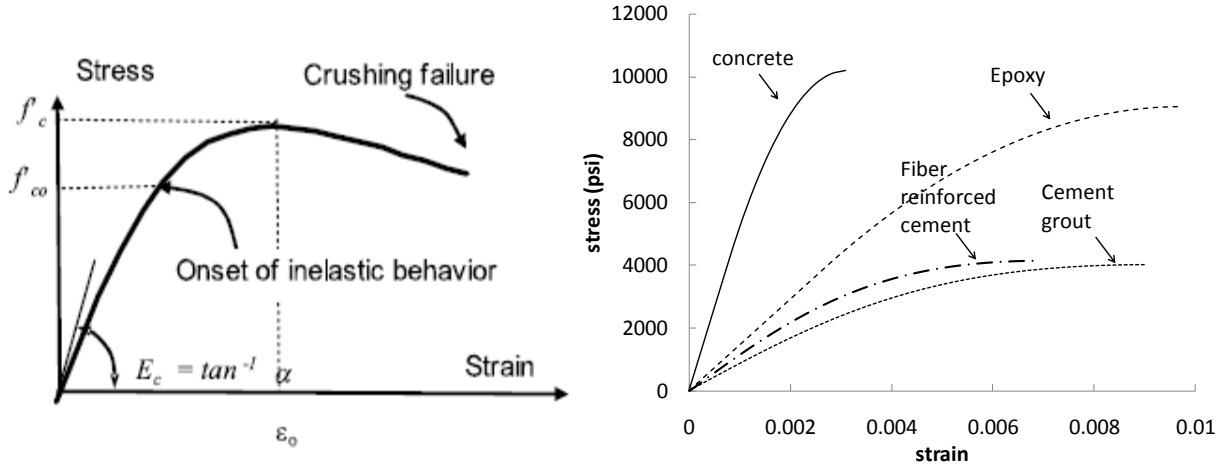

a) General curve b) Generated curves used for FE analysis

Figure 4.3 Analytical stress-strain behavior of concrete and grouting materials under uniaxial compression

Table 4.1 Material properties used in the numerical models

Material	Concrete	Epoxy Grout	Concrete-epoxy Interface	Cementitious Grout
Density (lb•s^2/in)	0.00022487	0.00022487	0.00022487	0.00022487
Compressive strength (psi)	11329	10036	11329	4474
Splitting tensile strength (psi)	741	1325	730	100.3
Modulus of elasticity (psi)	5.26 x 10^6	1.46 × 10^6	5.26 x 10^6	8.37 x 10^5
Fracture energy (lb/in)	0.9022	1.613	0.6652	0.05082

Elastic modulus: The elastic modulus of the grout (cementitious and epoxy) was determined experimentally. The values presented in Table 4.1 were used in the numerical models. For the concrete, epoxy grout, and concrete-grout interfaces, the elastic modulus was determined analytically using the ACI Committee 363 proposed equation for high-strength concrete:

$$E_c = 40{,}000\sqrt{f_c'} + 1.0 \times 10^6 \qquad \text{Eq. (4.3)}$$

where *f'c* is the uniaxial compressive strength in psi.

Tensile strength: Experimental results from the splitting tensile tests were used as tensile strength of the concrete, grouting materials, and the concrete-grout interfaces. Table 1 shows the values used in the numerical models.

Dilation angle: Based on previous numerical work conducted by the PI's research group (Coronado and Lopez 2010), the dilation angle was assumed to be 38 degrees for all materials.

Fracture energy: The plastic-damage model described above uses the concept of fracture energy, G_F (energy, per unit area, needed to create and propagate a crack in a particular material or interface) to predict the inelastic behavior of the concrete, grout and their interfaces. A softening curve is used to predict the damage progression. This curve is often approximated using a linear model, as shown in Figure 4.4c. The cohesive fracture energy is calculated as the total area under the load-LVDT curves obtained from the notched beam tests described in Chapter 2. Specific details of this procedure, described in Coronado and Lopez (2008) and Elices et al. (2002), were used to calculate the fracture energy values presented in Chapter 2, section 2.2.1. In particular, fracture energies of concrete-epoxy (or more specifically for this study, concrete-grout interfaces) were obtained. Table 4.1 shows the fracture energy values used in the numerical models. It should be pointed out that all values were obtained experimentally, except for the fracture energy of the epoxy grout, which was calculated based on the relative strength of the epoxy versus concrete.

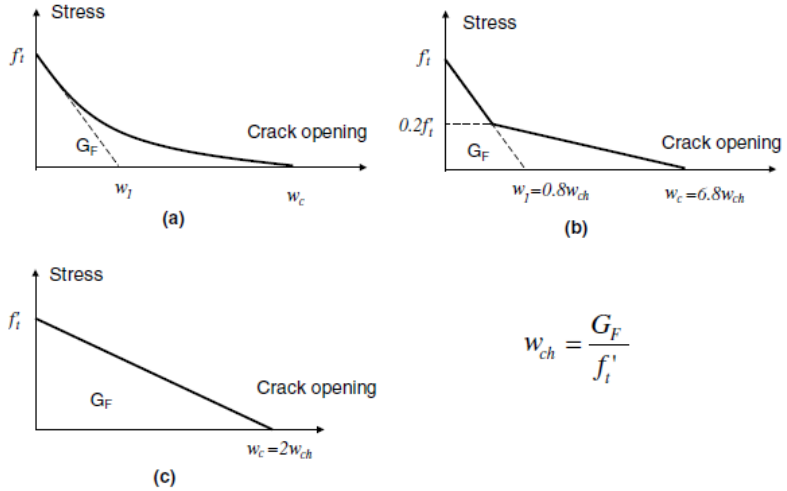

Figure 4.4 Softening model for concrete (Coronado and Lopez 2006)

The concept of “damage band” has been used to model the behavior of the interface between concrete and epoxy in adhesively bonded FRP repairs (Coronado and Lopez, 2007, 2008, 2010). In the numerical model of the shear test, it was used to characterize the interface between the concrete and the grouting material. Physically, a region where damage or cracking occurs between two dissimilar materials can be represented as a damage band. This “band” has similar fracture properties as plain concrete, but its fracture energy and tensile strength could be different. Experimentally, it was found that the shear tests of epoxy-grouted specimens failed in the concrete region prior to any failure in the grout. Therefore, for the modeling of this type of failure, the damage band was placed on the concrete side in the vicinity of the epoxy shear key. Figure 4.5a) shows the dimensions of the damage band used in the numerical model of the shear test. When modeling the cementitious grout, the damage band was not assigned as a region in the model because the cementitious grout is weaker than plain concrete (its fracture energy is two orders of magnitude smaller than that of plain concrete) and therefore its properties would control failure. Test observations were consistent with this assumption: cracks occurred at the shear key interface (edge) between the two materials. Therefore, the shear key was modeled using the material properties of the cementitious grout and the fracture energy of the concrete-cement interface. The numerical model of the cement-grouted shear test specimen is shown in Figure 4.5b).

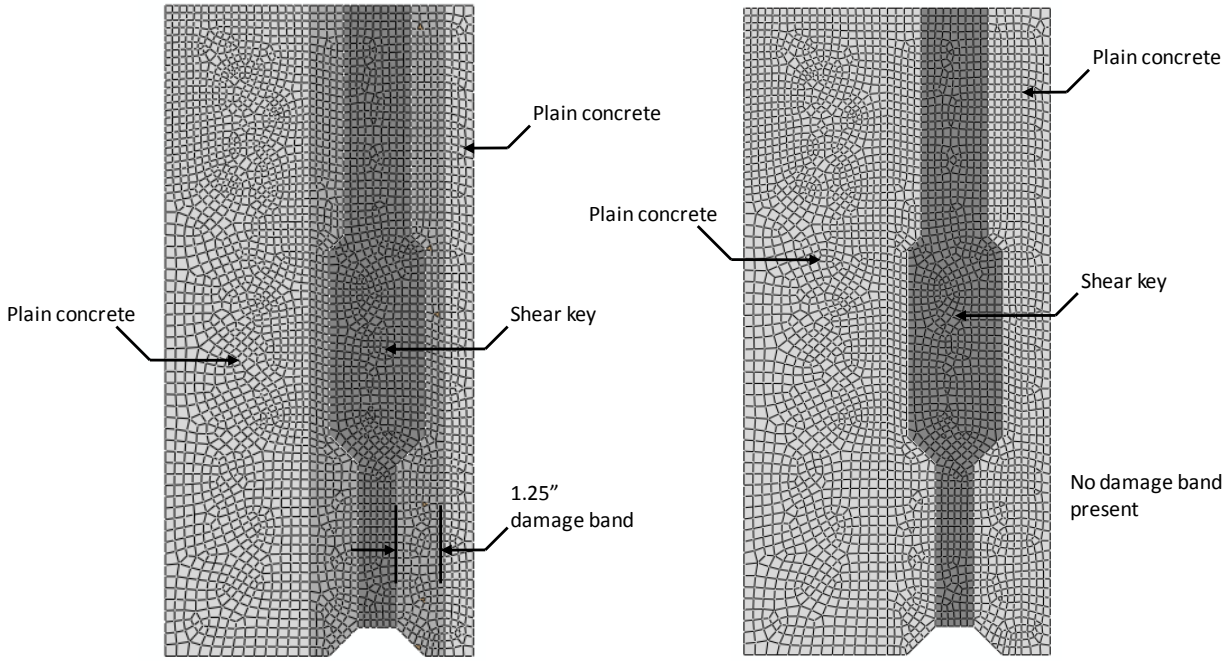

a) Epoxy-grouted shear key specimen b) Cement-grouted shear key specimen

Figure 4.5 Material property assignments in the epoxy grout models

4.2.3. Elements and Mesh

The element type used for all materials of the shear test model was a four-node plane strain (CPE4R) element, where each node consisted of two DOF, as shown in Figure 4.6. A plane strain element was selected because the strain in the out-of-plane direction was assumed to be

uniform; the thickness in the out-of-plane direction was significantly large (4.75 in) with respect to the dimensions of the model in the in-plane directions.

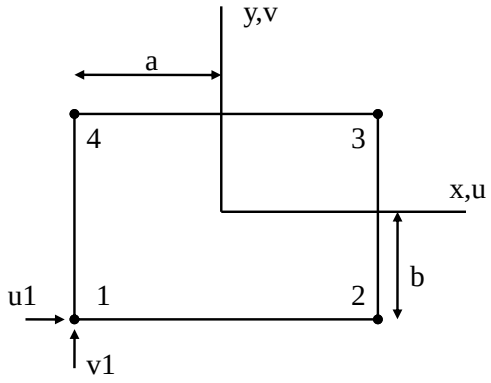

Figure 4.6 Nodes bilinear element

The R in the element type designation indicates reduced integration. Reduced integration uses a lower-order integration to form the element stiffness, thereby reducing running time. For example, CPE4 uses four integration points, whereas CPE4R uses one integration point. Consequently, element assembly is approximately four times more costly for CPE4 than for CPE4R. Element distortion control and hourglass control were enabled to help with convergence because one integration point tends to cause the element to distort in such a way that the strains calculated at the integration are all zero, which, in turn, may lead to uncontrolled distortion of the mesh.

Meshing of the model is shown in Figure 4.7. Areas of interest in the model have a finer mesh. Region 1 may experience stress concentration due to the concentrated load; region 2 represents the damage band where the possibility of crack occurrence is high; and region 3 is the shear key. All three regions are given a fine mesh. Region 4 is an area of less interest; therefore the meshing of region 4 is coarser and tries to accommodate the meshing of other regions. The typical mesh size for fine mesh in the model is about 0.2 in while that of the coarse mesh is around 0.5-1 in. In addition, the mesh in the model was arranged so that it was composed of rectangles for the most part or four-node elements, as shown in region 1. The meshes in region 2 and 3 were non-rectangular because of the irregular geometry of the shear key.

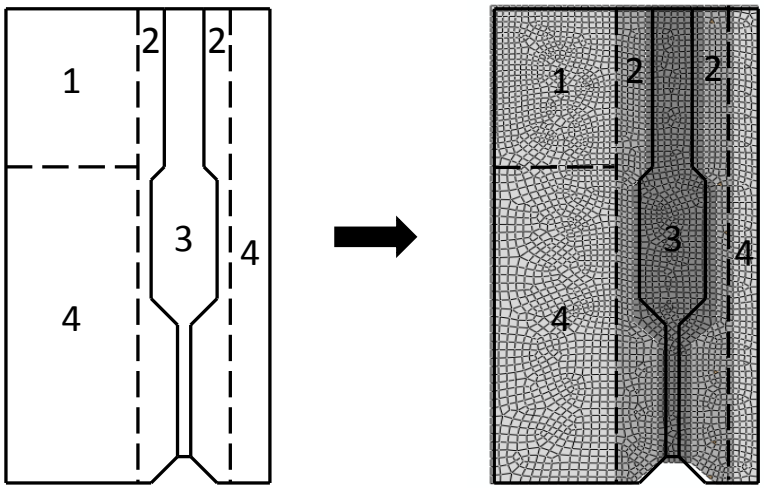

Figure 4.7 Mesh configurations for the FE model of the concrete-grout shear key specimen

In the model of epoxy grout shear key, the bond between the epoxy grout and concrete is very strong. Therefore, the surfaces of epoxy grout and concrete are modeled using a TIE command, which means that all degrees of freedom at the interface are locked together. As proved by the experimental data, any crack that occurred in the epoxy-grouted specimens went through the epoxy grout-concrete interface as if they had perfect bond. The same constraints were used in the cement grout model. However, due to the large differences in orders of magnitude of the fracture energies of the concrete and the cementitious grout, cracking was expected to occur within the shear key following its edge.

4.2.4 Results and Discussion

Results from the numerical modeling of one epoxy and one cementitious (no fibers) grouted specimen are presented in this section. Only the first cementitious test is used for comparison, since results from the second test appear to be influenced by the surface preparation of the shear key (see Section 2.3.4).

Failure modes

Both numerical models failed by shear, as indicated by the orientation of the main cracks connecting the loading region with the support. The numerical models were able to show differences in crack patterns as well as failure load, as were found in the experimental tests (see Chapter 2). At failure, the FE model of the epoxy grout specimen showed areas of damage (defined in terms of plastic strain) in the damage band region and shear key similar to the experimental tests, as shown in Figure 4.8a. The cracks occurred at a predicted load of approximately 85.5 kips and propagated through the entire shear key at a failure load of 115.7 kips.

The cementitious grout model showed all major cracks occurring inside the shear key. The adjacent concrete did not fail. Moreover, the cracks in the shear key region generally followed

the interface (edge) of the shear key. Top and bottom cracks are joined diagonally through the shear key. This damage pattern is very similar to the one observed in the experimental test, as described in more detail next.

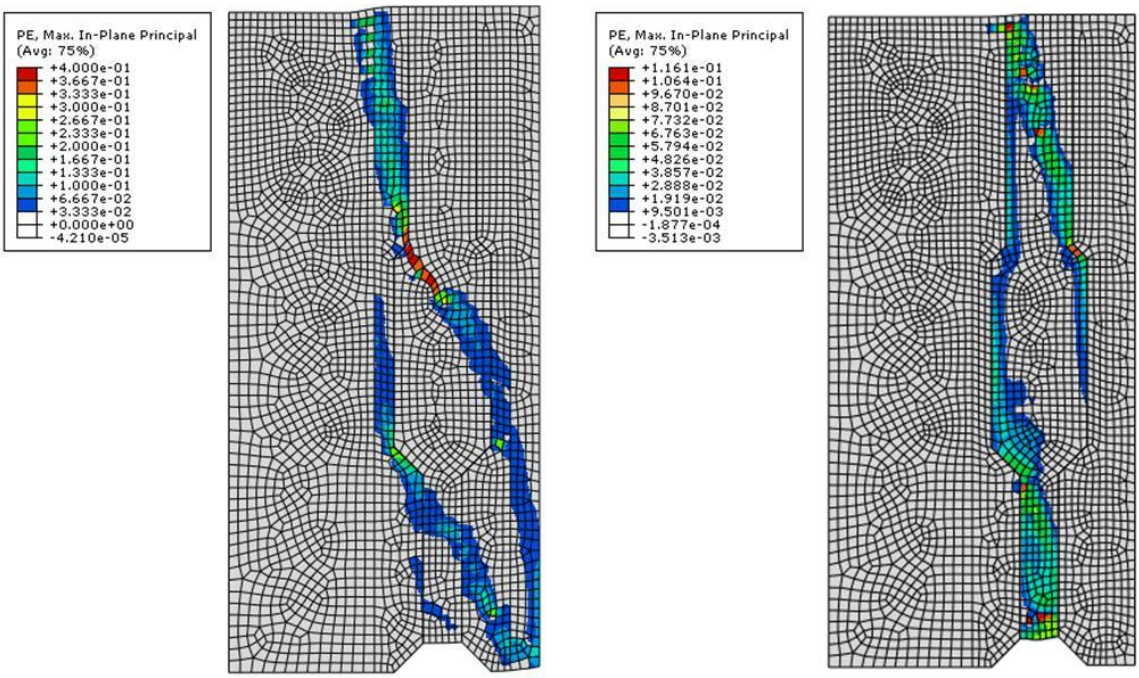

a) epoxy grout model b) cement grout model

Figure 4.8 Damage regions at failure for epoxy and cement grout models

Crack Sequence

Epoxy grout specimen

The crack sequence on the FE model of the epoxy grout specimen was characterized by three stages, shown in Figure 4.9. In stage 1 the applied load increased from zero to 76 kips (in the numerical model). In this initial stage, plastic strain, which can be used as an indicator of damage, develops as the load increases. The applied load creates shear forces that produce a maximum principal tensile stress in a diagonal direction in the specimen. Just before the first major crack occurs, a sloped strip of plastic strain concentration develops near the fixed supported edge in the model. Minor cracks formed in the vertical direction initiating from the bottom of the support. This type of crack was observed during the experimental tests and is captured by the numerical model, as shown in Figure 4.9a. The load at which this crack occurred experimentally is 10% smaller than the numerical one. The second stage of the crack sequence occurred at an applied load of 85.5 kips (in the numerical model). A major crack was initiated at the loading point and propagated diagonally toward the bottom support, as shown in Figure 4.9b). This main crack was also observed in the experimental test at a smaller load level, see Table 4.2. At this load level the crack width of the main crack was small and a few additional shear cracks developed at the top corner near the support. The last stage of the

crack sequence (stage 3) was the opening of the main crack, while another crack propagated from the loading point toward the bottom support on the top region of the shear key; see Figure 4.9c. This failure mechanism occurred at a load level of 115.7 kips. Note that the experimental test was stopped at 90 kips as the specimen underwent large deformation and approached the clearance at the bottom of the test setup.

Table 4.2 Crack sequence of epoxy grout model

Crack Designation	Load Level in FE Model (kips)	Load Level in the Test (kips)
1	76	67.3
2	85.5	76.3
3	115.7	90.1

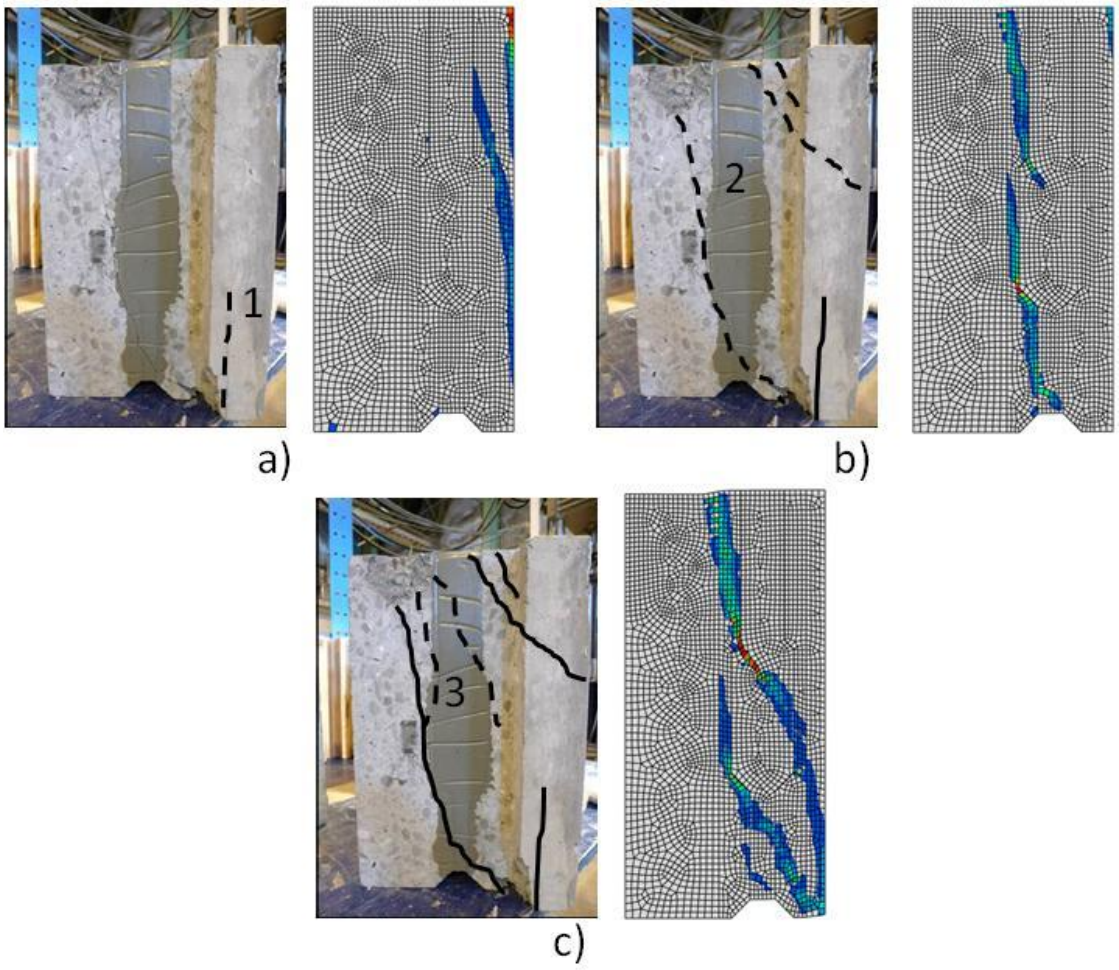

Figure 4.9 Crack sequence of the experimental and numerical shear test of epoxy grout: a) Step 1; b) Step 2; c) Step 3

Cementitious grout specimen

The crack sequence on the FE model of the cementitious grout model can be described in two stages. In the first one, cracks started to form at the interface between the concrete and the shear key at a very early loading level (8.6 kips). Experimentally, cracks at such early stage will be of the size of hairlines, making it difficult to detect with the eye. However, the experimental response shows a change in stiffness around 5 kips of load (see Figure 2.29). At the load level of 60.7 kips, the FE model predicted that the specimen would fail by total debonding of the interface between the concrete and the shear key. At this second stage, shear cracks developed with increasing loads, as shown in Figure 4.10b. The FE results indicate that this type of failure is brittle in nature. Similarly, in the experimental tests, no major cracks were found by visual inspection up to a load level of 38.1 kips when a major crack initiated at the bottom of the shear key region and propagated in a sudden manner along the interface. The experimental test was stopped at this point so photographs could be taken of the cracks without further damaging the shear key region.

Table 4.3 Crack sequence of the cementitious grout model

Crack Designation	Load Level in FE Model (kips)	Load Level in the First Test (kips)
1	8.6	<5
2	60.7	>38.1

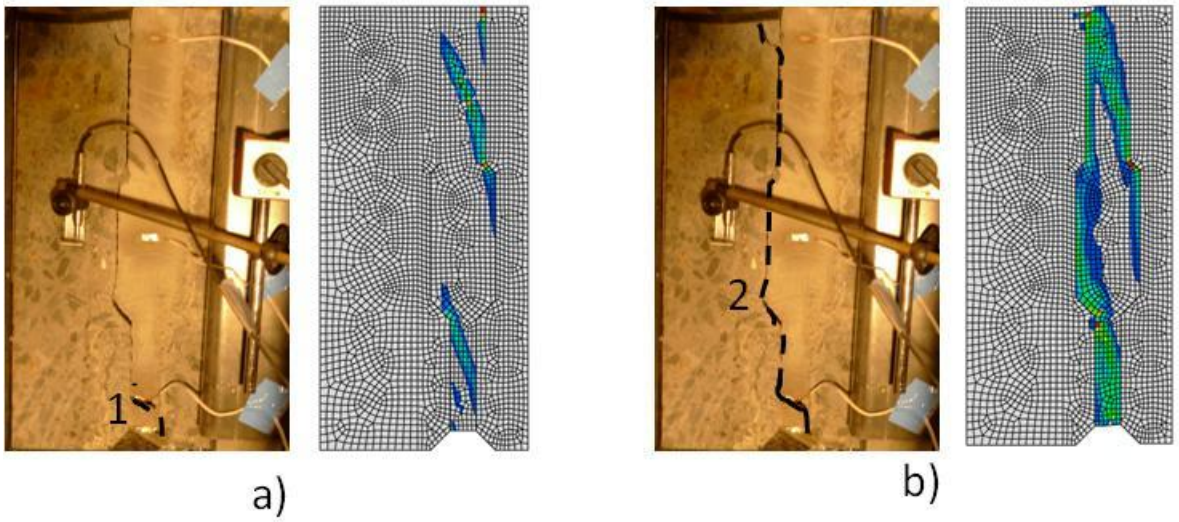

Figure 4.10 Crack sequence of the experimental and numerical shear test of cementitious grout: a) Step 1; b) Step 2

4.2.5 Modeling Remarks

Results from the numerical models developed in this section were compared with the experimental observations from the shear tests of concrete-grout specimens. The FE models were able to predict the differences in failure modes observed in epoxy and cementitious grout specimens as well as the experimentally observed crack sequence and patterns, and strength

levels. Therefore, the modeling approach discussed in this section was extended to model the shear keys of the bridge model developed in Chapter 3.

4.3. Modeling of the Shear Key Region

4.3.1 Modeling Approach

The modeling approach developed in Section 4.2 was used in this section to model the shear key region between adjacent precast box girders. Moments and shear forces obtained from the grillage analysis developed in chapter 3 were used as external loading for this region. The effects of changes in the shear key configuration, grouting material, post-tensioning, and bearing pad positioning were evaluated. The numerical model of an isolated shear key was created following the shear key geometry in accordance with PennDOT's specifications (PennDOT BC775M). Details of the geometry, loading, and material properties used are described next. Note that a partial depth shear key with cementitious grout was used as the basic case for comparison with other models. Figure 4.11 shows this shear key under a combination of positive shear force and positive moment.

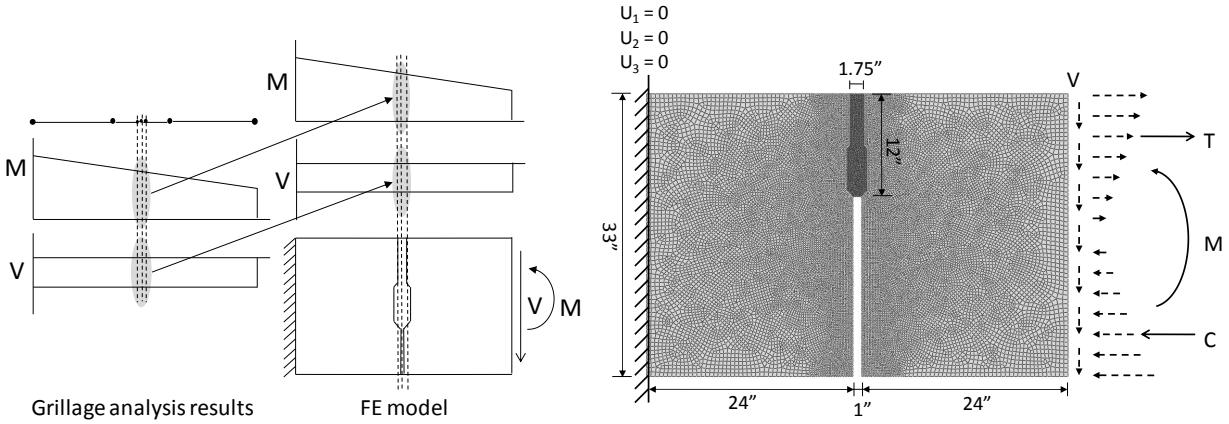

Figure 4.11 Numerical model on an isolated partial-depth shear key with cementitious grout under a combination of shear and moment

Geometry

Since the objective of this model was to assess the effect of different shear key modifications on the shear key region between adjacent precast concrete box girders, the geometry of this model reflects the geometry of the prototype bridge discussed in Chapter 3. The same box beam (BII-48) used in the grillage analysis was modeled as shown in Figure 1 (right): two halves of the box beams are connected by a shear key in the middle. The concrete box girders are assumed solid. There are two reasons for this modeling approach: (1) the maximum moments and shear occur at mid span (as described in Chapter 3) where there is a diaphragm, as shown in Figure 3.6; and (2) without modeling the steel reinforcement, the web of the box beam may undergo large deformations and most likely cracks under shear and flexural effects. It should be

pointed out that the main objective of this analytical evaluation was to accurately model the shear key region, not the entire precast box girder.

Boundary conditions and loading

To recreate the state of stresses in the shear key of the real bridge, the moments and shear forces from the grillage analysis were applied to the geometry described above using a statically determinate system. The left edge of the model was assumed to be fixed (u1=0, u2=0, and u3=0). Loading was applied on the right edge of the model by a combination of axial stress distribution and vertical shear stress distribution to create a resultant moment and shear at the shear key location that matched the combinations of moment and shear obtained from the grillage analysis. Recall that in the grillage analysis, the maximum moment and shear forces were calculated at the shear key location, as shown in Figure 4.11a.

Element type and meshing

As used in the shear test models described in section 4.2, a four-node bilinear plane strain element (CPE4R) was used in this model. Each shear key model represented one isolated shear key with a thickness in the transverse direction of 48 in, based on the grillage analysis developed in Chapter 3. The large majority of the elements were rectangular to increase the accuracy of the numerical model. The concrete region in the vicinity of the shear key (Region 1 in Figure 4.12a) as well as the shear key itself were considered areas of interest where cracks were likely to occur; therefore, a fine mesh (0.2 in) was assigned to these regions. Other regions were assigned a coarser mesh (0.5 in for region 2).

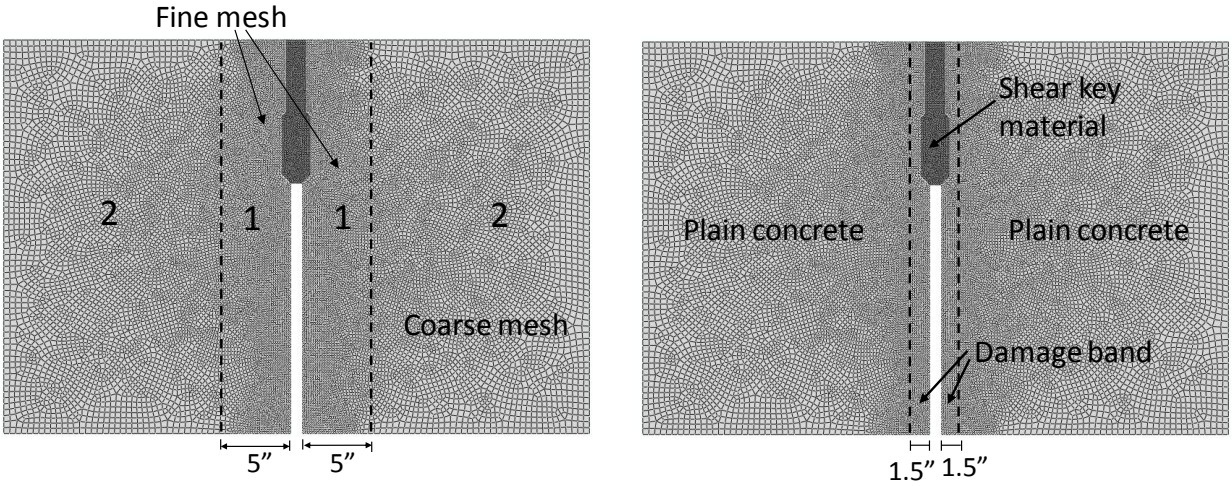

Figure 4.12 a) Mesh configuration of the shear key FE model; b) Material used in the shear key FE model

Material properties

After verifying the validity of the material models used in the concrete-grout shear key specimens, the same material properties were used for the shear key model in the real bridge. The material properties are listed in Table 4.1. Figure 4.12b shows the assignment of the material properties. For models using epoxy grout, a damage band was used (1.5-in thick) in the region enclosed by the shear key contour and the dotted lines. Material properties for this damage band are listed in Table 4.1. For models using cementitious grout, no damage band was assigned, as discussed in section 4.2. The shear key was assigned material properties of either epoxy or cementitious grout. These properties are listed in Table 4.1. Plain concrete properties were assigned to the remaining regions of the numerical model, also listed in Table 4.1.

4.3.2 Analysis of Typical PennDOT Shear Keys

To better understand the effect of each possible shear key modification (shear key configuration, grouting material, post-tensioning, and bearing pad positioning) on shear key behavior, each individual effect was evaluated independently. Thus, the first step of this analytical study was to examine the state of stresses (and possibility of cracking) of shear keys designed with current PennDOT design procedures.

Load cases

Based on the results from the grillage analysis, three load cases were chosen to represent the critical combinations of moment and shear force that act on the shear keys of a typical bridge (described in Chapter 3). The three load cases create the maximum negative moment, the maximum positive moment, and the maximum shear on shear keys. The magnitudes of the load cases are presented in Table 4.4. All three load effects happen at the mid span of the bridge. Their transverse locations are illustrated in Figure 4.13 and listed in Table 4.4.

Table 4.4 Load cases used in shear key FE model

	Moment (kip-in)	Shear (kips)	Location
Load case 5, Max M-	-1470	0	6
Load case 6, Max M+	2701	0	6
Load case 4, Max V	306	26.7	3

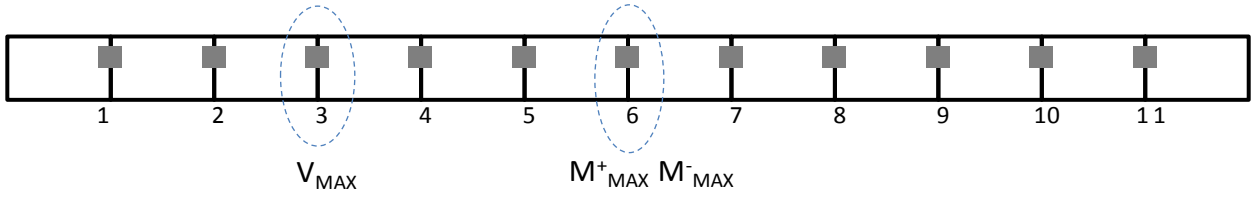

Figure 4.13 Location of shear keys along the transverse direction of the bridge

An FE model of a partial-depth shear key with cementitious grout was evaluated under these three load cases. Results indicated that the shear key cracked under all three load cases. The predicted crack pattern for all three load cases is shown in Figure 4.14. These results also show the locations of crack initiation on the shear key, which coincide with the regions of higher tensile stresses (before cracking). As shown in Figure 4.14, under maximum positive moment, cracking propagates along the middle of the shear key from the bottom toward the deck of the bridge; whereas under negative moment, cracking starts from top to bottom along the centerline of the shear key. In both load cases, the shear key is completely damaged and not able to retain any residual strength. Under a combination of maximum shear and corresponding moment, cracking also propagates from the bottom, but the crack follows the geometry of the shear key, similar to a debonding failure. Based on the experimental tests of shear keys with cementitious grout, it can be expected that the geometry of the shear key could still provide a locking effect on the box beams, if they are restrained laterally.

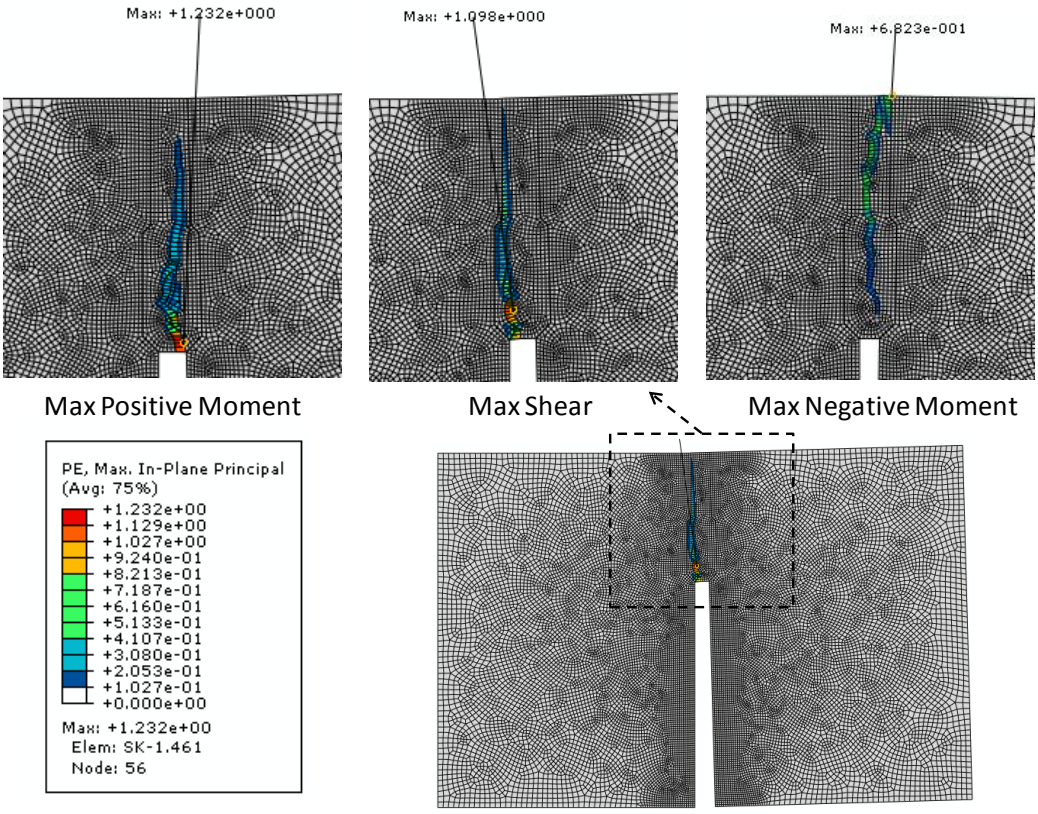

Figure 4.14 Crack patterns of a partial depth shear key with cementitious grout under the three maximum load cases

To avoid convergence problems in the numerical models, the applied stresses that create the resultant moment and shear were applied in load increments. Under the three load cases described here, the numerical models indicated that cracking occurred at a very early stage. The shear key cracked at 10% of the maximum negative moment; cracking occurred at 5% of the maximum positive moment and at 40% of maximum shear force. These results confirm that

the shear forces and moments generated by full live load on the prototype bridge analyzed in this study were very likely to produce cracking on the corresponding shear keys.

Table 4.5 Performance of the partial-depth cementitious grout under three load cases

Load Case	Percent of Load at Failure	Maximum Principal Stress at Applied Load (psi)	
		Top of Shear Key	Bottom of Shear Key
Maximum -M	10%	101 (tension)	260 (compression)
Maximum +M	5%	124 (compression)	103 (tension)
Maximum V	40%	201 (compression)	103 (tension)

Discussion

Results described in this section indicate that a partial-depth shear key with cementitious grout is very likely to crack under the load cases developed in this study. These results, however, do not explain the reason why shear keys may fail before the bridge is subjected to full live load. They do indicate that live load does contribute to the cracking of these elements. Shear key modifications (configuration, grouting material, post-tensioning, and bearing pad positioning) are explored in the next sections to evaluate the likelihood of avoiding (or minimizing) cracking in the shear keys.

4.3.3. Grouting Material

Epoxy grout

First, shear key models using the combination of partial depth and epoxy grout were analyzed for the three loading cases described previously (Max M+, Max M-, Max V). Results show that the shear key cracked under maximum positive and negative moments. No cracking was observed under the maximum shear force. As expected, under the maximum negative moment, the shear key cracked from the top and cracking propagated toward the bottom, whereas under maximum positive moment, the cracks propagated from the bottom toward the top, as shown in Figure 4.15. In both cases, shear keys were completely damaged and not able to retain any residual strength. It was observed that the epoxy-grouted shear keys cracked in the damage band, as observed in the experimental tests and modeled in section 4.2.

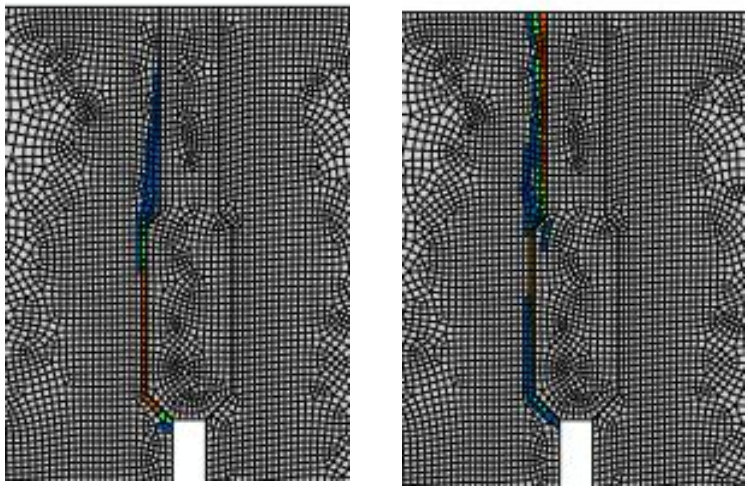

a) maximum positive moments b) maximum negative moments

Figure 4.15 Crack patterns of partial-depth epoxy grout shear key

Numerical results indicate that the partial-depth shear key with epoxy grout cracked at a later stage compared to the case with cementitious grout. The shear key cracked at 80% of the maximum negative moment and at 35% of the maximum positive moment. Therefore, the use of epoxy grout can be successful at preventing cracking due to shear under full live load conditions. For bending, even though it cannot be shown to prevent cracking under full live load, the percentage of maximum bending moment that it can withstand before cracking is at least seven times higher than for the cementitious grout. For the maximum shear force, maximum in-plane principal stresses generated on the shear key were 792.5 psi in tension (at the bottom of the shear key) and 272.7 psi in compression (at the top of the shear key), which are 59.8% of the tensile strength of the grout and 2.7% of compressive strength of the grout.

Table 4.6 Performance of the partial-depth epoxy grout under three load cases

Load Case	Percent of Load at Failure	Maximum Principal Stress at Applied Load (psi)	
		Top of Shear Key	Bottom of Shear Key
-M	>80%	760 (tension)	2230 (compression)
+M	35%	645 (compression)	889 (tension)
V	No crack	273 (compression)	793 (tension)

Fiber-reinforced cementitious grout

The same models substituted with fiber-reinforced cementitious grout were evaluated. The material properties of fiber-reinforced cementitious grout used in the model are listed in Table 4.7. All three load cases showed cracking. However, they cracked at a later stage compared with cementitous grout. The fiber-reinforced cementitious grout cracked at 20% of the maximum negative moment and at 10% of the maximum positive moment. At the maximum shear, the model just began to crack. The maximum tensile stresses developed in each load case prior to failure were around 368 psi, which is close to the splitting tensile strength of the

material. Overall, the performance of fiber-reinforced cementitious grout was slightly superior compared with cementitious grout.

Table 4.7 Material properties of fiber-reinforced cementititous grout used in the model

Material	Fiber-reinforced Cementitious Grout
Density (lb•s^2/in)	0.00022487
Compressive strength (psi)	4606
Splitting tensile strength (psi)	331
Modulus of elasticity (psi)	1.12 x 10^6
Fracture energy (lb/in)	0.2815

Table 4.8 Performance of partial-depth shear key using fiber-reinforced cementitious grout

Load Case	Percent of Load at Failure	Maximum Principal Stress at Applied Load (psi)	
		Top of Shear Key	Bottom of Shear Key
Maximum -M	20%	351 (tension)	1120 (compression)
Maximum +M	10%	351 (compression)	363 (tension)
Maximum V	100%	305 (compression)	372 (tension)

Discussion

Based on the results obtained in this section, it was shown that the use of epoxy grout improves the performance of the shear key under full live load. It can be inferred that it probably also improves the performance of the shear key under other load effects (such as thermal). However, the higher stress concentrations found on the partial-depth geometry prior to cracking indicate that changes in shear key configuration may also improve performance and therefore decrease the likelihood of cracking.

4.3.4 Shear Key Configuration

Full depth

The behavior of the FE models of full-depth shear keys with cementitious and epoxy grouts were evaluated under the three loading cases. The results show that under the maximum positive moment (Max M+), the cementitious grout cracked whereas the epoxy grout did not. Figure 4.16 shows the crack pattern of the full-depth shear key with cementitious grout. For the cementitious grout, using partial depth or full depth did not prevent cracking under maximum positive moment; however, the percentage of the applied moment at cracking increased from 5% to 40%. For the epoxy grout, using a full-depth shear key avoided cracking. The shear key withstood the maximum positive moment without cracking. Maximum in-plane principal stresses generated on the shear key were 302.1 psi tension (at the bottom of the shear key) and 298.3 psi compression (at the top of the shear key), which are 22.8% of the tensile strength of grout and 3.0% of compressive strength of grout.

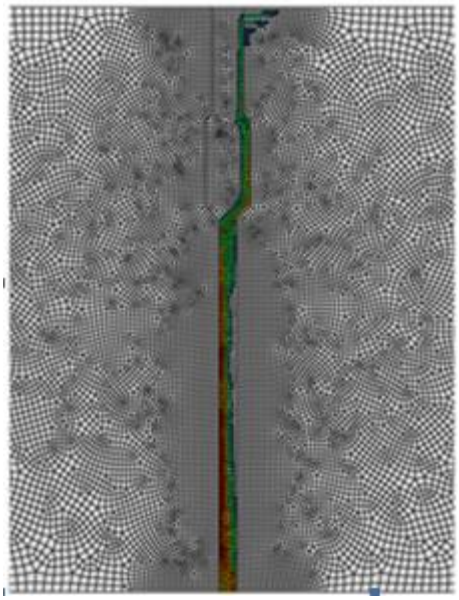

Figure 4.16 Plastic strain (crack patterns) of cementitious grout full-depth shear key

Location of key way

The location of the key way (top tier versus mid depth) and its effect on the behavior of the shear key under full live load was explored. FE models of mid-depth shear key with cementitious and epoxy grouts were analyzed and the results are summarized in Table 4.9. Both top tier and mid-depth shear keys with cementitious grout cracked at 40% of the maximum positive moment. Neither top tier nor mid-depth shear keys with epoxy grout cracked under the maximum positive moment. Stress distribution for these two epoxy cases was further evaluated. Maximum stresses were found to be about 302 psi at the bottom of the shear key regardless of the shear key location. These results suggest that when using a full-depth grouted shear key, the location of key way does not affect its performance.

Table 4.9 Performance of mid-depth shear key versus top-tier shear key

Load Case	Percent of Load at Failure	Maximum Principal Stress at Applied Load (psi)	
		Top of Shear Key	Bottom of Shear Key
Full-depth epoxy grout	No crack	298 (compression)	302 (tension)
Mid-depth epoxy grout	No crack	300 (compression)	303 (tension)
Full-depth cementitious grout	40%	127 (compression)	102 (tension)
Mid-depth cementitious grout	40%	139 (compression)	102 (tension)

Shear key width

FE models of two full-depth epoxy shear keys with two different key widths (¼ in and 1 in) were evaluated. The results indicate that neither of the shear keys cracked under the maximum positive moment. Moreover, the maximum principal stresses, which occurred at the bottom of both keys, were very close in magnitude (see Table 4.10), indicating that a change in the width

of a full-depth shear key does not affect its performance. It is assumed that the epoxy grout can flow in such a narrow key way and form a good bond with the concrete surface. Experimental testing is needed to confirm the validity of this idea.

Table 4.10 Performance of ¼-in shear key versus 1-in shear key (full-depth epoxy grout under Max +M)

	Percent of Load at Failure	Max Principal Stress at the Maximum Load (psi)	
		Top of Shear Key	Bottom of Shear Key
¼ ” full-depth epoxy grout	No crack	294 (compression)	308 (tension)
1” full-depth epoxy grout	No crack	298 (compression)	302 (tension)

4.3.5 Post-tensioning Effect

Post-tensioning

Based on current PennDOT specifications (PennDOT BD651M), the transverse post-tensioning layout of the prototype bridge was defined as shown in Figure 4.17a. The prototype bridge has a span length of 80 ft and no skew (90-degree skew angle); therefore its transverse post-tensioning details follow the plan B layout from PennDOT BD651M with an end void zone of 16 ft. According to PennDOT BC775M, each post-tensioning force represents a ½-in 270 ksi poly-strand tendon, post-tensioned up to at least 30 kips and placed at the centroid of the shear key (Figure 4.17b). It is noted that the end diaphragm is not specified to have a transverse post-tensioning tendon.

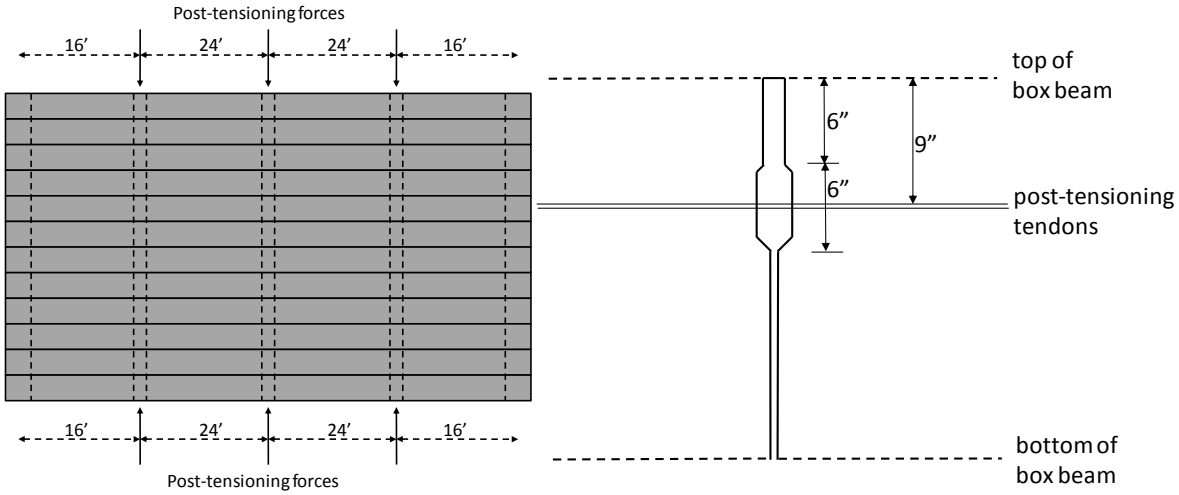

Figure 4.17 a) Transverse post-tensioning layout for the prototype bridge, b) Location of post-tensioning in the shear key area

The transverse post-tensioning tendons are expected to provide a confinement effect to the box beams and shear keys. In particular, properly designed transverse post-tensioning could counterbalance part of the tensile stresses developed in the shear key at early construction stages (such as temperature and shrinkage) as well as during service conditions under full live

load. Therefore, In order to use this information in the FE shear key model described previously, the stress distribution developed in the shear key due to this transverse post-tensioning was determined.

Because the post-tensioning force was not applied at the centroid of the box girder, the post-tensioning stresses varied linearly through the shear key cross section. Two FE models were generated to evaluate the post-tensioning effect: The first 2D model looks at the distribution of the compressive stresses over the entire bridge. This model was used to evaluate the areas of confinement due to the post-tensioning forces. For an isolated shear key, such as the one used in this study, the variation of the stresses due to the eccentricity of the post-tensioning force and geometry of the shear key were further explored with a second FE model.

FE model of bridge superstructure with post-tensioning forces

The 2D FE model of the bridge superstructure, including the post-tensioning forces defined previously, is shown in Figure 4.18. Each arrow represents a force of 30 kips. Plane stress elements (CPS4) were used, since the thickness of the model was small compared to in-plane dimensions of the model. It was assumed that the entire model was made of plain concrete. Sections that are light gray represent the void in the box beam or the flanges (thickness = 11 in), whereas the darker gray sections represent solid section in the box beam, due to intermediate and end diaphragms (thickness = 33 in). The concrete deck was not included in the model because the transverse post-tensioning was put in place before the placement of deck. Post-tensioning forces were applied at the centerlines of the intermediate diaphragms. This FE model was artificially pinned at one point (u1=0 and u2=0) to avoid rigid boy deformations. A mesh size of 5 in was used for the entire model.

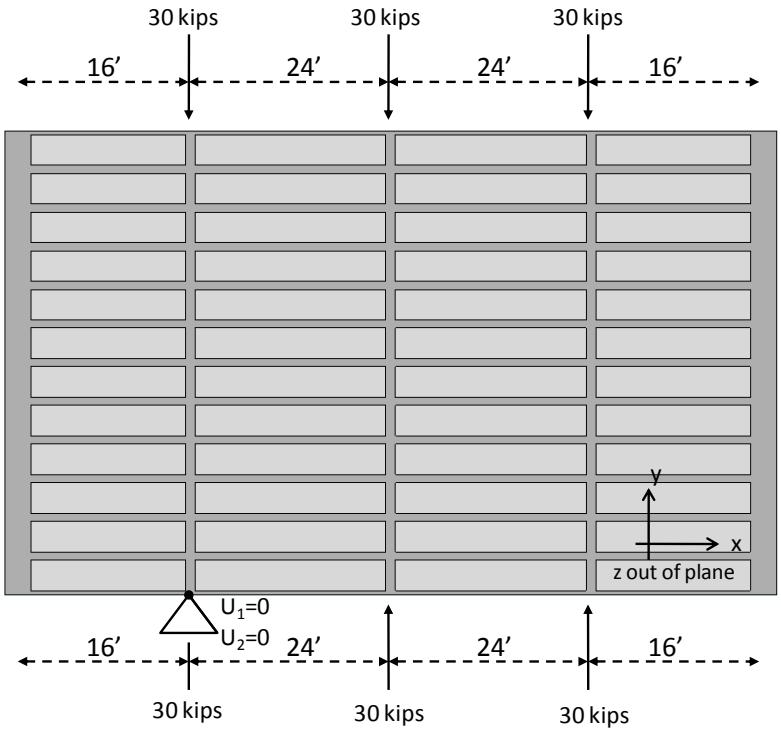

Figure 4.18 2D FE model of bridge superstructure with transverse post-tensioning

Figure 4.19 shows the distribution of normal stress in the y direction (s22) across the superstructure of the bridge. The compression stress ranged from 0 to 163.5 psi (stress concentration at the loading point). The stress distribution of the FE model shows that post-tensioning forces produced confinement only in the region near the loading points. The area of influence can be approximated on average to two adjacent box girders in the transverse y direction and a maximum width of 4 ft. This area experienced a range of compression stress between 15 psi and 45 psi. In regions further away from the loading points, the compressive stress distribution became more uniform. Shear keys in this region were found to be subjected to 10 psi of compressive stress, on average. In particular, for the two full-depth shear keys evaluated using the load cases from the grillage analysis (shear keys 3 and 6, see location in Figure 4.13), the average compressive stresses were 4.2 psi and 3.7 psi, respectively. It can be concluded that the post-tensioning layout used in the prototype bridge, which follows current PennDOT specifications, had a limited confinement effect on the overall bridge. Only shear keys in the immediate proximity to the loading points may benefit from this compressive force.

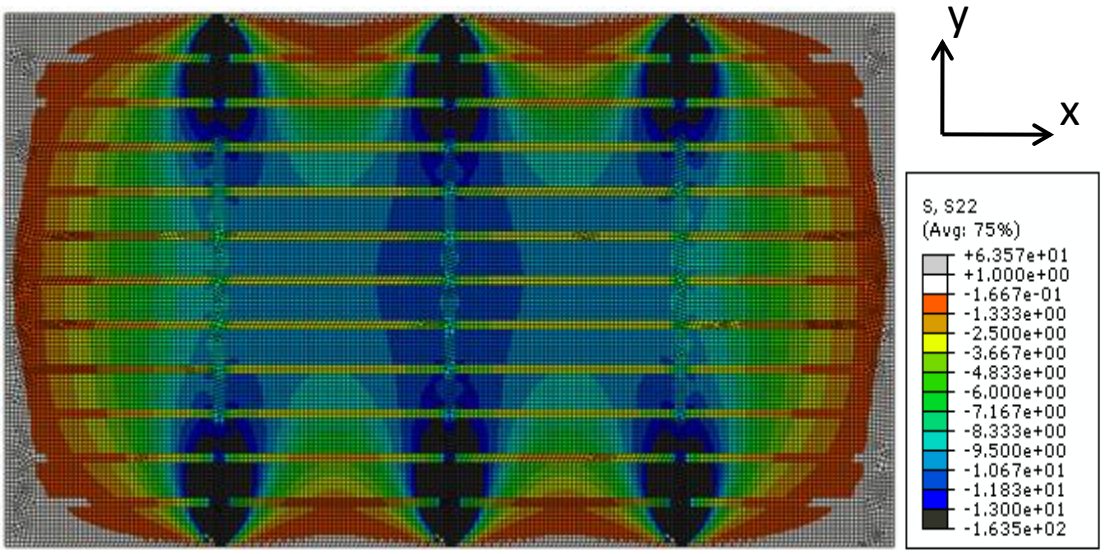

Figure 4.19 Stresses in the transverse y direction (s22) due to post-tensioning

FE model of two adjacent box girders subjected to a post-tensioning force

Because current PennDOT shear key specifications indicate partial depth and a post-tensioning tendon located at the centroid of the shear key, the variations of stresses along the shear key height needed to be evaluated. Figure 4.20 shows the FE model of two adjacent box beams connected with a shear key. The concrete box beams were assumed to be fully solid to represent behavior on a diaphragm. A post-tensioning force was applied as point load at the centerline of the shear key. The same modeling details from previous FE analysis were incorporated into this model.

The results, shown in Figure 4.20, indicate that compressive stresses fan out from the loading point toward shear key. However, only the top portion of the box beam experienced the confining effects of the post-tensioning. The highest compressive stress in the shear key region was found to be 44.3 psi. The magnitude of this compressive stress was smaller than the tensile stress created by the vehicle loading (live load). Moreover, the top portion of the shear key exhibited a negligible amount of compression. Therefore, it can be concluded that the current PennDOT transverse post-tensioning details provide limited confinement of the shear key region.

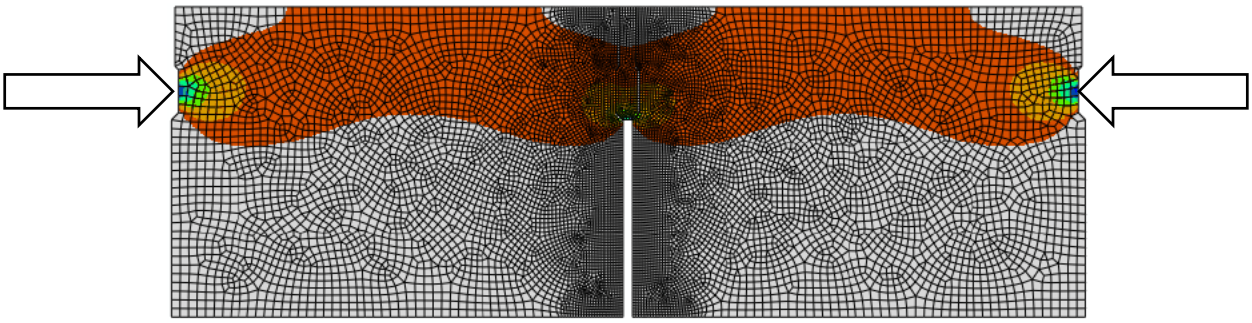

Figure 4.20 Maximum negative principal stress of a partial-depth cementitious grout shear key model under a single post-tensioning force

When a full-depth shear key with epoxy grout was used, the distribution of the maximum principal stresses was similar to the one observed for partial depth shear key, as shown in Figure 4.21. The magnitude of stresses did change: compressive stresses developed in the shear key at the top (7.6 psi) and tensile stresses developed at the bottom (1.25 psi). When under positive moment, the tensile stress induced by the post-tensioning tendons may help the initiation of cracks. Moreover, the compressive stress developed at the top was insignificant compared with the stresses developed by vehicle loadings. This finding suggests that a higher post-tensioning force should be applied at the centroid of the entire cross section to effectively confine the shear key region.

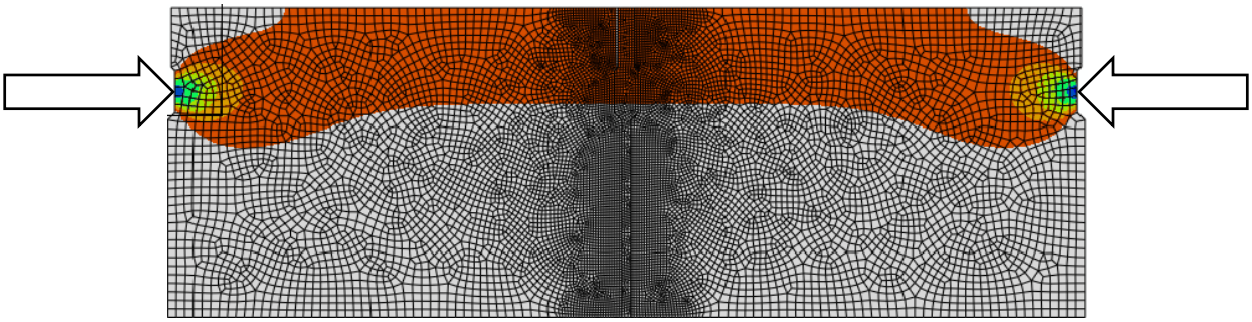

Figure 4.21 Maximum negative principal stress of a full-depth epoxy grout shear key model under one post-tensioning force

Effect of three post-tensioning tendons in a full-depth epoxy grout shear key

In order to create uniform compressive stress across the entire box beam section, three post-tensioning tendons were provided, as shown in Figure 4.22. Each post-tensioning tendon was jacked up to 30 kips. The results show that the entire out-of-plane cross-section of the shear key was undergoing the same compressive stress (10.9 psi).

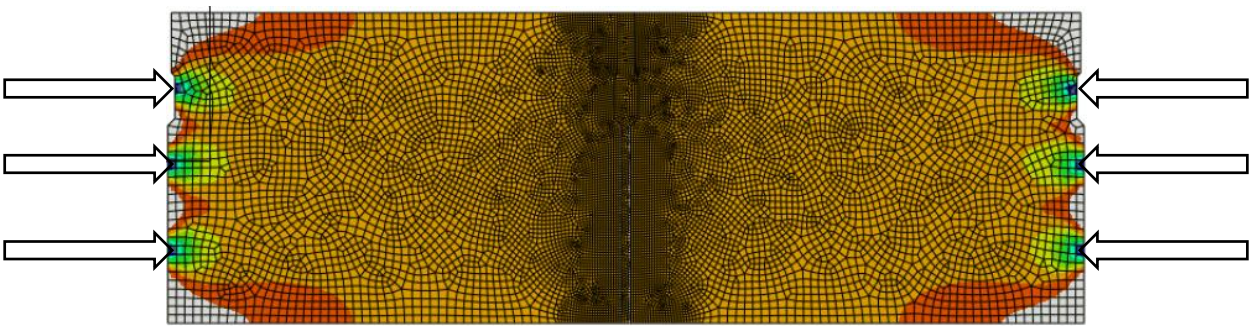

Figure 4.22 Maximum negative principal stress of a full-depth epoxy grout shear key model under three post-tensioning forces

The magnitude of post-tensioning should be calculated based on the stress level developed by vehicle load. If the stress exceeds the strength of the grouting material, post-tensioning should be calculated to balance the tensile stress so that cracking does not occur. Based on the magnitude of the post-tensioning force calculated, the spacing and layers of the post-tensioning tendons can then be determined. It is recommended that the transverse post-tensioning tendons be uniformly spread longitudinally. Current PennDOT bridge design standards specify no tendons at the end span of the bridge for span lengths greater than 55 ft. Crack patterns provided by PennDOT and other studies (Miller et. al 1999) show cracks initiating at the end of the span.

4.3.6 Bearing Pad

Model details

To analyze the effect of bearing pad on shear key, the following finite element was developed. The same model details of box beams and shear key from the shear test model were incorporated into this model. Full-depth epoxy grout was used for the model. The new component in this model was the bearing pad. The bearing pad was modeled using simple spring elements that are able to mimic the shear stiffness and compressive stiffness of the bearing. The shear modulus of the bearing pad was assumed to be 135 psi, which was selected from the recommended range (80 psi – 189 psi) from PennDOT DM4. Based on the selected shear modulus of the bearing pad, the shear stiffness and effective compressive modulus of the bearing pad were calculated (AASHTO 14.6.3.1-2 and C14.6.3.1-2). The shear stiffness of the bearing pad was determined to be 13.7 kips/in, whereas the compressive modulus of the bearing pad was 12.98 ksi.

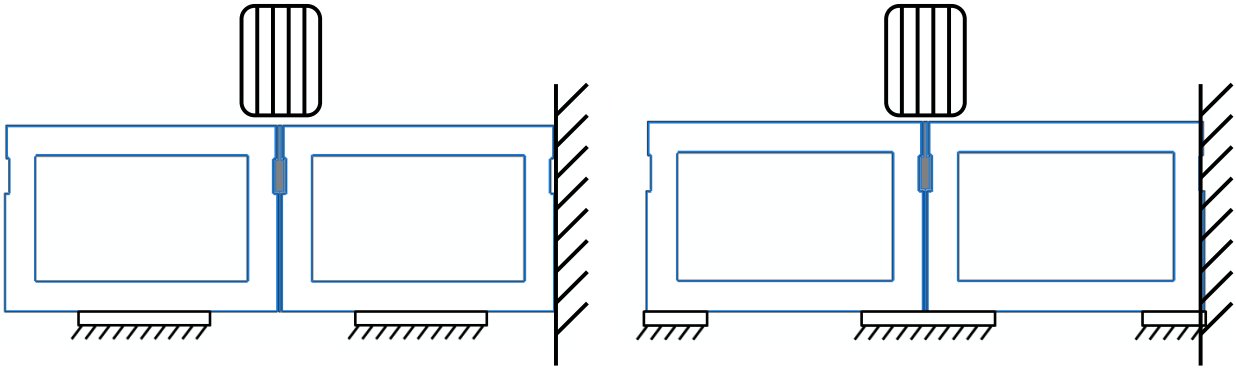

Figure 4.23 a) Bearing pad alternative 1 b) bearing pad alternative 2

The two box beams modeled were located on the edge. One side of the box beam was fixed assuming symmetry. One wheel load of 25 kips with a width of 12 in was applied as a uniformly distributed load at two locations, one at a time. One location was at the centerline of the exterior box beam and the other was the shear key. Two bearing pad alternatives for an adjacent box beam bridge were evaluated with the FE model; see Figure 4.23. The width of bearing pad in both alternatives was 24 in. The contact between the box beam and the bearing pad was modeled using surface-to-surface contact; the box beam elements could not penetrate into the geometry of the bearing pad; however, they were free to deform away from the bearing pad.

The graphic results of the distribution of maximum principal stress are plotted in Figure 4.24. The maximum principal stress in each case can be found in Table 4.11. Shear key in case 2 developed the highest tensile stress as expected because, with the absence of support below the shear key, the shear key was able to deflect more under the same level of loading. Depending on the level of the truck load, the stress can exceed the tensile strength of the grouting material and lead to cracking. This qualitative study of the effect of the bearing pad configuration suggests that putting bearing pad below shear key can greatly reduce the stress developed.

Based on a request from PennDOT's technical advisor, a new numerical model was analyzed. It incorporates recent PennDOT (District 1) designed bearing pad details (PennDOT Design Drawing SR0006, Section B04 2008). According to this design drawing, two 10-in-wide bearing pads are placed under each box beam with an edge clearance of 5 in (case 5, Figure 24). This pad configuration was evaluated under wheel loading on top of the shear key. Results show that the maximum principal tensile stresses developed near the bottom of the shear key. The magnitude of the maximum tensile stress was 132 psi, which is 50% smaller than the tensile stresses generated using the bearing pad alternative 1 (case 2, Figure 2.24). However, bearing pad alternative 2, in which the bearing pads were placed right under the shear key (case 4), showed the smallest tensile stress (50% smaller than case 5) for all bearing pad configurations under the same loading conditions, as shown in Table 4.11.

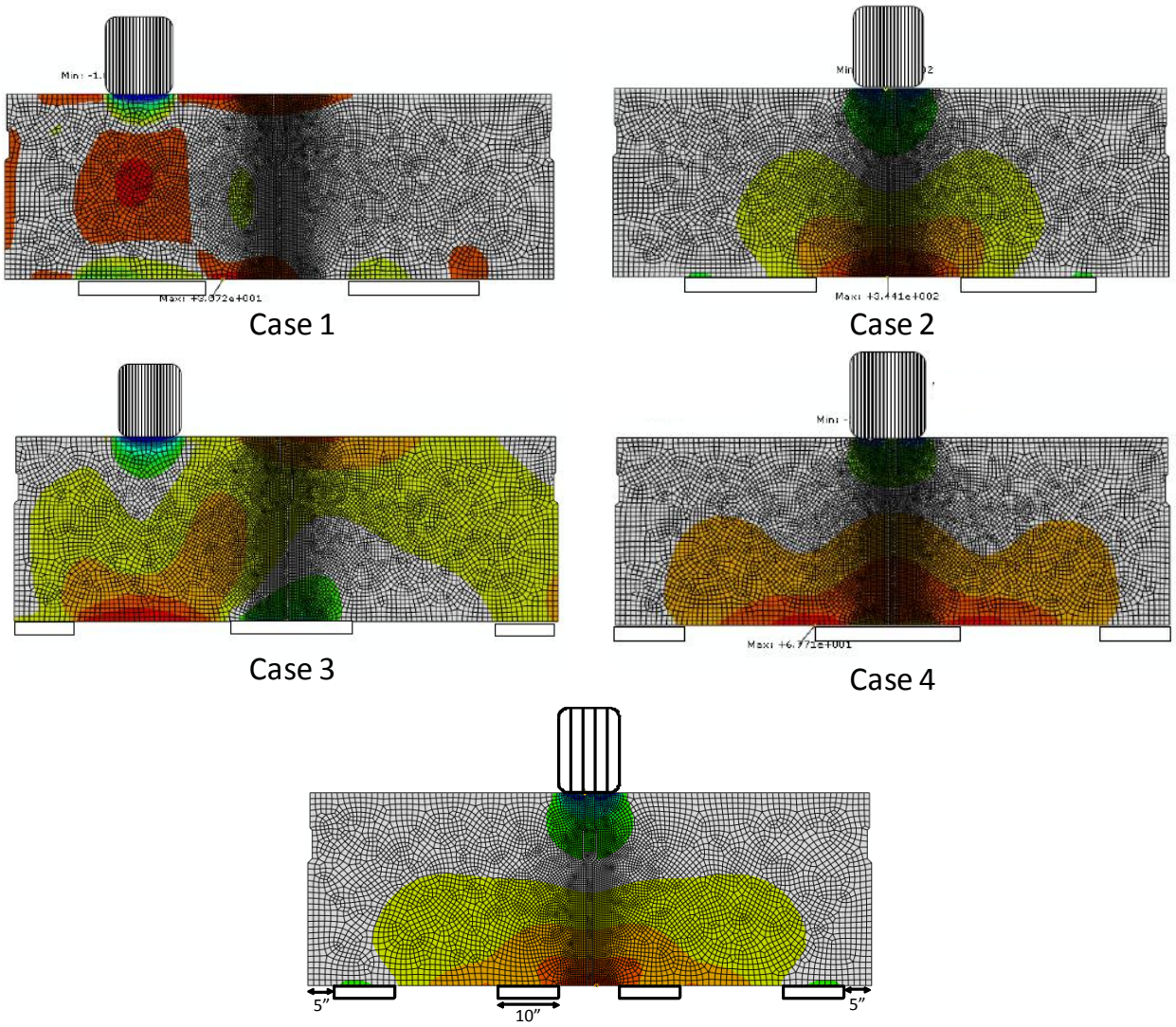

Figure 4.24 Maximum principal stress distribution of five bearing pad models

Table 4.11 Maximum principal stress in the shear key developed in five cases

	Maximum Principal Stress in the Shear Key (psi)
Case 1	15.1 (tension)
Case 2	341.0 (tension)
Case 3	16.4 (tension)
Case 4	60.5 (tension)
Case 5	132 (tension)

4.4 Table Summary

Table 4.12 Summary of modifications based on the findings from FE modeling

Modification		Summary
Load cases		• Maximum positive moment is the most critical load case. Crack propagates from bottom of shear key toward top.
Material	Cementitious grout	• Cementitious grout cracks in all cases. • It has weak bond strength, cracks tend to develop along the interface between cementitious grout and concrete.
	Epoxy grout	• Epoxy grout does not crack except for the partial depth shear key case. • It has very strong bond strength and fracture properties. Cracking is likely to occur in the concrete when failure happens.
	Fiber-reinforced cementitious grout	• It has better bond strength compared with cementitious grout. • It still cracks in most cases except when full-depth shear key is used.
Configuration	Grouting depth	• Full-depth shear key relieves the stress developed in shear key and therefore is more effective in preventing cracking than partial-depth shear key.
	Location	• Location of shear key does not significantly affect the performance of the shear key.
	Width	• For epoxy grout, the width of shear key does not affect the performance of the shear key as long as the grout can flow through key way and form a good bond with concrete.
Post-tensioning		• The current PennDOT specified post-tensioning is insufficient in resisting cracks. • Higher post-tensioning force is recommended to help with the cracking problem. • It is also recommended that post-tensioning extend through the mid height of the box beam to create uniform compressive stress.
Bearing pad		• Putting bearing pad directly under shear key can reduce the stress developed in the shear key under the same loading.

Chapter 5. Summary and Conclusions

The objective of this project was to evaluate improved design, construction, and repair practices that have the potential to reduce shear key grout failure in the Pennsylvania Department of Transportation's precast box beam bridges. To meet the objective, a comprehensive literature review of the performance of connection details of adjacent precast box beams was conducted, followed by experimental and analytical evaluation of shear key connection modifications.

Based on the findings of the literature survey documented in this report, the following parameters were found to be the most likely sources for shear key cracking: partial grouting depth and top-tier shear key location (related to shear key geometry), bearing details that induce relative beam deflection, insufficient transverse post-tensioning reinforcement, and inadequate strength and shrinkage incompatibility of grouting materials.

PennDOT's technical advisor, in discussion with the Penn State research team, agreed to further exploration of the following alternatives: shear key configuration (full-depth grouted shear key, geometry and location of the shear key), grouting material (fiber-reinforced mortar and epoxy-based grout), transverse post-tensioning and post-tensioning reinforcement details (location of tendons, level of prestress force), and bearing pad details.

Results from the experimental evaluation of the concrete and grouting materials indicated that the epoxy grout characterized in this report had a higher bond with respect to concrete than the selected cementitious grout. In particular, the fracture energy of the concrete-epoxy grout interface was one order of magnitude higher than the concrete-cementitious grout. The addition of fibers appears to provide a modest improvement in the bond between concrete and grout.

Experimental testing of concrete specimens with different grout materials showed that the epoxy-grouted specimens had the highest strength. Cracking originated on the concrete side of the shear keys, and no debonding failures were observed. By contrast, the specimens with cementitious grout failed at the shear key interface by debonding. Fractured shear key surfaces exhibited residual strength due to bearing failure and slip mechanisms.

Results from the analytical evaluation using a grillage model indicated that the shear keys most likely to be subjected to maximum moments and shear are located at midspan. Maximum positive and negative moments affect the shear key located at mid length in the transverse direction. Maximum shear force was found acting on a shear key located toward the exterior beams.

Numerical models developed to predict the behavior of the experimental shear tests of concrete-grout specimens were able to reflect the differences in failure modes observed in epoxy and cementitious grout specimens as well as the experimentally observed crack

sequence and patterns, and strength levels. Cracks were observed in the partial-depth cementitious grout in all the load cases studied, both numerically and experimentally. The test showed that the cracking at the shear key region may occur even at an early loading stage, well before it is subjected to full live load. The strength of a shear key with epoxy grouts, on the other hand, increased substantially.

Upon verification of the numerical model against test results, parametric studies were performed to investigate alternative design approaches that could alleviate the cracking problem at the shear key region. Parameters included the location and depth of the shear key. The results suggested that the use of a full-depth epoxy grouted shear key has the highest potential to reduce shear key grout failure. The amount of transverse prestressing tendons and the effect of the bearing pad at supports also plays an important role in reducing maximum tensile stresses and thus cracking.

Other than these design considerations, the following construction practices are recommended as well:

- Sandblast the shear key surface of the box beams before shipping to provide a better bonding surface for the grout.
- Clean the shear key surface with compressed air or water before the erection of the box beams to provide a better bonding surface.
- Provide proper curing of the grouting material to prevent excessive shrinkage of grout.
- Conduct quality control of the grouting materials used to ensure proper strength and bond of the shear key.

References

AASHTO LRFD Bridge Design Specification (2008). F. E., American Association of State Highway and Transportation Officials, Washington, D.C., plus 2008 Interim Revisions.

AASHTO/PCI Bridge Design Manual (1997). F. E., American Association of State Highway and Transportation Officials, Washington, D.C.

ACI Committee 446 (2007). "Fracture Toughness Testing of Concrete." American Concrete Institute, Farmington Hills, Michigan.

Ahlborn, T. M., Gilberstson, C. G., Aktan, H., and Attanayake, U. (2005). *Condition Assessment and Methods of Abatement of Prestressed Box-Beam Bridges*. Research Report RC-1470, Michigan Technological University.

ASTM C 39 (2005). "Standard Test Method for Compressive Strength of Cylindrical Concrete Specimens." American Society for Testing and Materials, West Conshohocken, Pennsylvania.

ASTM C 496 (2004). "Standard Test Method for Splitting Tensile Strength of Cylindrical Concrete Specimens." American Society for Testing and Materials, West Conshohocken, Pennsylvania.

ASTM C 531 (2005). "Standard Test Method for Linear Shrinkage and Coefficient of Thermal Expansion of Chemical-Resistant Mortars, Grouts, Monolithic Surfacings, and Polymer Concretes." American Society for Testing and Materials, West Conshohocken, Pennsylvania.

ASTM C 579 (2006). "Standard Test Methods for Compressive Strength of Chemical-Resistant Mortars, Grouts, Monolithic Surfacings, and Polymer Concretes." American Society for Testing and Materials, West Conshohocken, Pennsylvania.

ASTM C 580 (2008). "Standard Test Method for Flexural Strength and Modulus of Elasticity of Chemical-Resistant Mortars, Grouts, Monolithic Surfacings, and Polymer Concretes." American Society for Testing and Materials, West Conshohocken, Pennsylvania.

ASTM C 882 (2005). "Standard Test Method for Bond Strength of Epoxy-Resin Systems Used with Concrete by Slant Shear." American Society for Testing and Materials, West Conshohocken, Pennsylvania.

Attanayake, U., and Aktan, H. (2008). "Issues with Reflective Deck Cracks in Side-by-Side Box Beam Bridges." *Proceedings of the 2008 Concrete Bridge Conference*, Federal Highway Administration, National Concrete Bridge Council, Missouri Department of Transportation, American Concrete Institute, 18 pp.

Attanayake, U., and Aktan, H. M. (2009) "Side-by-side Box-beam Bridge Superstructure: Rational Transverse Posttension Design." Transportation Research Board Annual Meeting, Washington, D.C.

Badwan, I. Z., and Liang, R. Y. (2007a). "Performance Evaluation of Precast Post-Tensioned Concrete Multibeam Deck." *Journal of Performance of Constructed Facilities*, 21(5), 368-374.

Badwan, I. Z., and Liang, R. Y. (2007b). "Transverse Post-Tensioning Design of Precast Concrete Multi-beam Deck." *PCI Journal*, 52(4), 84-92.

Coronado, C. A., and Lopez, M. M. (2006). "Sensitivity Analysis of Reinforced Concrete Beams Strengthened with FRP Laminates." *Cement and Concrete Composites*, 28, 102-114.

Coronado, C. A., and Lopez, M. M. (2007). "Damage Approach for the Prediction of Debonding Failure on Concrete Elements Strengthened with FRP." *Journal of Composites for Construction*, 11(4), 391-400.

Coronado, C. A., and Lopez, M. M. (2008). "Experimental Characterization of Concrete-cement Interfaces." *Journal of Materials in Civil Engineering*, 20(4), 303-312.

Coronado, C. A., and Lopez, M. M. (2010). "Numerical Modeling of Concrete-FRP Debonding Using a Crack Band Approach." *Journal of Composites for Construction*, 14(1).

Dong, L., Yue, L., and Ahlborn, T. M. (2007). "Performance of Joint Connections between Decked Prestressed Concrete Bridges Girders." *Proceedings, PCI National Bridge Conference*, Phoenix, AZ.

El-Remaily, A., Tadros, M. K., Yamane, T., and Krause, G. (1996). "Transverse Design of Adjacent Prestressed Concrete Box Girder Bridges." *PCI Journal*, 41(4), 96-107.

Elices, M., Guinea, G. V., Gomez, J., and Planas, J. (2002). "The cohesive zone model: advantages, limitations and challenges." *Eng Fract Mech*, 69(2): 137–63.

Greuel, A., Baseheart, T. M., Rogers, B. T., Miller, R. A., and Shahrooz, B. M. (2000). "Evaluation of a High Performance Concrete Box Girder Bridge." *PCI Journal*, 45(6), 60-71.

Gulyas, R. J., Wirthlin, G. J., and Champa, J. T. (1995). "Evaluation of Keyway Grout Test Methods for Precast Concrete Bridges." *PCI Journal*, 40(1), 44-51.

Hanna, K. E., Morcous, G., and Tadros, M. K. (2007) "Transverse Design and Detailing of Adjacent Box Beam Bridges." *Proceedings, PCI National Bridge Conference*, Phoenix, AZ.

Hanna, K. E., Morcous, G., and Tadros, M. K. (2008). "Non-Post-Tensioned Transverse Design and Detailing of Adjacent Box Beam Bridges." NCBC Concrete Bridge Conference, St. Louis, MO.

Hawkin, N. M., and Fuentes, J. B. (2003). *Structural Condition Assessment and Service Load Performance of Deteriorated Pretensioning Deck Beam Bridges*. FHWA-IL-UI-285, Illinois Cooperative Highway and Transportation.

Hlavacs, G. M., Long, T., Miller, R. A., and Baseheart, T. M. (1997). "Nondestructive Determination of Response of Shear Keys to Environmental and Structural Cyclic Loading." *Transportation Research Record*, 1574, 18-24.

Huckelbridge, A. A., El-Esnawi, H., and Moses, F. (1993). *An Investigation of Load Transfer in Multi-beam Prestressed Box Girder Bridges*. Case Western Reserve University, Ohio Department of Transportation, Federal Highway Administration.

Huckelbridge, A. A., and El-Esnawi, H. H. (1997). *Evaluation of Improved Shear Key Designs for Multi-beam Box Girder Bridges*. Case Western Reserve University, Ohio Department of Transportation, Federal Highway Administration.

Huckelbridge, A. A. J., El-Esnawi, H., and Moses, F. (1995). "Shear Key Performance in Multi-beam Box Girder Bridges." *Journal of Performance of Constructed Facilities*, 9(4), 271-285.

Issa, M. (2002). *Experimental Evaluation of Full Depth Precast/Prestressed Concrete Bridge Deck Panels*. University of Illinois, Chicago, Illinois Transportation Research Center.

Issa, M. A., Ribeiro do Valle, C. L., Abdalla, H. A., and Islam, S. (2003). "Performance of Transverse Joint Grout Materials in Full-Depth Precast Concrete Bridge Deck Systems." *PCI Journal*, 48(4), p. 92-103.

Kim, J. J., Nam, J. W., Kim, H. J., Kim, J. H., Kim, S. B., and Byun, K. J. (2008). “Overview and Applications of Precast, Prestressed Concrete Adjacent Box-beam Bridges in South Korea.” *PCI Journal*, July-August 2008, pp. 83-106.

Koller, William (2008). Personal correspondence.

Lall, J., Alampalli, S., and DiCocco, E. F. (1998). "Performance of Full-Depth Shear Keys in Adjacent Prestressed Box Beam Bridges." *PCI Journal*, 43(2), 72-79.

Lee, J. (2010). “Performance of Uwrap as an Anchorage System in Externally Bonded FRP Reinforced Concrete Elements.” Ph.D. Dissertation, The Pennsylvania State University.

Lubliner, J., Oliver, J., Oller, S., and Onate, E. (1989). “Plastic-damage model for concrete.” *Int J Solids Struct*, 25(3), 299–326.

Macioce, T. P., Rogers, H. C., Anderson, R., and Puzey, D. C. (2007). "Prestressed Concrete Box Beam Bridges - Two DOTs' Experience." PCI National Concrete Bridge Conference, Phoenix, AZ.

Miller, R. A., Parekh, K., and Halsey, J. H. (1995). *Destructive Load Testing of a Damaged and Deteriorated Prestressed Concrete Box Beam*. UC-CII 93/03, Cincinnati Infrastructure Institute, University of Cincinnati.

Miller, R. A., Hlavacs, G. M., and Long, T. W. (1998). *Testing of Full Scale Prestressed Beams to Evaluate Shear Key Performance*. Cincinnati University, Ohio Department of Transportation, Federal Highway Administration.

Miller, R. A., Hlavacs, G. M., Long, T., and Greuel, A. (1999). "Full-scale testing of shear keys for adjacent box girder bridges." *PCI Journal*, 44(6), 80-90.

Nottingham, D. (1995). “Discussion of Evaluation of Keyway Grout Test Methods for Precast Concrete Bridges". *PCI Journal*, 40(4), 98-103.

PCI Bridge Design Manual, P. P. C. I., Chicago, IL, 1997. Updated July 2003.

PennDOT (2007). “Standard Miscellaneous Prestress Details” Technical document BC-775M. Pennsylvania Department of Transportation, Harrisburg, PA.

PennDOT (2007). “Design Manual Part 4.” Pennsylvania Department of Transportation, Harrisburg, PA.

PennDOT (2008). “Design Drawing SR0006, Section B04.” Pennsylvania Department of Transportation, Harrisburg, PA.

PennDOT Publication 35, Bulletin 15 (2004). “Approved Construction Materials.” Pennsylvania Department of Transportation, Harrisburg, PA.

Scott, D. L., and Tremblay, J. A. (2007). "New Hampshire's First Use of Full-Depth Precast Concrete Deck Panels." PCI National Concrete Bridge Conference, Phoenix, AZ.

Tang, J. (1992). *Shear Key Construction for Precast Unit Bridges*. Client Report 58, Engineering Research and Development Bureau, New York State Department of Transportation, Albany, NY.

Todeschini, Claudio E., Albert C. Bianchini, and Clyde E. Kesler (1964). “Behavior of Concrete Columns Reinforced with High Strength Steels.” *ACI Journal, Proceedings*, Vol. 61, No. 6.

Thorenfeldt, E., Tomaszewicz, A., and Jensen, J.J. (1987). “Mechanical Properties of High Strength Concrete and Application to Design.” *Proceedings of the Symposium: Utilization of High-Strength Concrete*. Stavanger, Norway, pp. 149-159.